MISCELLANEOUS PAPER S-73-57

RADIOGRAPHIC, PETROGRAPHIC, AND SEM EVALUATION OF BALLISTICALLY LOADED CLAY

by

D. M. Patrick

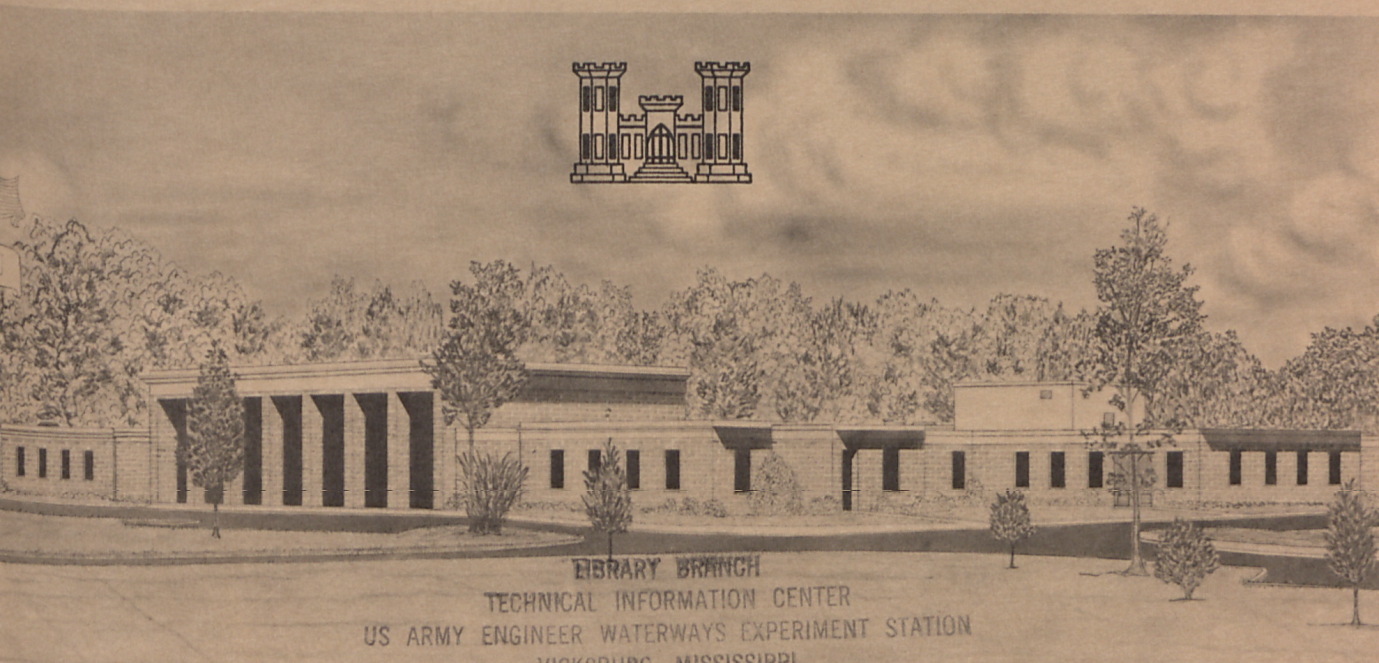

June 1973

Sponsored by Directorate of Military Engineering and Topography

Conducted by U. S. Army Engineer Waterways Experiment Station
Soils and Pavements Laboratory
Vicksburg, Mississippi

MISCELLANEOUS PAPER S-73-57

RADIOGRAPHIC, PETROGRAPHIC, AND SEM EVALUATION OF BALLISTICALLY LOADED CLAY

by

D. M. Patrick

June 1973

Sponsored by Directorate of Military Engineering and Topography
Project No. 4A061102B52E

Conducted by U. S. Army Engineer Waterways Experiment Station
Soils and Pavements Laboratory
Vicksburg, Mississippi

ARMY-MRC VICKSBURG, MISS.

THE CONTENTS OF THIS REPORT ARE NOT TO BE USED FOR ADVERTISING, PUBLICATION, OR PROMOTIONAL PURPOSES. CITATION OF TRADE NAMES DOES NOT CONSTITUTE AN OFFICIAL ENDORSEMENT OR APPROVAL OF THE USE OF SUCH COMMERCIAL PRODUCTS.

FOREWORD

The study reported herein was funded by the Department of the Army, Project 4A061102B52E, "Research in Military Engineering Construction (RMEC)," Task 03, Work Unit 009, sponsored by the Directorate of Military Engineering and Topography.

The study was conducted in the Soils and Pavements Laboratory of the U. S. Army Engineer Waterways Experiment Station under the direct supervision of Dr. E. L. Krinitzsky, Chief, Engineering Geology Research Facility, and the general supervision of Dr. C. R. Kolb, Chief, Engineering and Geology Division, and Mr. J. P. Sale, Chief, Soils and Pavements Laboratory.

Specimens were prepared and X-rayed by Messrs. R. O. Pichulo and J. T. Lewis. Firing was conducted by the Soil Dynamics Division under the general supervision of Dr. B. Rohani. Quantitative density standards were prepared in the Soils Testing Branch under the supervision of Mr. R. C. Horz, Jr.

X-ray diffraction analyses, thin-section preparation, and scanning electron microscope (SEM) photographs were provided by Messrs. A. P. Buck and C. R. Hallford under the general supervision of Mrs. K. Mather, Chief, Petrography and X-ray Branch, Concrete Laboratory.

Quantitative density analyses, petrographic and scanning electron microscope studies, and writing of the report were undertaken by Dr. D. M. Patrick, Engineering Geology Research Facility.

Directors of WES during this investigation were COL Levi A. Brown, CE, and COL Ernest D. Peixotto, CE. Technical Director was Mr. F. R. Brown.

CONTENTS

CONTENTS

CONVERSION FACTORS, BRITISH TO METRIC UNITS OF MEASUREMENT

British units of measurement used in this report can be converted to metric units as follows:

Multiply	By	To Obtain
inches	2.54	centimeters
pounds per cubic foot	16.0185	kilograms per cubic meter
feet per second	30.48	centimeters per second
grain (1/7000 lbm avoirdupois)	0.00006479	kilogram

SUMMARY

Specimens of highly plastic clay were prepared at densities and water contents ranging from 106 to 128 pcf and 26 to 67 percent, respectively. These specimens were ballistically loaded by impact of a projectile traveling at both low (1660 fps) and high (3327 fps) velocities. Radiographic examination of the specimens revealed the extent and nature of disturbance including crater size and shape, depth of projectile penetration, and projectile deformation. Radiography of thin slabs and isodensitometer studies provided the basis for density measurements. The radiography was supplemented by clay-fabric studies utilizing petrography and scanning electron microscopy (SEM). These techniques indicated that the impact produced negligible fabric disturbance and that some densification had occurred beneath the projectile. Techniques, procedures, and recommendations are given for studying ballistic loading of materials.

RADIOGRAPHIC, PETROGRAPHIC, AND SEM EVALUATION OF BALLISTICALLY LOADED CLAY

PART I: INTRODUCTION

Purpose

1. The use of soils for protection against conventional weapons has stimulated interest in the effects of ballistic impact on earth materials. This interest has been directed toward practical aspects such as penetrability of soils and, as a consequence, has generated interest in the changes which occur in the soil due to impact.

2. The purpose of this study was to investigate the techniques and applicability of X-radiography and related techniques to the study of ballistic loading of clays. The applications investigated are considered to be of potential usefulness for other materials and other types of loading.

Scope

3. The intent of this report is not to analyze the mechanisms of ballistic deformations but to illustrate specific techniques of studying them. The examination of the results of ballistic loading for clay specimens prepared under various conditions will form the basis of this study.

4. Although the radiographic aspects are of primary concern, scanning electron microscopy (SEM), petrography, and X-ray diffraction techniques are also included. These supplemental techniques provide a basis for comparison and permit the study of small-scale features in the specimens.

Materials

5. The clay that was subjected to ballistic loading was highly

plastic (CH), contained less than 5 percent sand, and consisted of approximately 50 percent clay particles. It was dark gray to black due to the presence of organic material.

6. The mineralogy was determined by X-ray diffraction (XRD) including both randomly oriented powder and sedimented slide techniques. The sand and silt fractions were predominantly quartz with minor amounts of feldspar and mica. Calcite and dolomite were present in minor amounts in some samples. The clay fraction was of subequal kaolinite and montmorillonite, some quartz, with minor amounts of illite and chlorite. The clay also contained concretions of hematite, limonite, and possibly siderite, ranging from 1/8 to nearly 1 in.* in diameter.

Specimen Preparation

7. Five 2-in. lifts of the clay material were compacted in a 4-1/8- by 4-1/2- by approximately 12-in.-side masonite box. An impact hammer striking an aluminum plate was used to compact each lift and distribute the impact uniformly over the surface of the clay.

8. The clay was compacted at bulk densities ranging from 106 to 128 pcf and water contents ranging from 26 to 67 percent. Lead shot was placed on the surface of each lift in order to define the relative position of each lift before and after impact.

9. The masonite box containing the five lifts of compacted clay was placed in the aluminum firing box shown in fig. 1. The firing box was supported by two cables fastened to the ceiling of the firing chamber.

10. Seven linear variable differential transformers (LVDT) mounted on the top and sides of the firing box measured the dilation of the box at the mounting point. One LVDT mounted at the midpoint of the rear face measured translation of the box in the firing direction. However, the dilation and translation data are not contained in this report.

---

* A table of factors for converting British units of measurement to metric units is presented on page ix.

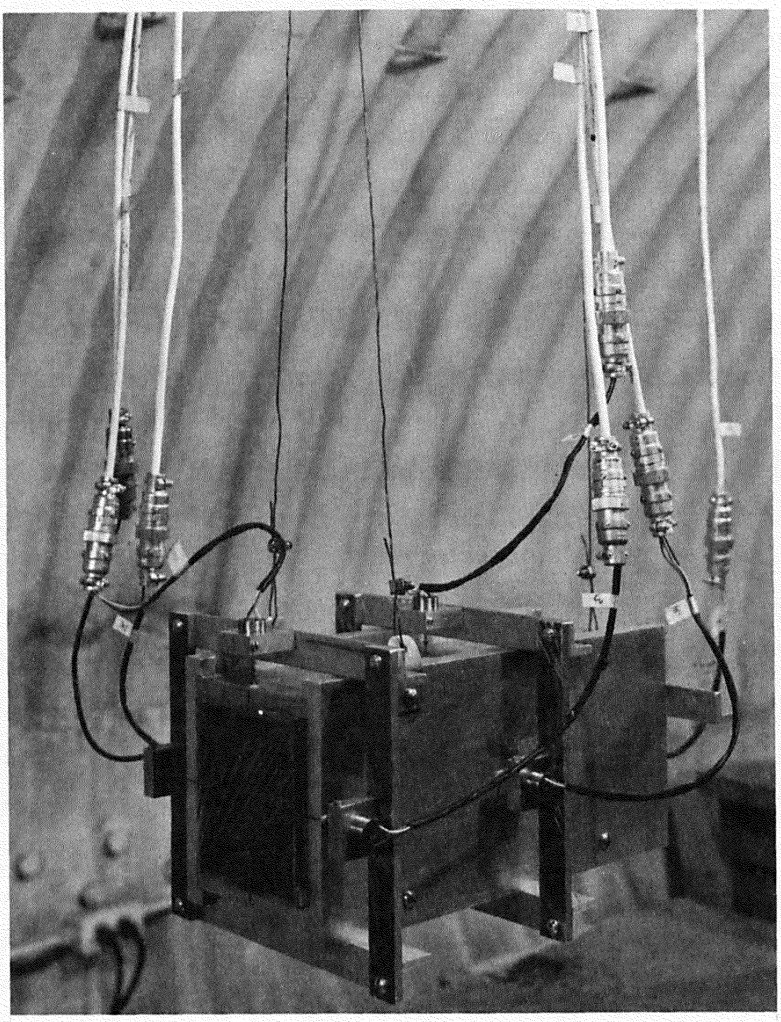

Fig. 1. Aluminum firing box

11. Table 1 is a summation of the test parameters for fired and control specimens.

12. A sample of clay was cut from the specimen and frozen in Freon-12. After freezing, the sample was "dried" in a vacuum, and the ice was removed by sublimation. This procedure permits the removal of pore water with a minimal disruption of fabric.* The pore space was then filled by impregnating the sample with an epoxy resin. The resin,

---

* Fabric as used herein refers to the size, shape, and arrangement of the soil particles.

after setting up, preserves the particle-to-particle arrangement and acts as a cement during final grinding.

13. There are two general procedural problem areas that must be considered when studying clay fabrics by SEM. These are: (1) fabric alteration during sample preparation and (2) fabric alteration associated with the vacuum within the microscope. The first problem stems from the necessity of examining a surface within the sample. In order to view this surface, the sample must be opened in some manner to permit observation. Fracturing or breaking the sample at the desired location has been found to produce significantly less disturbance than either slicing or sawing, both of which have a tendency to smooth out the clay at the exposed surface.

14. The second problem centers around the dehydration effects produced by the vacuum of the microscope itself. The loss of pore water as well as interlayer water, if present, produces shrinkage within the sample and also may cause curling of the clay platelets. The procedure found to be most effective consists of freeze-drying, fracturing, and finally impregnation prior to examination.

Firing Techniques

15. The firing direction was normal to the surface of the lifts. A rifle firing 5-1/2-mm cubes of steel weighing approximately 45 grains was used in these tests to ballistically load the clay specimens. Each cube was housed in a plastic sabot. Projectile velocities ranged from 1660 to 3327 fps, as measured by photoelectric cells.

PART II: RADIOGRAPHIC EXAMINATION

16. Prior to firing, each specimen was examined by X-radiography. This examination provided a means of quality control of specimen preparation and served as a basis for posttest evaluation and comparison. The posttest radiographs were taken under the same conditions as the pretest radiographs. In order to detect small-scale changes in the clay, the specimens were also cut into slabs and radiographed.

17. The pretest and posttest radiographs of the specimens are included as figs. 2-5. The photo tone gives a relative measure of the density of the material for a particular specimen. The darker areas indicate higher soil densities. This rule cannot be applied in comparing different specimens, because differences between samples required that the developing processes be adjusted to give maximum contrast for a particular specimen. The dark circles represent the lead shot that delineates the lift boundaries. The dark areas around the sides and bottom of most of the radiographs do not represent areas of higher density but are due to scattering of radiation, which generally occurs along edges. This can be overcome by placing lead shielding around the periphery of the sample. Such a technique was utilized for the radiography of the slabs.

Pretest Radiography

18. Generally, the effectiveness of the compaction can be seen to be quite good. The photo tones are uniform and the lift boundaries are distinct. Specimens 09BC and 010BC (fig. 4), which were prepared by hand-placing the soil, do not, however, exhibit distinct lift boundaries as would be expected. The shot in this case merely serve as control points within the specimen. Specimens 011BC and 012BC (fig. 5) indicate that the compaction was poor; this is evident from the numerous void spaces within the specimens. The lower water contents (26 percent) are most likely responsible for lack of uniformity in density.

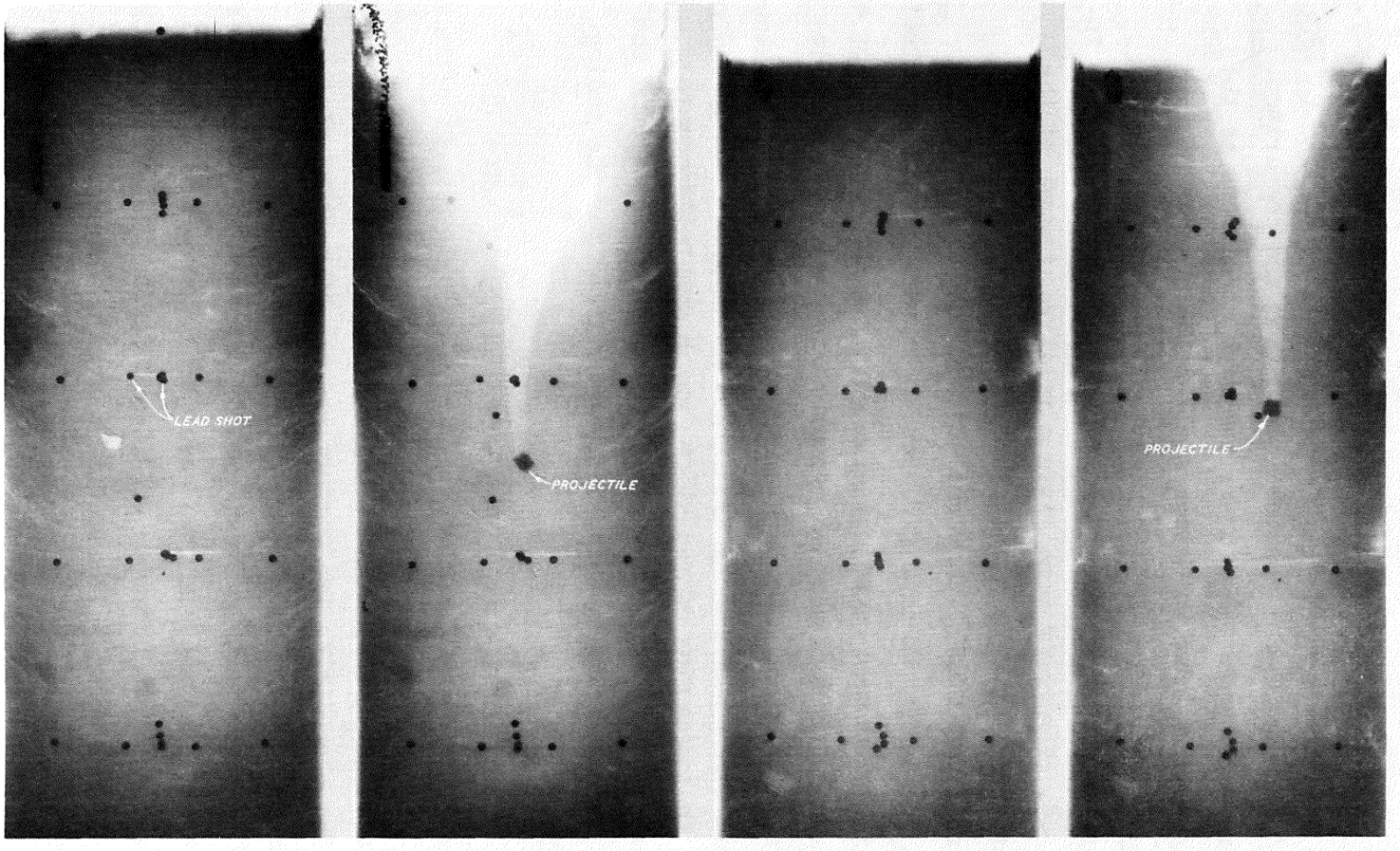

PRETEST POSTTEST PRETEST POSTTEST

a. SLAB 02BC

BULK DENSITY	120.0 PFC
WATER CONTENT	35.9 %
NO. OF BLOWS PER LIFT	25
PROJECTILE VELOCITY	3226 FPS

SCALE IN INCHES

1 0 1 2 3

b. SLAB 03BC

BULK DENSITY	126.9 PFC
WATER CONTENT	31.3 %
NO. OF BLOWS PER LIFT	25
PROJECTILE VELOCITY	1795 FPS

Fig. 2. Pretest and posttest radiographs of specimens 02BC and 03BC

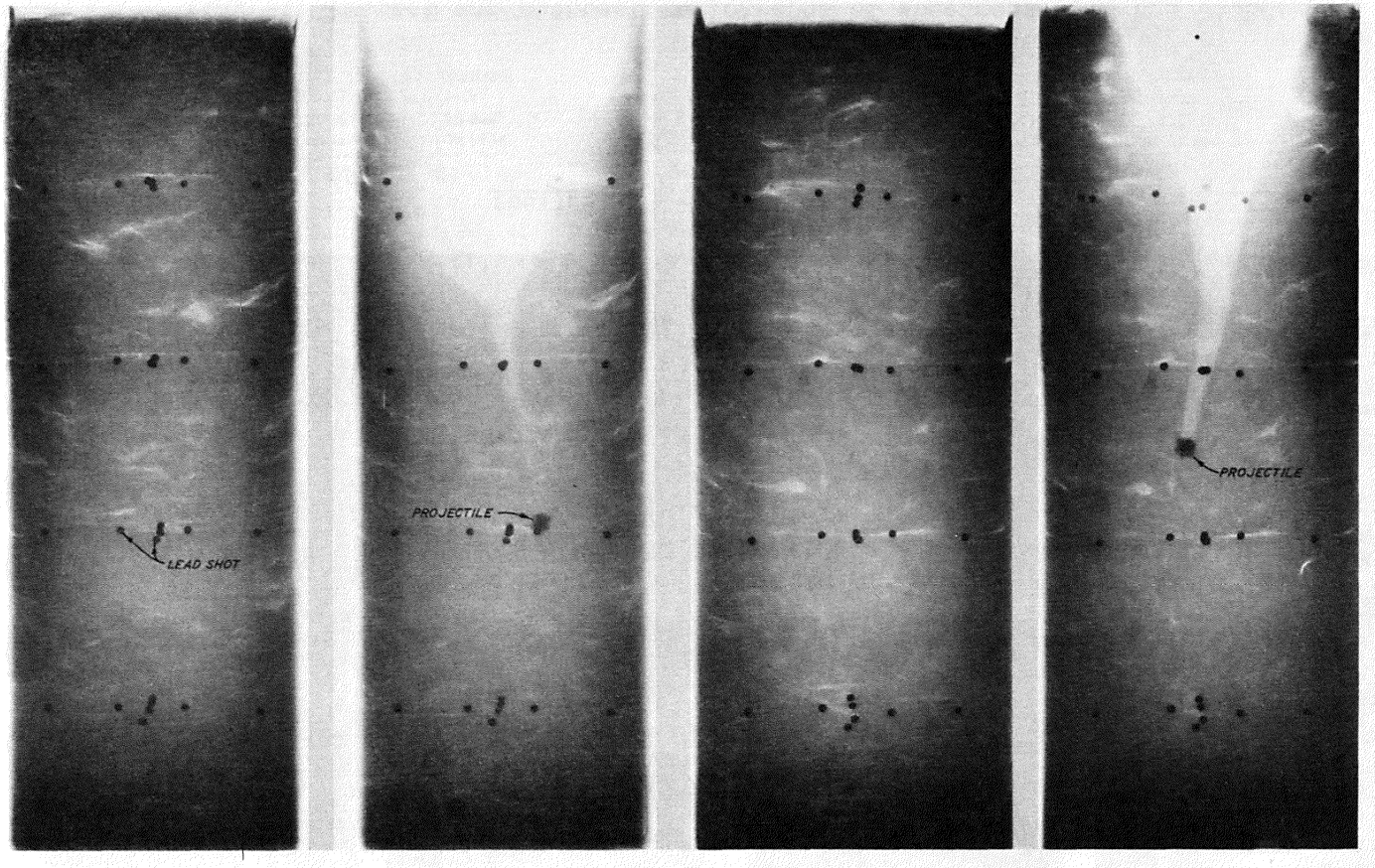

Fig. 3. Pretest and posttest radiographs of specimens 04BC and 05BC

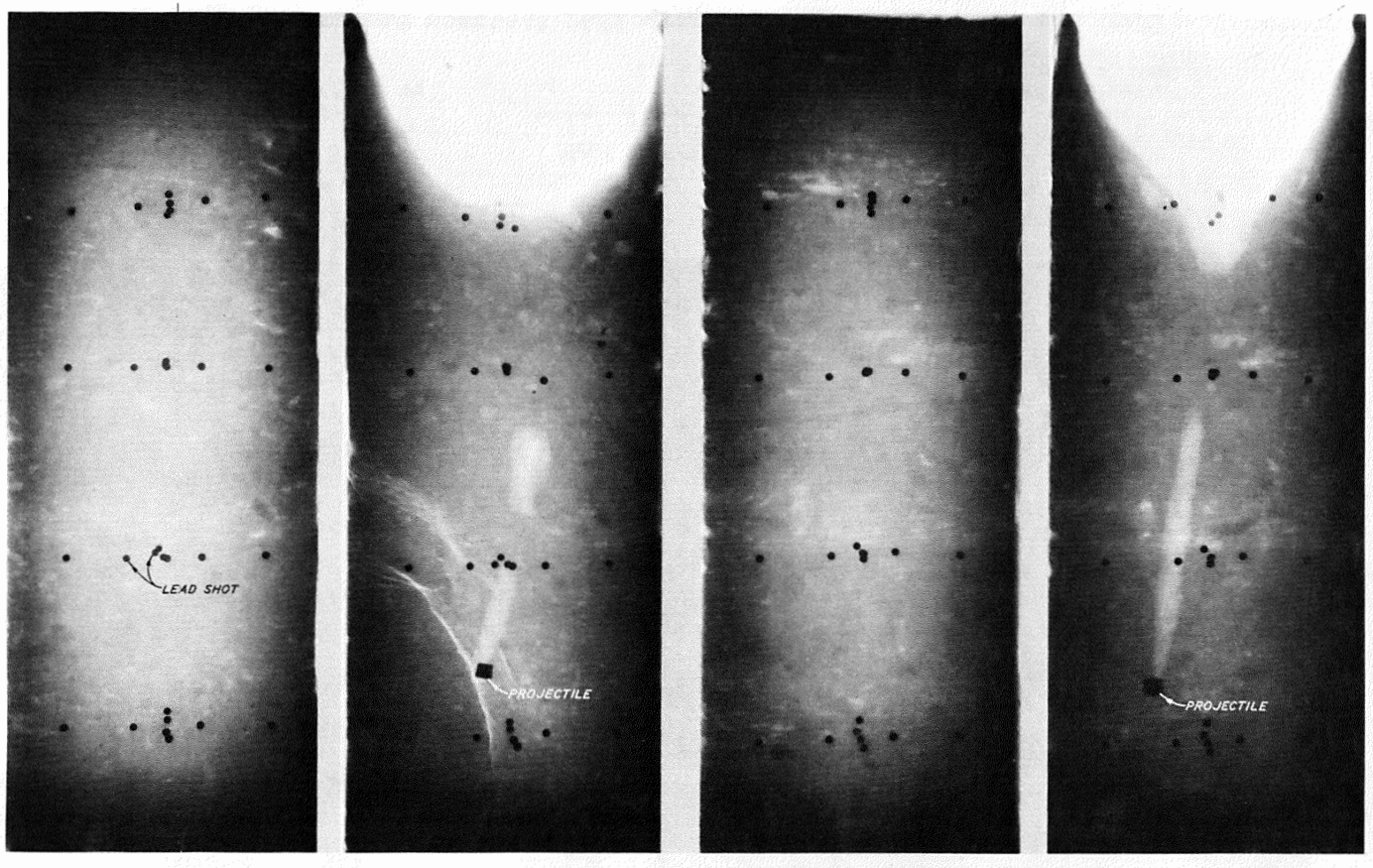

Fig. 4. Pretest and posttest radiographs of specimens 09BC and 010BC

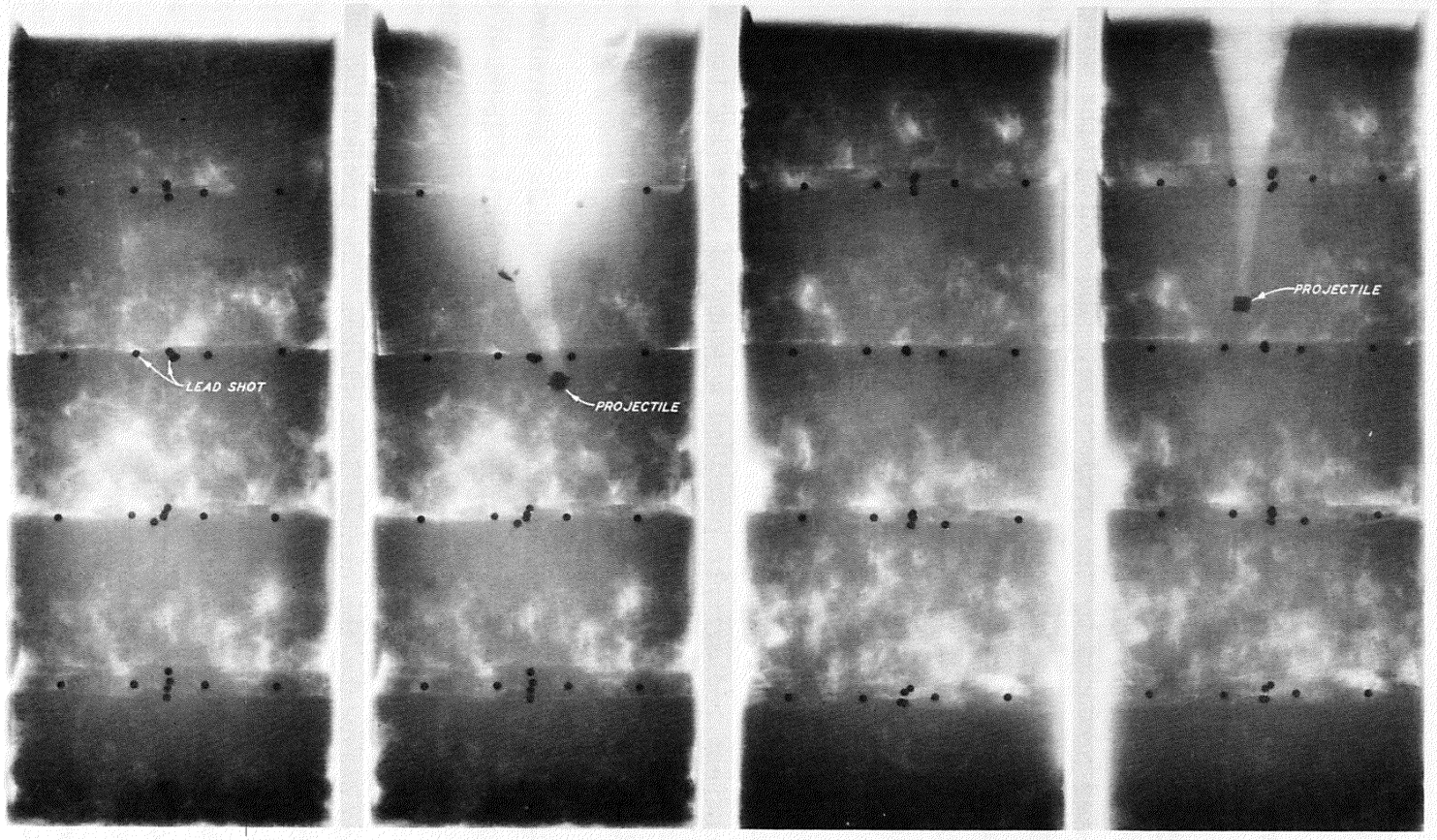

Fig. 5. Pretest and posttest radiographs of specimens 011BC and 012BC

Posttest Radiography

19. After firing, the masonite box containing the specimen was removed from the aluminum firing box and X-rayed. The posttest radiographs were then compared with the pretest radiographs. This comparison and examination revealed the general results described below of the ballistic impact on the clay specimen.

Crater size and shape

20. The posttest radiographs illustrated the configuration and extent of the crater produced by the projectile. The radiographs were particularly useful for some impacted specimens in which the projectiles had penetrated several inches beyond the crater and were hidden from visual observation. For most specimens two radiographs taken normal to each other provided sufficient information. The lower crater shown in fig. 4, specimen 09BC, would not be detected in a strictly visual examination.

Location of projectile

21. The posttest radiographs provided a means of locating the projectile, determining the extent of deformation, and providing information on the nature of clay-projectile relations in the area around the projectile.

22. The depth of penetration of the projectile can be determined from posttest radiographs. Fig. 6 represents an X-ray source located at a focal distance f from a specimen of thickness t. The specimen has a height h and is in contact with X-ray film. Lead shot at top and bottom of specimen delineate the center line (t/z). The projectile is located a distance d from the top of the specimen. The X-ray source should be positioned facing the center of the specimen.

23. The X-ray source is shown in fig. 6 to be a point source. This is not strictly true, but it may be considered a point for this application.

24. The geometrical considerations relevant to the solution for d require that the projectile be roughly centered in the x and z directions as shown in the inset in fig. 6. Two posttest radiographs

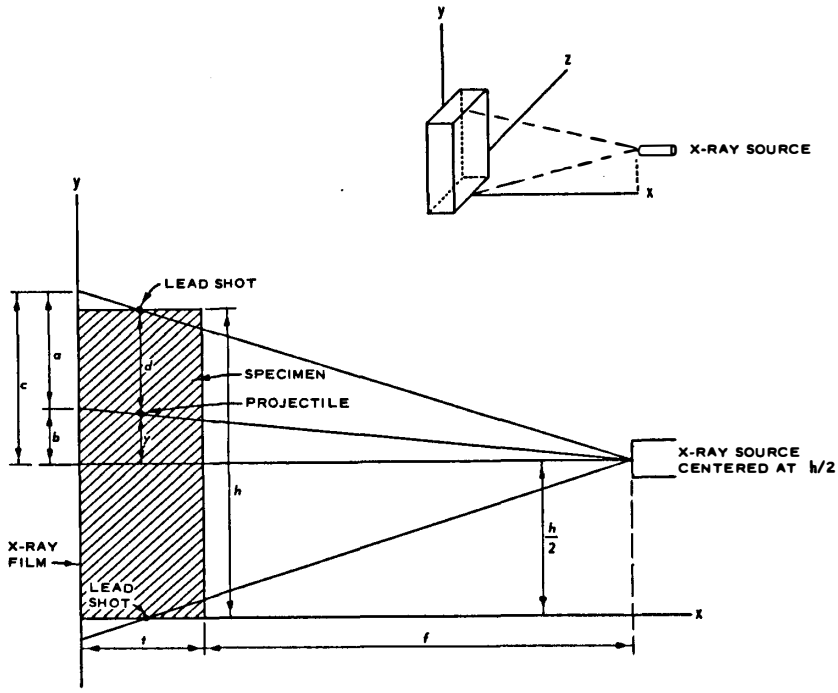

$$d = \frac{ha}{2c} \qquad (1)$$

WHERE: d = DEPTH OF PENETRATION OF PROJECTILE IN SPECIMEN
h = HEIGHT OF SPECIMEN
a = DEPTH OF PENETRATION MEASURED ON RADIOGRAPH
c = ONE-HALF SPECIMEN HEIGHT MEASURED ON RADIOGRAPH
f = FOCAL DISTANCE

Fig. 6. Schematic illustration of the geometrical relations that control measurements on radiographs

will provide information on the position of the projectile. If the radiographs indicate that the projectile has veered excessively away from the center line of the specimen, the row of lead shot should be aligned in the x direction with a point directly above the projectile, and the X-ray source should be moved in the z direction to that point on line with the projectile. If the projectile has moved only slightly off center, the source should be moved back, thereby increasing f and, therefore, providing better accuracy. As a general rule, f should be as great as practical considerations permit.

25. When the preceding adjustments have been made and the specimen has been re-X-rayed, c and a can be measured on the radiograph and, knowing h , equation 1 (in fig. 6) can be solved for d .

Specimen disturbance beyond crater

26. The examination of posttest radiographs and their comparison with pretest radiographs lead to increased understanding of the nature and degree of disturbance in the specimen beyond the crater. The disturbance here is manifest by disruption of the lifts, production of cavities, and a separation of the material at lift boundaries and elsewhere.

Deformation of projectile

27. The extent of deformation of the projectile can be readily determined by examination of the posttest radiographs. Deformation is manifest by the enlargement of the front of the projectile and its more curved appearance. Those specimens (02BC, 04BC, 09BC, and 011BC) that were impacted at velocities over 3200 fps exhibited some degree of projectile deformation. The deformation of the projectile in specimen 04BC is more apparent in the thin-slab radiograph (fig. 10), discussed below, than in fig. 3. It is interesting to note in comparing specimens 09BC and 010BC that the projectile that penetrated the furthest (specimen 010BC) suffered the least deformation.

Summary

28. The radiographic examination of the bulk specimens has been shown to provide a rapid, nondestructive method for observing the general nature and characteristics of the ballistically loaded clay. The radiography of bulk specimens, however, does not lend itself to detailed specimen analysis in that here the radiographic image is a composite of all features within the entire thickness of the sample.

Radiography of Thin Slabs

Slabbing

29. For a more detailed inspection of specific areas, it is useful to cut the specimens into thin slabs. Each ballistically loaded specimen was sectioned according to the diagram shown in fig. 7. In all cases the path and final resting place of the projectile were restricted to the central three 1-1/4-in. slabs (B, C, and D). These three slabs

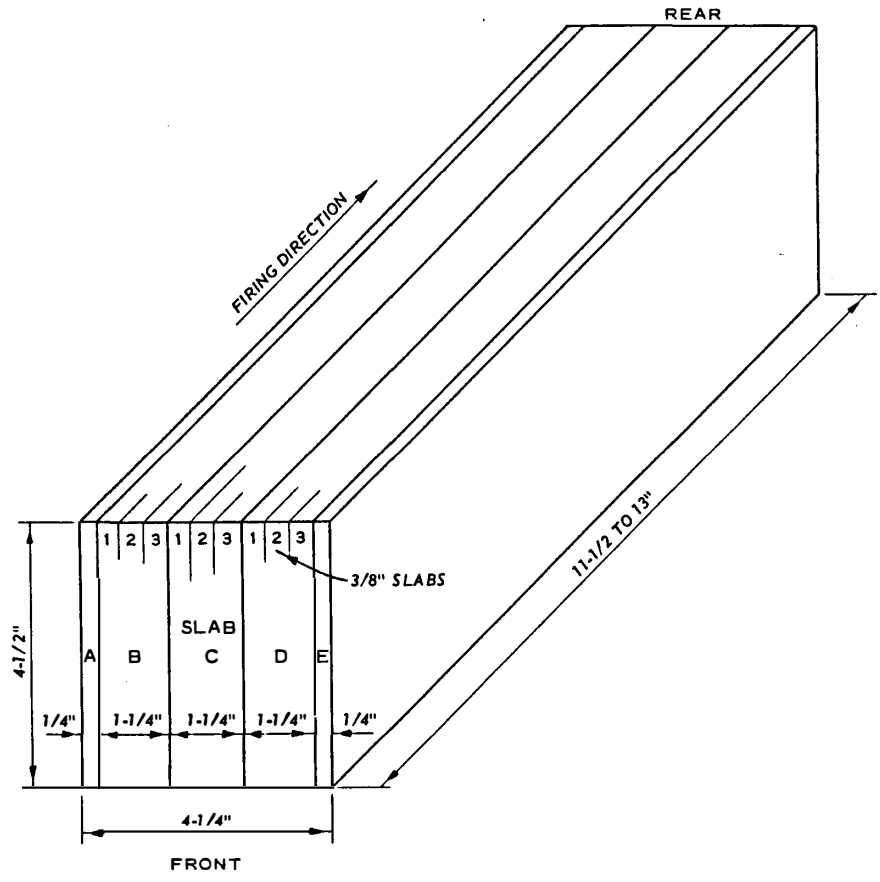

Fig. 7. Specimen slabbing and labeling scheme

were radiographed and, in most cases, were cut into 1/8-in. slabs. The 1/8-in. slabs were also radiographed.

30. To minimize disturbance, each specimen was securely held in an aluminum cutting frame and sliced with piano wire. Experience has demonstrated that this procedure produces negligible fabric alteration in fine-grained materials.

Description of radiographs

31. The radiographs of the slabs provided a means of examining areas within the specimens and permitted observations of textural changes attributed to the impact of the projectile.

32. Figs. 8-15 are radiographs of the eight loaded specimens. Generally, the figures include the slab containing the projectile or the main portion of the projectile path, slabs adjacent to the projectile

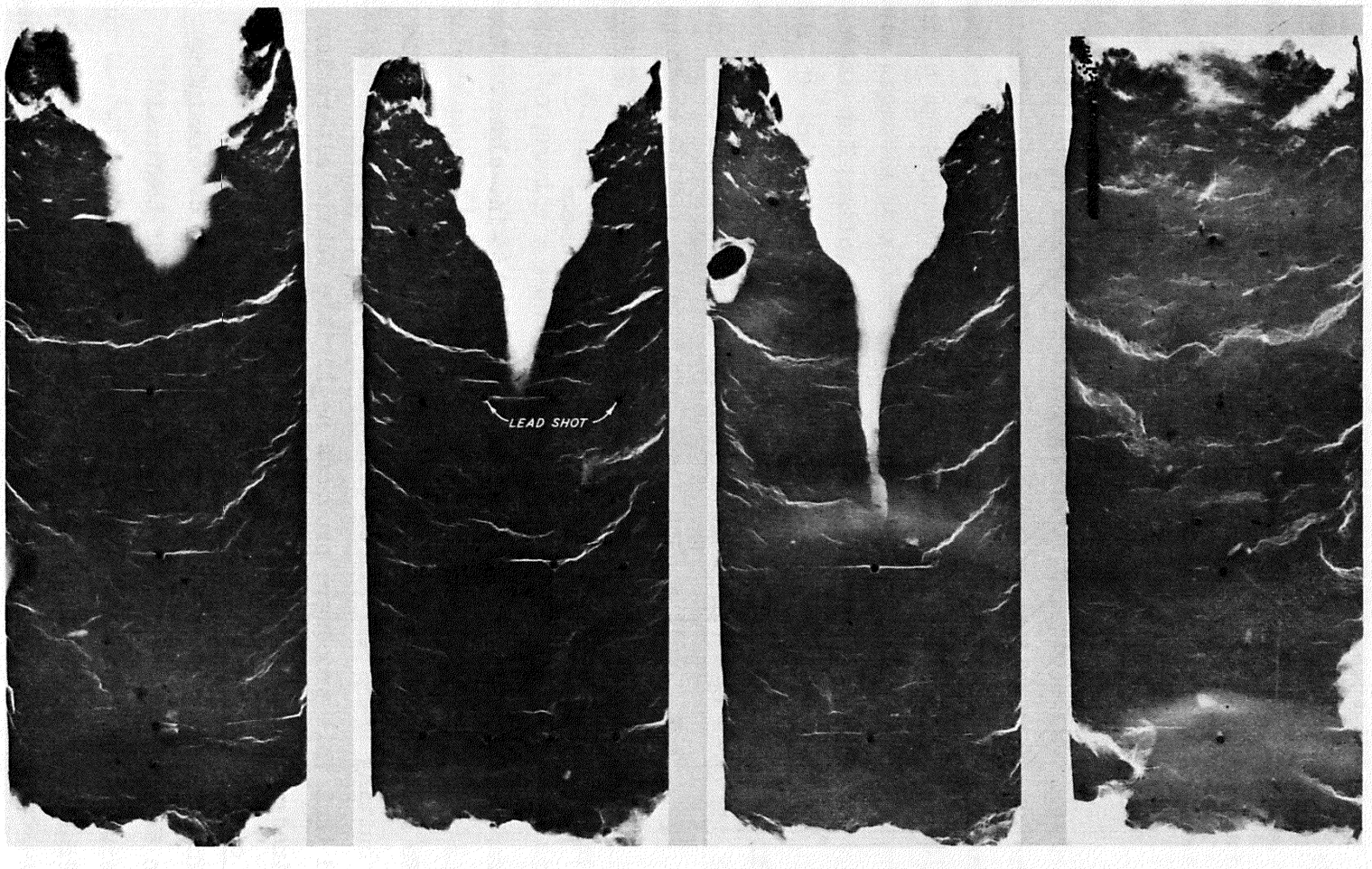

Fig. 8. Thin-slab radiographs, specimen 02BC (specimens are 3/8 in. thick)

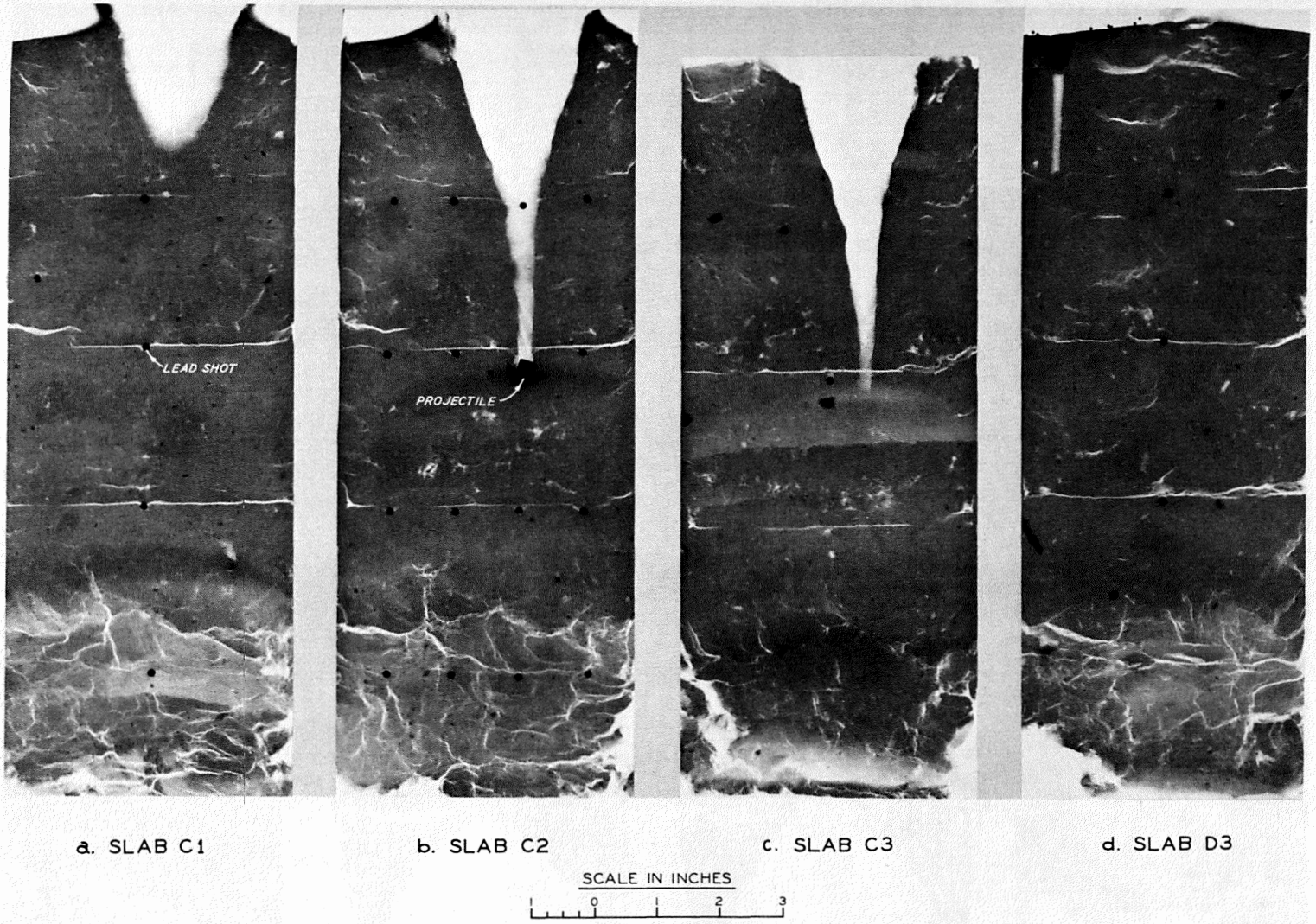

Fig. 9. Thin-slab radiographs, specimen 03BC (specimens are 3/8 in. thick)

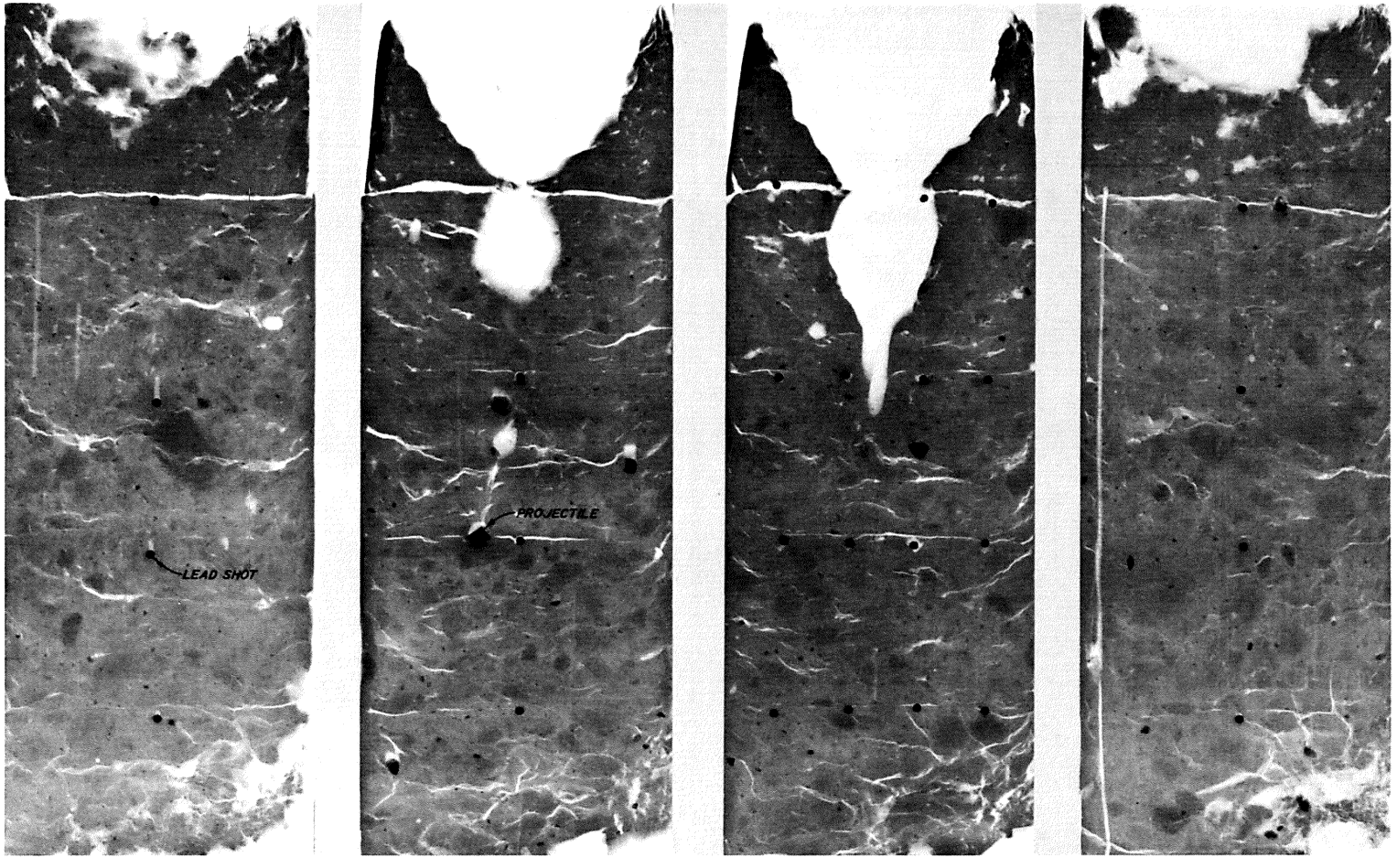

Fig. 10. Thin-slab radiographs, specimen 04BC (specimens are 3/8 in. thick)

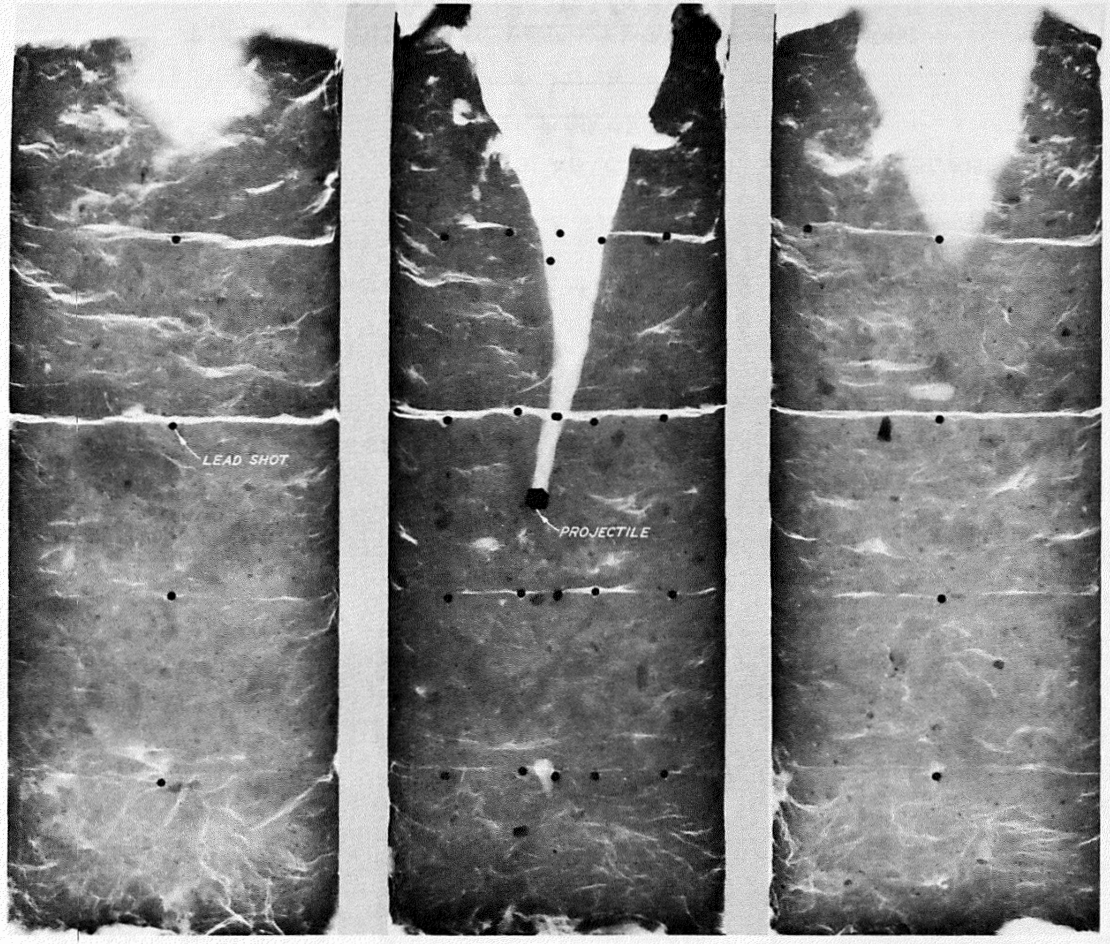

Fig. 11. Thin-slab radiographs, specimen 05BC
(specimens are 1-1/4 in. thick)

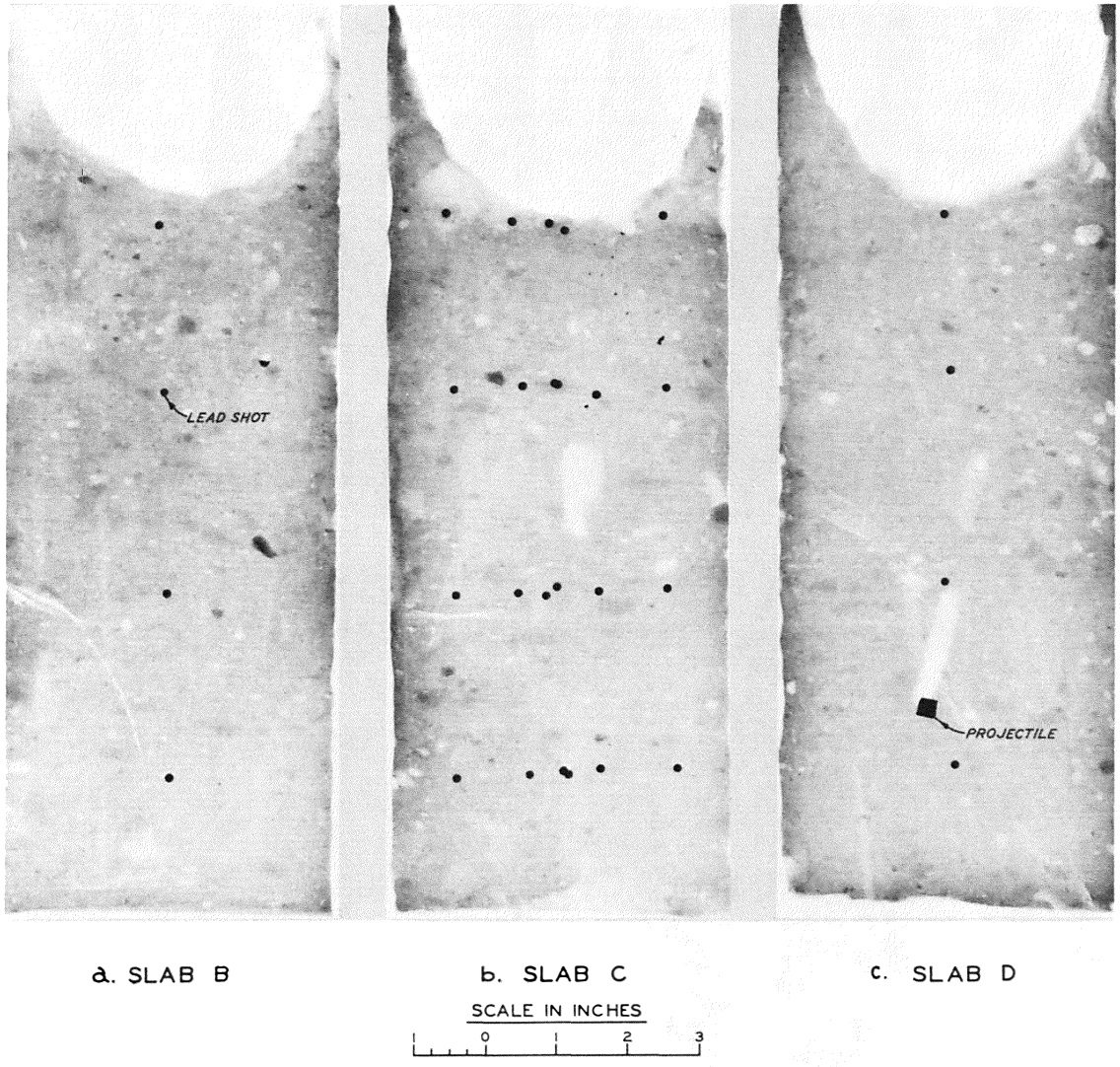

Fig. 12. Thin-slab radiographs, specimen 09BC (specimens are 1-1/4 in. thick)

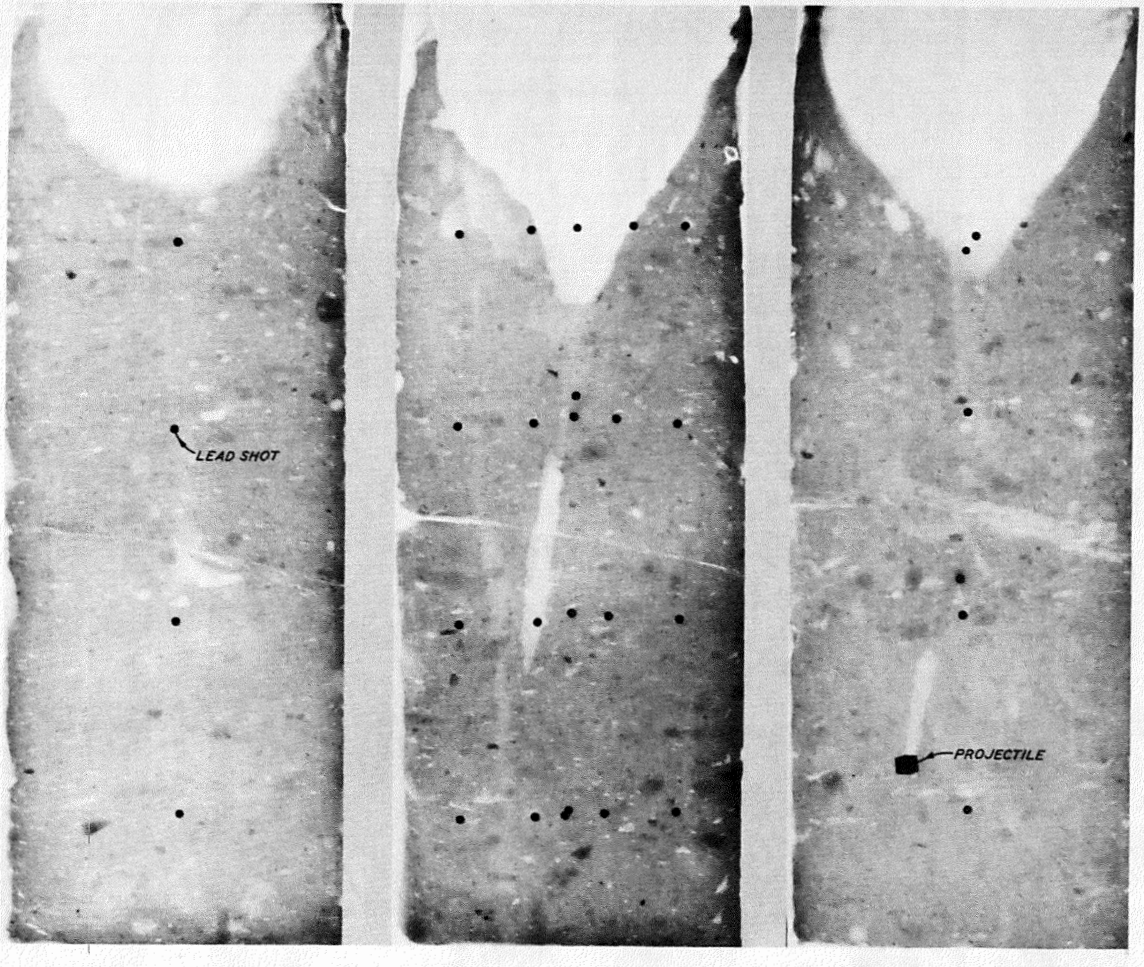

Fig. 13. Thin-slab radiographs, specimen O1OBC (specimens are 1-1/4 in. thick)

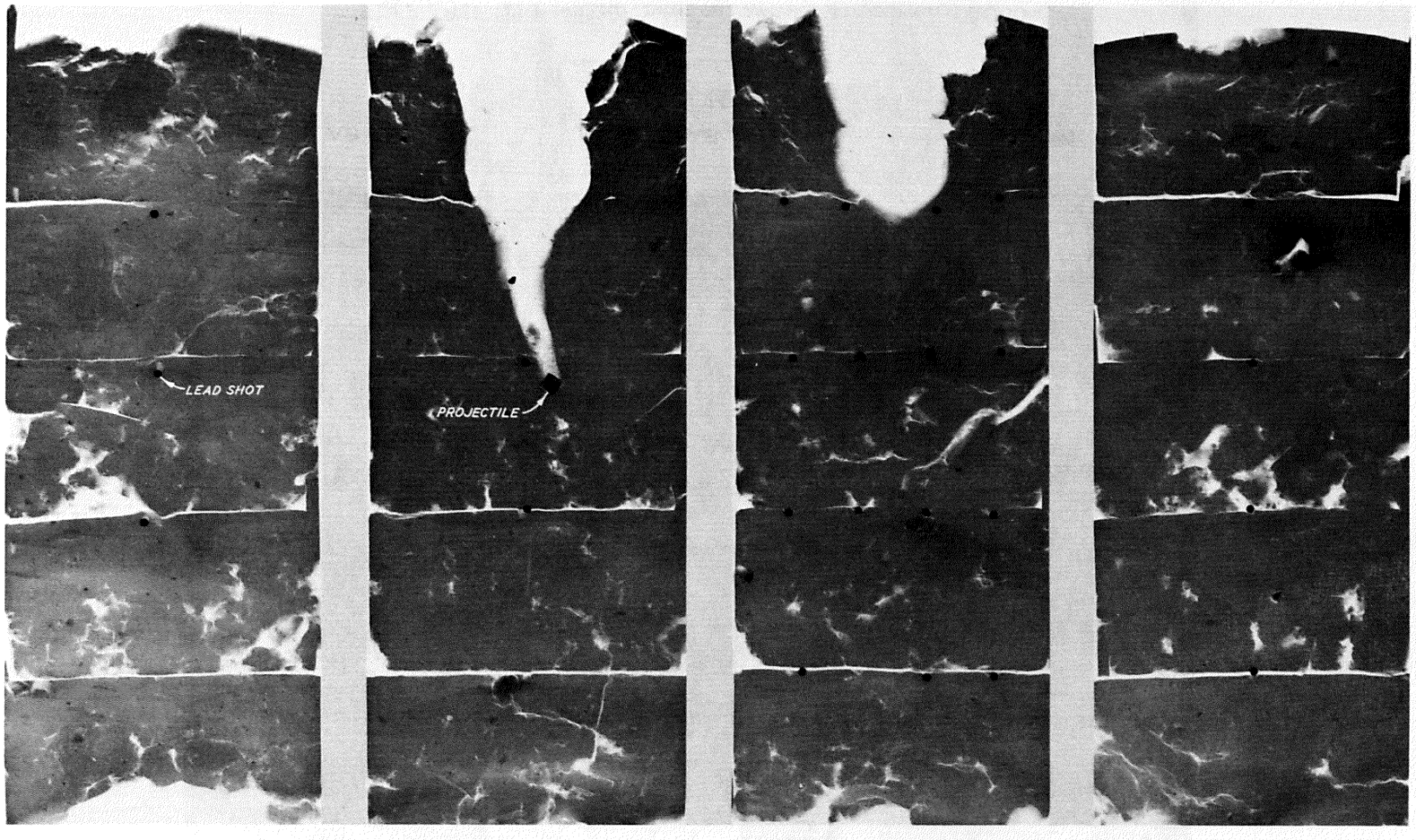

Fig. 14. Thin-slab radiographs, specimen O11BC (specimens are 3/8 in. thick)

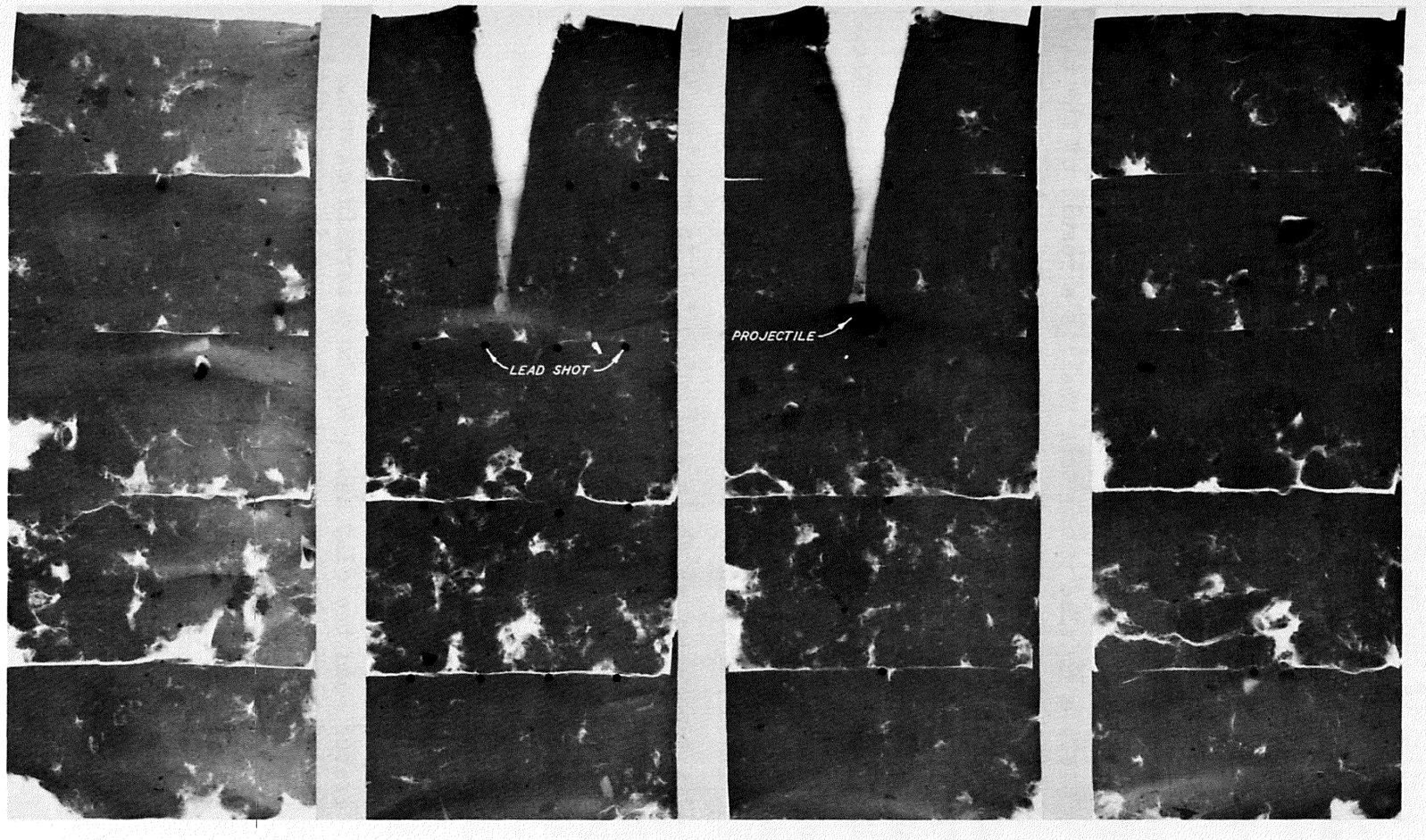

Fig. 15. Thin-slab radiographs, specimen 012BC (specimens are 3/8 in. thick)

that depict a portion of the impact crater, and a slab cut beyond the impact crater. The slab thicknesses are shown in the figures.

33. The radiographs of the slabs provide further information on the quality of the compaction as manifest by the uniformity of photo tone. Generally, the compaction is shown to be uniform, particularly in the upper portions of the specimens. The first lift placed exhibits the poorest compaction. The lead shot and the thin lines of separation indicate the lift boundaries. Specimens 09BC and 010BC (figs. 12 and 13, respectively) exhibit a mottled photo tone that is a result of the high water content and mode of preparation.

34. Specimen 02BC (fig. 8) possesses a distinct concave-up lineation which is an indication of nonuniform lift preparation. These curved features are present to a lesser extent in the other specimens and are treated in later discussions on petrography and scanning electron microscopy.

35. Generally, the slabs do not reflect any major disturbance in areas beyond the immediate vicinity of the crater. Near the crater there is some lift separation which is well exhibited in specimen 04BC (fig. 10). Specimens 03BC, 011BC, and 012BC (figs. 9, 14, and 15, respectively) show a thickening of the top lift adjacent to the crater.

36. The geometry of the crater appears to be a function of projectile velocity and specimen water content, and it consists of three types which are:

a. A relatively deep, roughly symmetrical crater that is not continuously connected to the area in which the projectile rests. The projectile has penetrated beyond the crater, and the clay has been, to a certain extent, healed along the trajectory. This type is restricted to the specimens (09BC and 010BC) of high water content.

b. Those specimens that were subjected to high-velocity impact (specimens 02BC, 04BC, and 011BC) exhibit crater systems consisting of three interconnected areas. The upper area is the largest and is generally cup-shaped. The next area is somewhat smaller than the one above but is similarly shaped. The lowest area is the smallest and has a tubelike shape.

c. The specimens receiving low-velocity penetration exhibit

- a more nearly uniform and narrow cavity (specimens 03BC, 05BC, and 012BC).

37. The depth to which the projectile penetrated was a function of density, water content, and velocity. The penetration depths are listed in table 1. Generally, the deepest penetration occurred in specimens having lowest density, highest water content, and highest projectile velocity.

38. Examination of the radiographs of specimens 02BC and 012BC (figs. 8 and 15, respectively) suggests that there may be some densification occurring in the region adjacent to the projectile. This densification is indicated by the darker photo tones in this area. The 3/8-in. slabs cut adjacent to the ones containing the projectile (slab C3 of specimen 03BC and slab C2 of specimen 012BC, figs. 9 and 15, respectively) suggest that there has been some decrease in density in this area.

PART III: MICRODENSITOMETER STUDIES

39. The analysis of radiographic negatives by a microdensitometer provides a means of detecting significant density variations within soil specimens.[1] The basis for this application is the inverse relation between soil density and radiographic film density. X-rays can more easily penetrate less dense soils than dense soils. Thus, the radiographic film of a less dense soil will exhibit a greater film density owing to the greater exposure to X-rays.

40. The Joyce & Loebl microdensitracer (the instrument used in this study) scans the radiograph along predetermined traverses, computes the relative optical density of the film, and utilizes multicolored pens to print out relative film densities. The end product is an isodensitracing of the soil depicting zones of equal density within the sample. The scanning rates, traverse spacings, as well as optical density increments, can be adjusted to accommodate the type of soil or the nature of the application.

41. Those areas represented by a particular color are areas of more-or-less equal film density. These areas are further subdivided by dots and dashes. The dots represent lower film density. The colored areas are separated by blank spaces.

42. Isodensitracings provide an excellent visualization of density variations within specimens. The uniformity of compaction, lift boundaries, and projectile location are evident and can be easily correlated with radiographs of the same specimens. Furthermore, the isodensitracings of the specimens in this study revealed subtleties in density changes which were due to the ballistic loading and which were entirely unsuspected from visual inspection of the radiographs.

Application

43. Isodensitracings were prepared for the 3/8-in. slabs of each control and each fired specimen. The boundaries separating areas of different density were drawn on tracing overlays on each isodensitracing.

This step is not required for general applications but does result in a more distinct visual separation of areas of unlike density. For highly detailed quantitative density studies, the drawn boundaries facilitate the calculation of the areal extent of a particular film density by planimeter. After calculating the areal extent of each film density within a specimen, the average film density can be determined.

44. The areas of equal film density on the isodensitracing locate the areas on the radiographs where film density measurements can be determined with a transmission film densitometer. In this manner, film densities were obtained for the 3/8-in. slabs of each fired and each control specimen.

Isodensitracings

45. Fig. 16 is a black and white copy of the isodensitracing of slab D3 of control specimen 4. This specimen was prepared at a water content of 67 percent and compacted to a density of approximately 107 pcf. The variable density and lack of lift boundaries are quite evident from the isodensitracing.

46. The isodensitracing of slab D3 of control specimen 5 is illustrated in fig. 17. This specimen had a water content of 28 percent and a density of approximately 128 pcf. The uniformity of the density and the presence of distinct lift boundaries are manifest here.

47. Generally, the isodensitracings of the ballistically loaded specimens did not exhibit any alteration in the clay beyond 2 in. of the impact cavity. The density variation in these regions appeared similar to that in the control specimens.

48. Fig. 18 illustrates the isodensitracing of slab C3 of specimen 012BC. The water content was 26 percent and the bulk density was 128 pcf. The film density appears more-or-less uniform in the upper regions of the specimen. The location of the projectile in the slab is evident. The projectile is bounded by three concentric bands whose film density decreases toward the projectile. The differential scattering and absorption characteristics of the clay and projectile are partially

responsible for these concentric density bands.

49. An area irradiated by X-radiation will produce a certain amount of scatter which is dependent, in part, on its ability to absorb radiation. Dense materials, such as the steel projectile, are highly absorptive and will produce less scatter than the less absorptive clay. The degree of film darkening in the area in question is due to the nature of the material comprising the area and the nature of the material in the neighboring areas as well.

50. In this case the area occupied by the projectile is highly absorptive and contributes little scatter to the neighboring areas resulting in a lowering of film density in the area around the projectile. This problem can be remedied by removing the projectile from the specimen and placing sand or clay in the cavity. In most circumstances these materials have similar absorptions.

51. The examination of slab C2 also from specimen 012BC (illustrated in fig. 19) suggests that the concentric density bands are not entirely due to differential scattering and absorption. This slab is adjacent to the trajectory and does not contain the projectile, yet the concentric density variation is present. The film density is lowest in the central ring and increases outwardly. It appears, however, that the film density beyond the concentric ring area is lower than that in the central ring.

52. These concentric density bands suggest densification of the clay in the vicinity of the projectile and demonstrate the usefulness of isodensitometer studies of ballistically impacted materials.

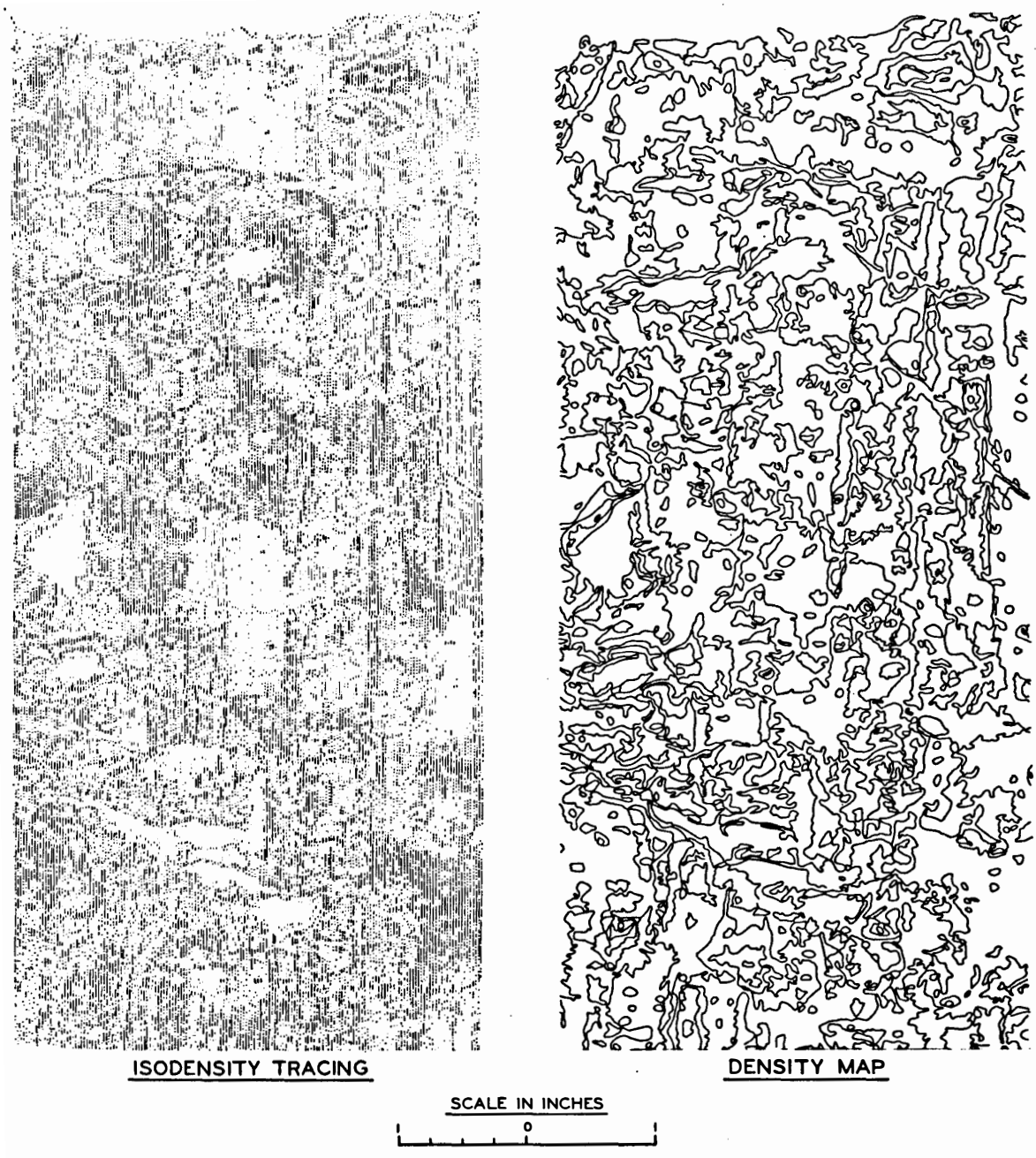

Fig. 16. Isodensity tracing (isodensitracing) and density map of control specimen 4, slab D3

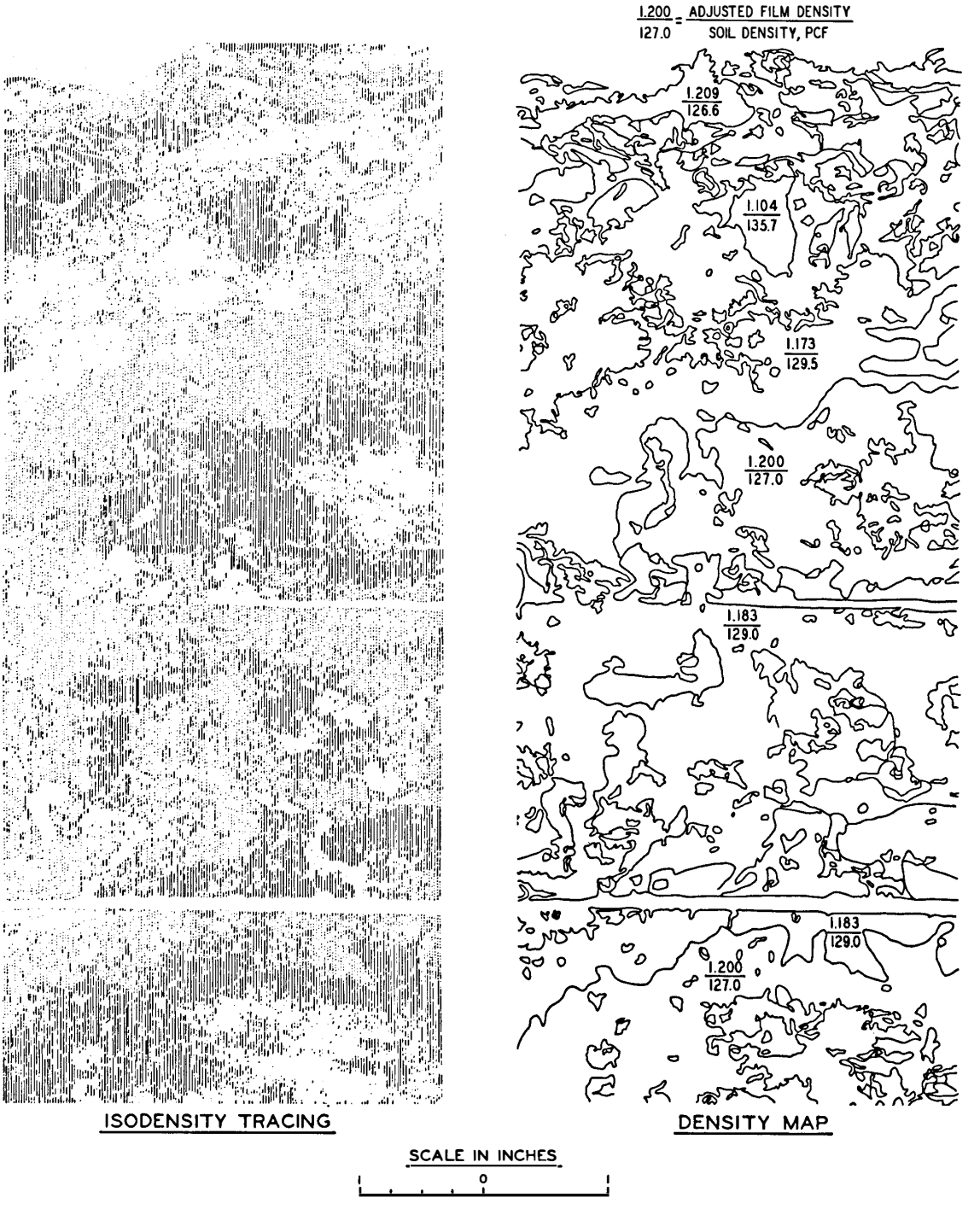

Fig. 17. Isodensity tracing (isodensitracing) and density map of control specimen 5, slab D3

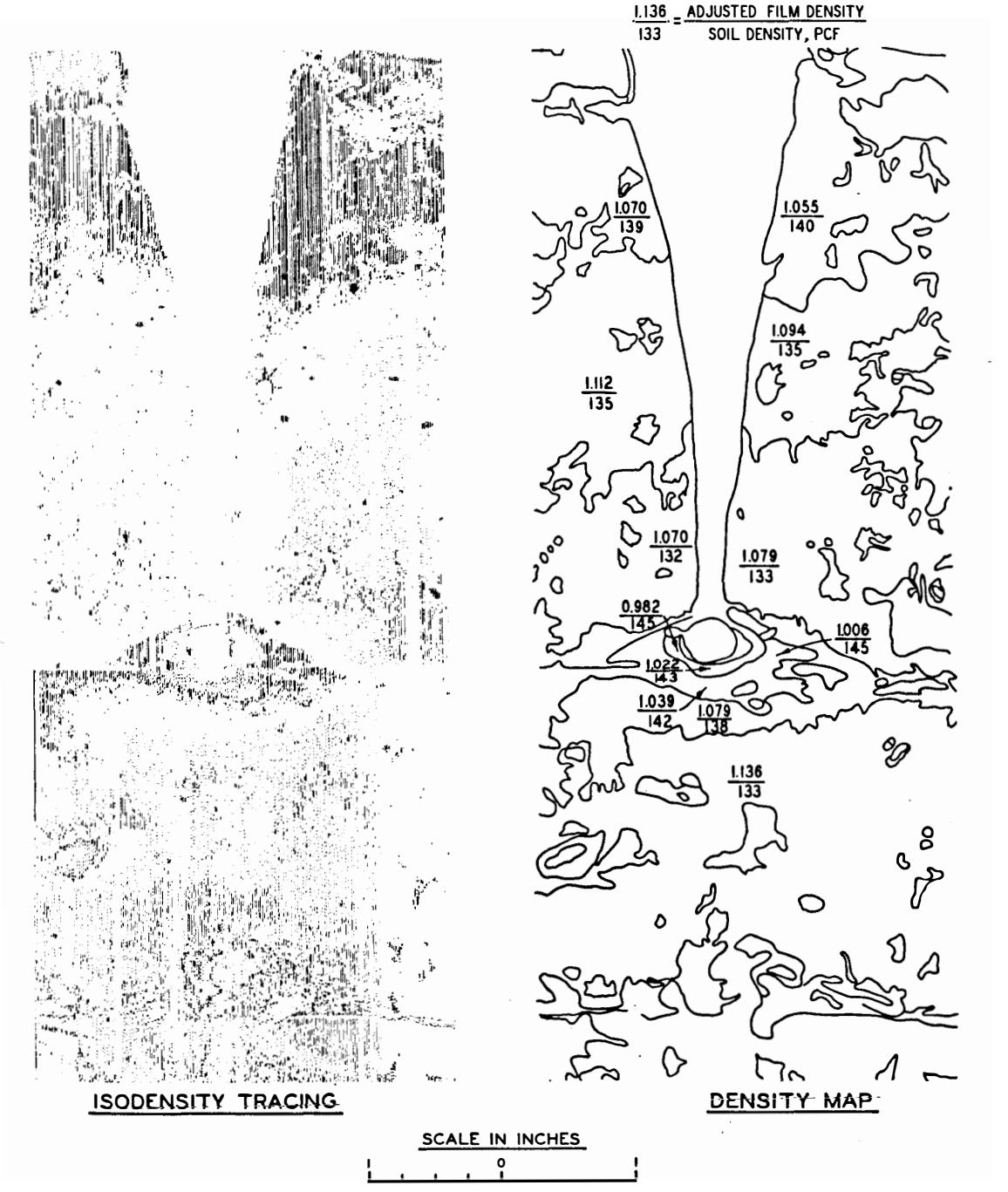

Fig. 18. Isodensity tracing (isodensitracing) and density map of specimen 012BC, slab C3

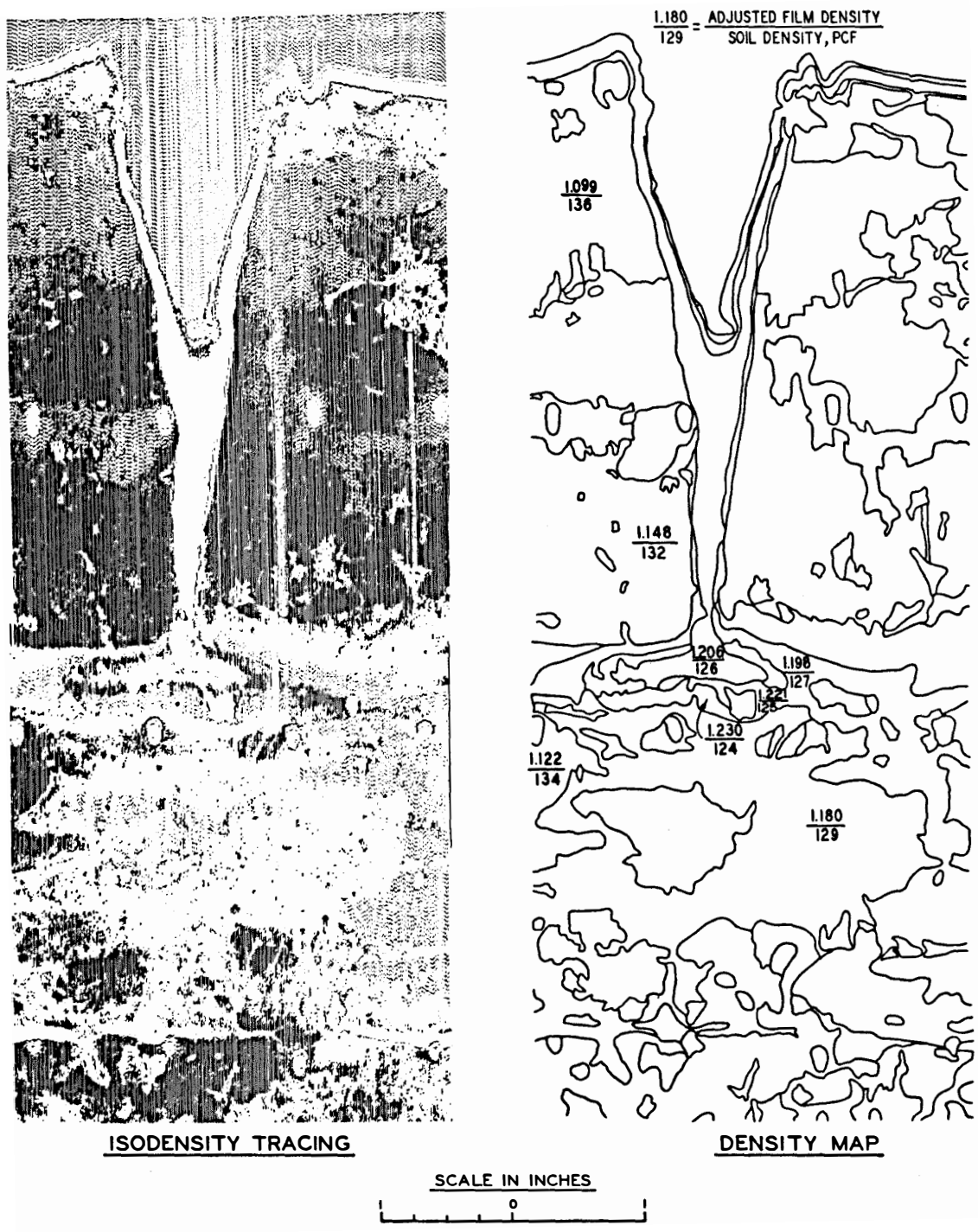

Fig. 19. Isodensity tracing (isodensitracing) and density map of specimen 012BC, slab C2

PART IV: QUANTITATIVE DENSITY

Theoretical Aspects

53. The absorption of X-ray energy passing through a material is controlled by the exponential decay equation[2]

$$I = I_o e^{-(M/\rho)\,\rho_T x}$$

where

I = intensity of transmitted radiation
I_o = initial radiation
(M/ρ) = mass absorption coefficient of mineral in soil
ρ_T = bulk density of soil
x = sample thickness

It can be seen that the bulk density of a sample can be related to film exposure as measured by film density if the exposure time and developments are controlled, and if the mass absorption coefficient and thickness of the sample are held constant.

Application

54. The application of this relation to several types of soil models has been demonstrated by Krinitzsky.[1] He has prepared samples compacted to various densities for several types of soil. For a given soil, calibration curves were prepared that related the soil density to measured film density. These calibration curves could be used to determine soil densities for test specimens of the same material.

55. The extrapolation of data from a calibration curve derived for sand in order to determine bulk densities of a clay, for example, may not always be appropriate. This is due to mineralogical differences between sand and clay which may be reflected in their mass absorption coefficients.

56. The mass absorption coefficient of a particular mineral is a function of its density, the relative abundance of its constituent chemical elements, and the individual mass absorption coefficients of these elements. In a similar fashion the mass absorption coefficient of a soil is a function of the mass absorption coefficients of its constituent minerals and their relative abundance.

Internal Standards

57. As a means of monitoring and, in effect, controlling the processing of the radiographic film, it has been found useful to include a 1/4-in. aluminum disk with all samples radiographed for quantitative density data. This disk allows comparison between different samples and facilitates the interpolation of data from calibration curves. Any significant changes that occur in the developing process between several samples or between samples and standards can be detected by an examination of the film density of the disk. If the disk film density has changed, the film density of the soil must be proportionately adjusted.

58. An example will add clarification. Consider two soil samples of similar nature and equal thickness. Both will be X-rayed under identical conditions. After developing and processing, the film density of soil and aluminum disk for both samples are as shown below.

Soil Sample	Film Density Aluminum Disk	Film Density Soil
A	1.10	1.30
B	1.00	1.15

59. It can be seen that the aluminum disk of soil A has a higher film density than soil B. Since both disks are of the same thickness and were X-rayed under identical conditions, the difference in film density must be due to differences in processing between the two samples. Furthermore, it follows that the film density of the soil in sample A is proportionately higher than that in soil B.

60. In adjusting the film density of the soil, either sample may

be the standard. In the example below soil B was selected.

Soil Sample	Film Density Aluminum Disk	Film Density Soil		Factor		Adjusted Film Density of Soil
A	1.10	1.30	×	$\frac{1.00}{1.10}$	=	1.18
B	1.00	1.15	×	$\frac{1.00}{1.00}$	=	1.15

61. This type of adjustment must be made for soil density standards that are to be used for the preparation of calibration curves and for test specimens of unknown density. The standard reference sample used in the calibration curve will also be the reference for the test specimens.

Calibration Curves

62. The density of compacted clays depends upon the water content and the compaction effort. It is important to have some compaction data available for the clay in question before preparing the density standards. If the data are available, one can select the appropriate water contents and compaction effort to produce the desired densities. The clay used in this study had been sufficiently studied that data were available.

63. In order to obtain standards in the density range of 110 to 140 pcf it was necessary to compact the standard sample at water contents between 10 and 38 percent. Calculated X-ray intensities are not appreciably affected by variations in water content.

64. The clay was mechanically compacted in five lifts in slightly tapered molds having a diameter of 4 in. and a height of 4.5 in. After compaction, the bulk density was determined and the sample was removed from the mold, and a 3/8-in. slab was cut from the center. The length of the slab was cut parallel to the vertical axis of the mold. These slabs were X-rayed under conditions identical with those of the tested specimens.

65. Isodensitracings of selected radiographs revealed that the compaction was quite uniform.

66. The average film density of each density standard was determined by measuring the film density of approximately 15 points in the central part of the radiograph. The curve representing a plot of film density versus soil density is shown in fig. 20.

Specimen Density Measurements

67. Radiographic film densities of the 3/8-in. slabs were measured with a transmission film densitometer. The areas on the radiographs where these measurements were made were selected by visually examining the isodensitracings and determining those representative film density regions.

68. The measured film densities for each selected area within each particular slab were averaged and corrected utilizing the aluminum control disk. The average corrected film density of a specimen was obtained by averaging the film densities of the individual slabs.

69. The bulk density of each specimen and control was determined from the calibration curve shown in fig. 20. Table 2 lists the actual and computed bulk densities of the specimens and controls. The table indicates that the computed soil densities were reasonably close to actual densities for half of the controls and specimens. Specimen 02BC exhibited the maximum observed error of 6.4 percent. There appears to be a tendency for the computed soil density to be somewhat greater than actual density.

Sources of Error

70. There are two factors which appreciably affect the accuracy of soil density determinations by radiography. Both of these factors become increasingly significant for larger specimens.

71. The first factor involves the determination of a representative film density for the specimen. In this study film density areas

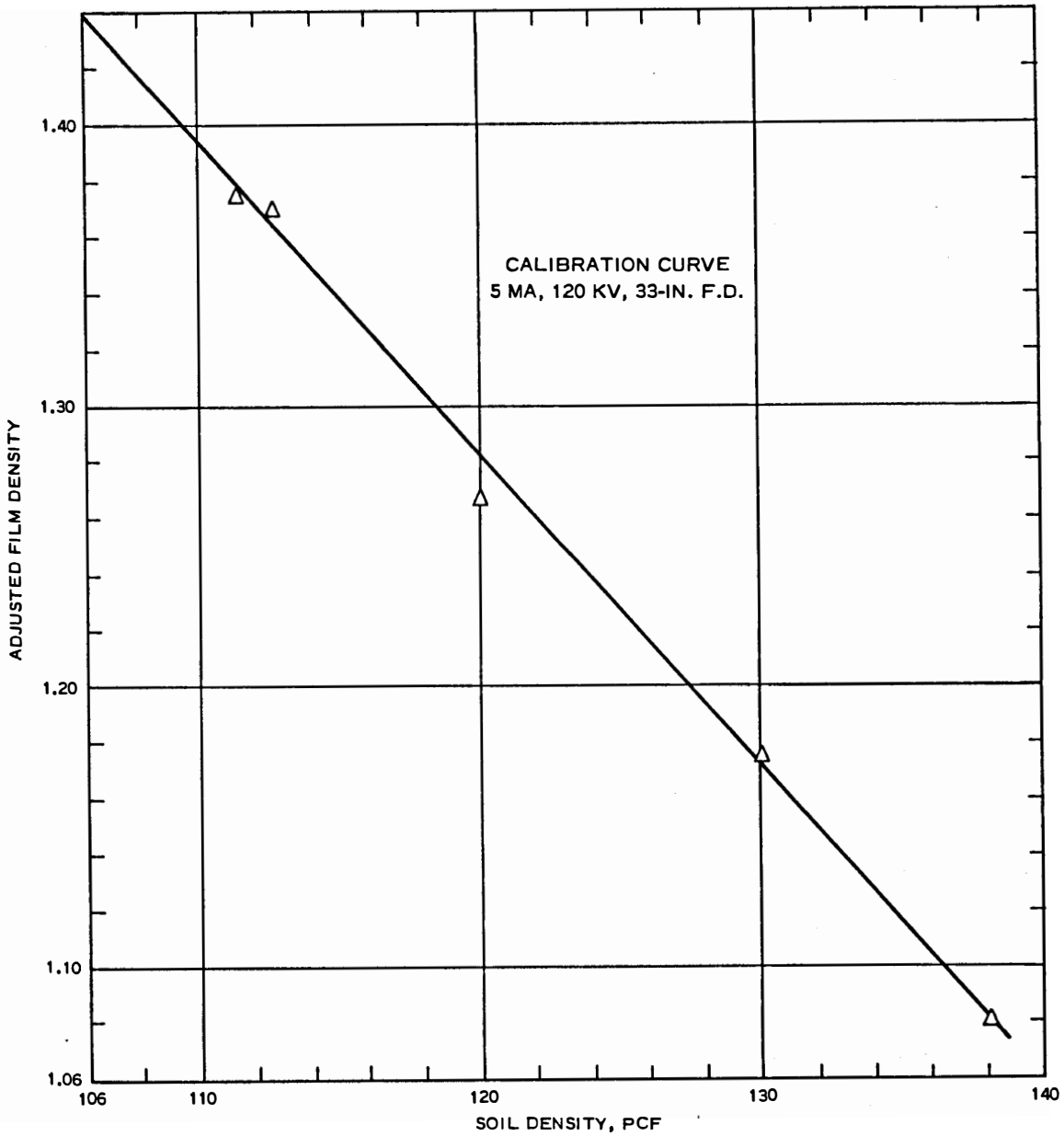

Fig. 20. Calibration curve relating adjusted film density to soil density

were visually determined prior to averaging. More accuracy would have resulted if the magnitudes of these areas had been measured by planimeter.

72. The second source of error results from the nonuniform areal distribution of X-ray intensity produced by the target. This nonuniform distribution is called the "heel" effect and consists of considerable reduction in X-ray intensity beyond the target-sample axis.[3] Fig. 21 illustrates the variations of radiation intensity in terms of angle of emergence.

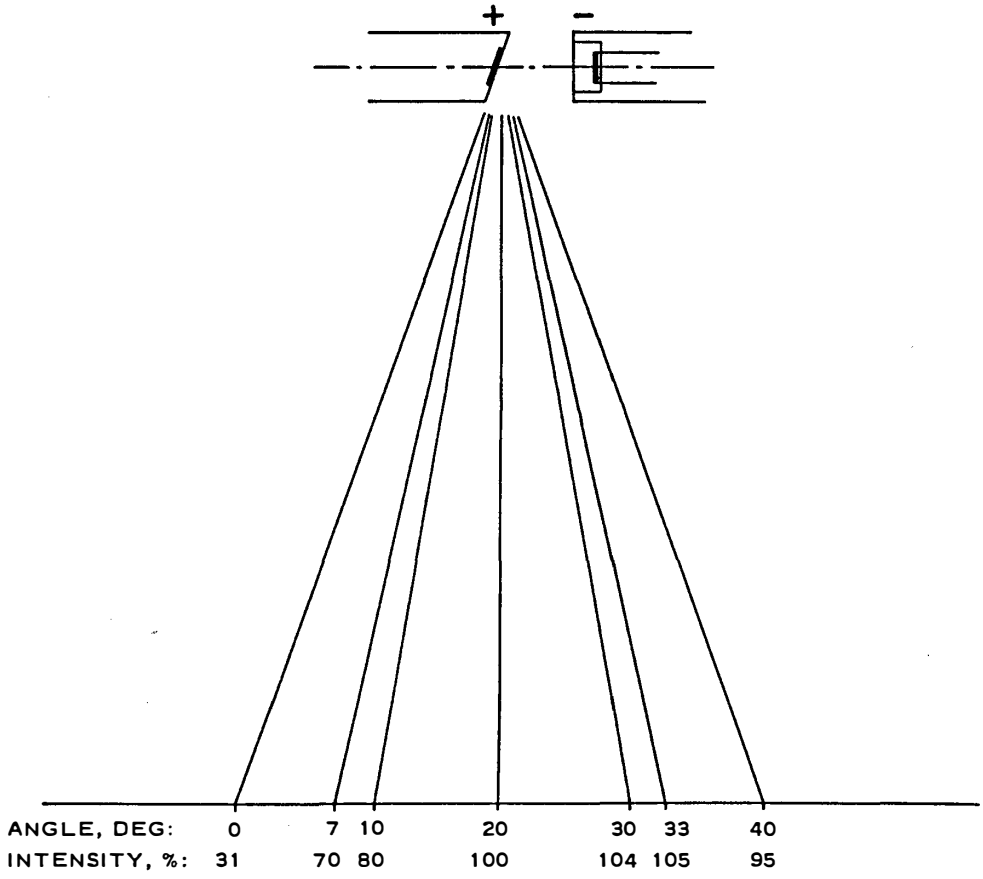

Fig. 21. Variations of radiation intensity in terms of angle of emergence (after McMaster[3])

73. It is evident from fig. 21 that large specimens will receive significantly different quantities of radiation in those areas that are subjected to extremely low and extremely high angles of emergence. The

intensities in these two areas are so different that soil density data obtained by film density measurements would most likely be in error.

74. Thus, for detailed analyses, it is necessary to limit the area under study to that area directly opposite the target. This would require several radiographs for large specimens. Also it is necessary to locate the aluminum control disk as near as possible to the area under study.

PART V: PETROGRAPHY

75. The petrographic examination of clays is an important supplement to X-ray diffraction studies. Whereas X-ray diffraction permits the rapid identification of the constituent mineralogy, the petrographic microscope provides information on the clay fabric as well as mineralogy. The usefulness of the petrographic examination is, however, dependent to a certain extent upon the clay size and the degree of secondary mineralization (e.g. iron staining) which the clay has undergone. The purpose of this aspect of the study was to determine the applicability of the petrographic microscope in the detection of fabric changes due to the ballistic impact.

76. As stated previously, fabric refers to the size, shape, and arrangement of the soil particles. Here we are primarily concerned with particle arrangement. Individual clay mineral grains or crystallites exist as platelets. The fabric of a clay is, therefore, the manner in which the platelets are arranged and their size.

77. The manner in which the clay platelets are arranged is a function of mineralogy, size, adsorbed and interlayer cations, ions in solution, concentration of clay in solution, and previous history of loading. Although the mode of arrangement may be quite complex, there are three general types of platelet arrangement.[4] These types consist of edge-to-face, edge-to-edge, and face-to-face associations. The edge-to-face and edge-to-edge associations result in a more-or-less random orientation of the clay platelets while the face-to-face association is considerably more uniform or nonrandom.

78. The clay crystallography and resulting orientation of the optic axis control the refraction of light through the clay. When the clay platelets are arranged in a face-to-face orientation, there will be an effective alignment of certain crystallographic and optic directions.[5] This alignment will impart to thin sections cut at selected attitudes a degree of optical continuity throughout the section.

79. A thin section cut parallel to the c-crystallographic axis (normal to platelet face) and viewed under crossed polarizers will

exhibit a position of maximum birefringence and a position of extinction (darkening) as the microscope stage is rotated. If the fabric is face-to-face alignment, the resulting optical continuity will extend the effect of maximum birefringence and extinction throughout the thin section. Thin sections cut subparallel to the c-axis will exhibit the same effects, but the extinction and maximum birefringence angles will be somewhat different.

80. Thin sections cut normal to the c-axis (parallel to platelet face) will exhibit a nonuniform, random extinction as the microscope stage is rotated. This also applies to randomly oriented fabrics such as edge-to-face.

81. Two thin sections cut normal to one another at a particular area are sufficient to detect platelet orientation if present. Two are required to preclude the possibility of cutting the thin section parallel to the faces of the platelets and concluding that random orientation exists due to the random extinction.

Application

82. Two ballistically loaded specimens were selected for thin-section study. For each specimen, one set of sections was taken as close as possible to the impact crater and the other set approximately half way between the face of the crater and the side of the specimen. The set consisted of two thin sections, one parallel and one perpendicular to the firing direction. Samples were also taken at these locations for SEM analysis which will be discussed later.

83. The applicability of thin-section techniques (and scanning electron microscopy as well) is predicated upon the identification of particle arrangement in the undisturbed clay. This arrangement will depend upon the type of clay mineral, adsorped ions, water content, and, more importantly, the nature of sample preparation. The comparison of undisturbed areas with areas near the impact crater would determine the extent of fabric alteration due to the ballistic loading.

84. Fig. 22 illustrates the locations of thin sections and SEM specimens for two ballistically loaded samples.

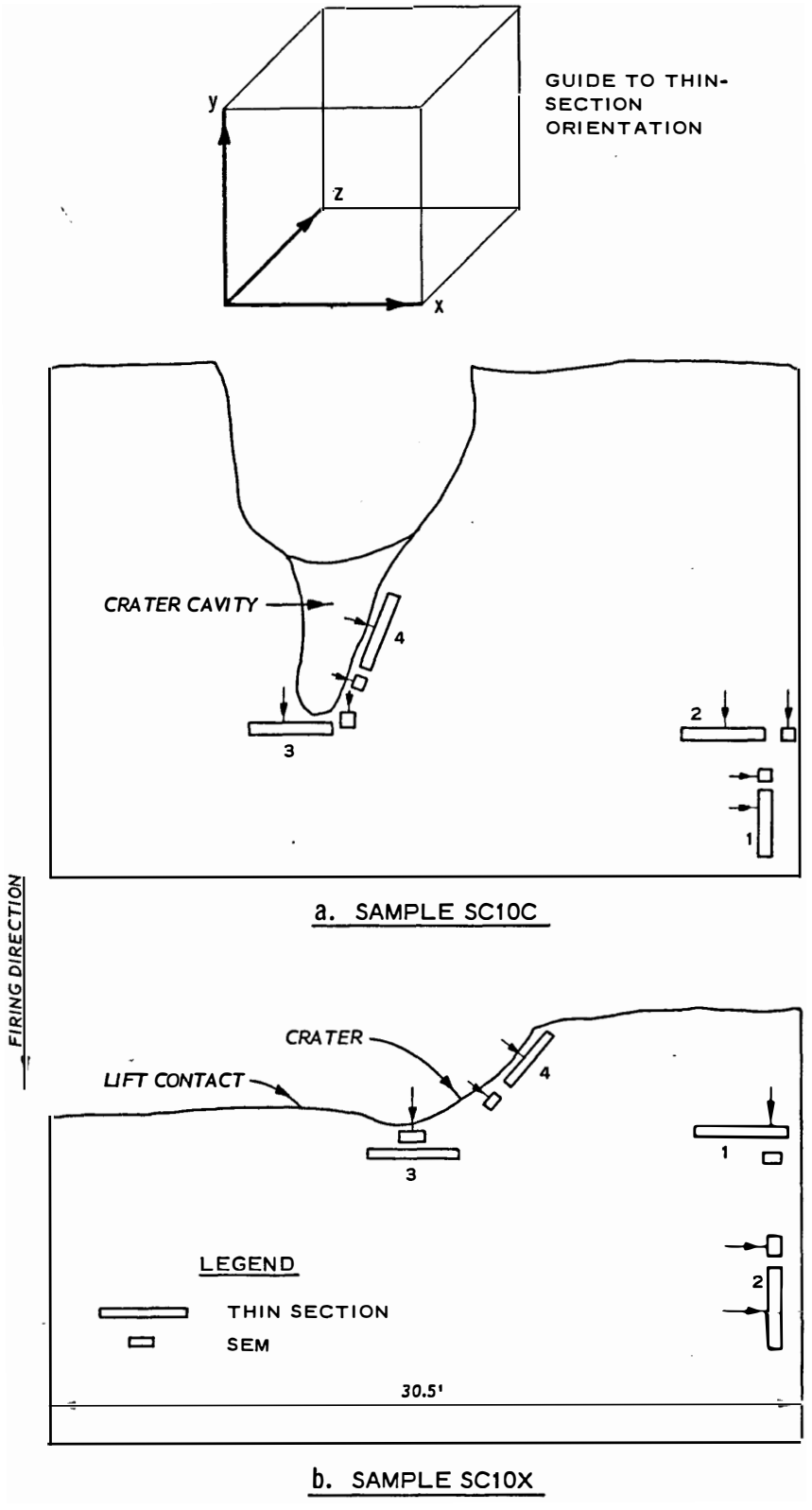

Fig. 22. Schematic representation showing locations of thin sections and SEM samples for specimens SC10C and SC10X

Description of Thin Sections

Specimen SC10C

85. Fig. 23 illustrates two photomicrographs (X20) of thin sections cut parallel to both the firing direction and the direction of compaction located in an undisturbed area. Polarizers are crossed. Fig. 23a shows a distinct lineation perpendicular to the firing direction. The white streaks are clay platelets. The angular, white, equidimensional grains are quartz or possibly feldspar. Some iron staining is apparent, and the dark spots represent highly stained areas or even very small concretions. Fig. 23b illustrates the same field rotated to extinction. The tone of this photomicrograph is considerably darker and indicates that the majority of the platelets are at extinction.

86. Fig. 24 illustrates photomicrographs of sections perpendicular to the firing direction. In fig. 24a there is no general overall grain orientation, although some areas appear less random than others. Rotation of the microscope stage (fig. 24b) results in appreciably no change in photo tone.

87. Figs. 25 and 26 represent areas adjacent to the impact crater. Fig. 25 is perpendicular to the firing direction; here there is no apparent preferred grain orientation in either the parallel or rotated position. Fig. 26 illustrates a view parallel to the firing direction showing distinct east-west grain orientation and darkening upon rotation.

Specimen SC10X

88. Fig. 27 illustrates sections (X20) taken perpendicular to firing direction and some distance from impact crater. There does not appear to be any preferred orientation. The section cut parallel to the firing direction (fig. 28) shows a rather distinct east-west trend in the upper part of the photomicrograph. The large grain in the upper portion is plagioclase feldspar. The rotated position illustrates moderately uniform extinction.

89. Figs. 29 and 30 illustrate sections taken adjacent to impact areas. These photomicrographs indicate random grain orientation in this area.

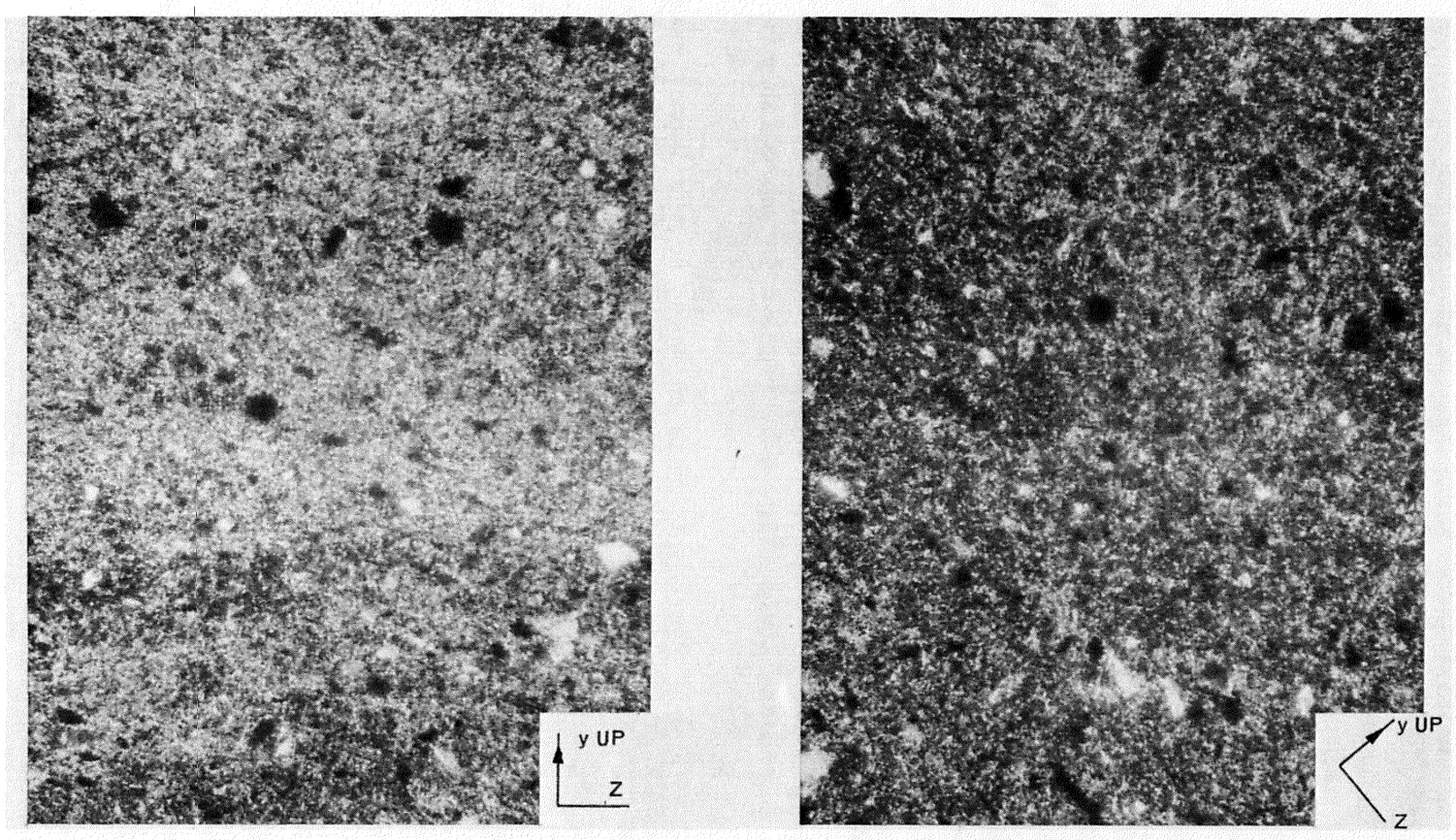

a) UPRIGHT POSITION

b) ROTATED POSITION

Fig. 23. Photomicrographs of specimen SC10C. Face is parallel to trajectory and beyond impact area. Crossed polarizers, X20

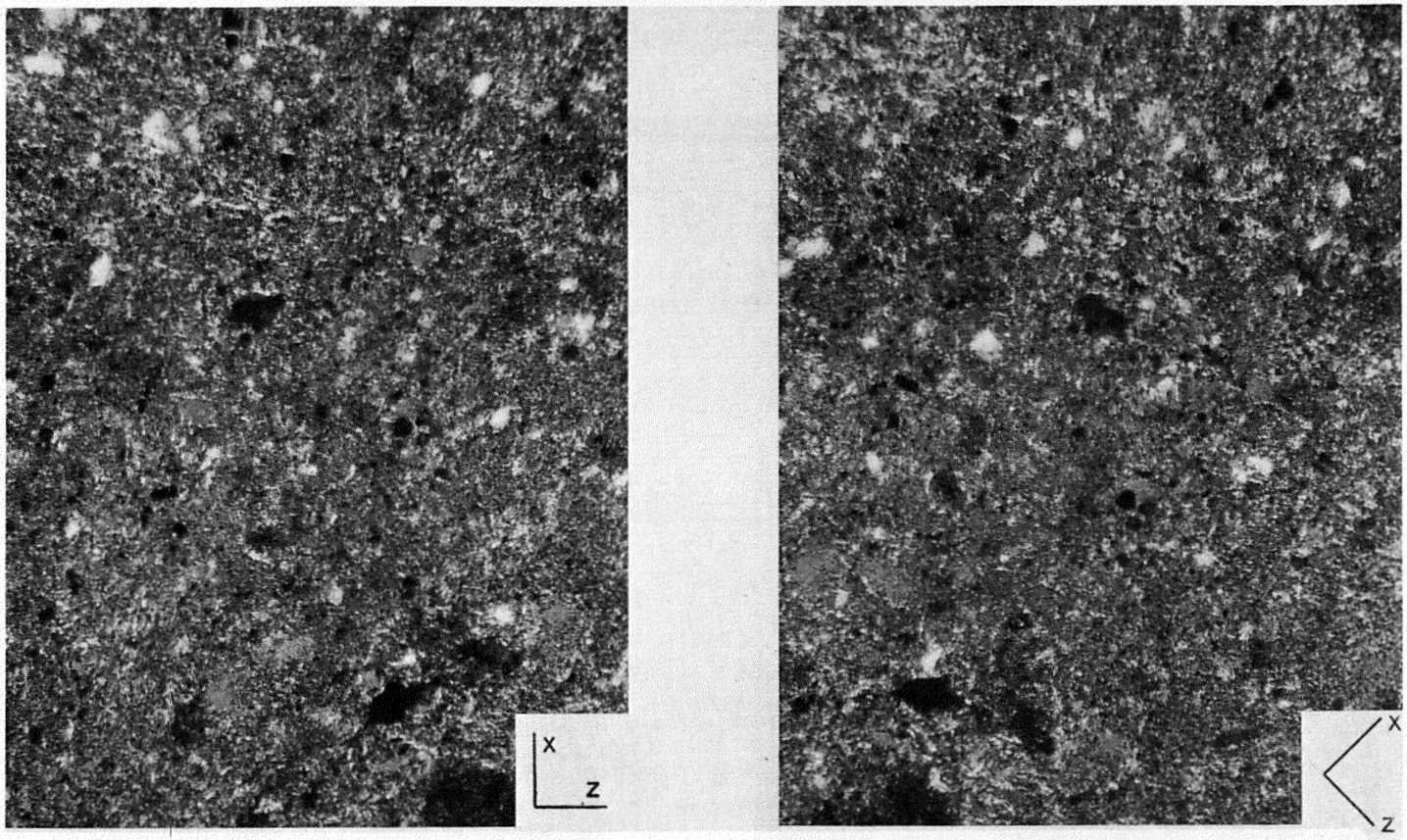

a) x-z PLANE

b) x-z PLANE ROTATED

Fig. 24. Photomicrographs of specimen SC1OC. Face is normal to trajectory and beyond impact area. Crossed polarizers, ×20

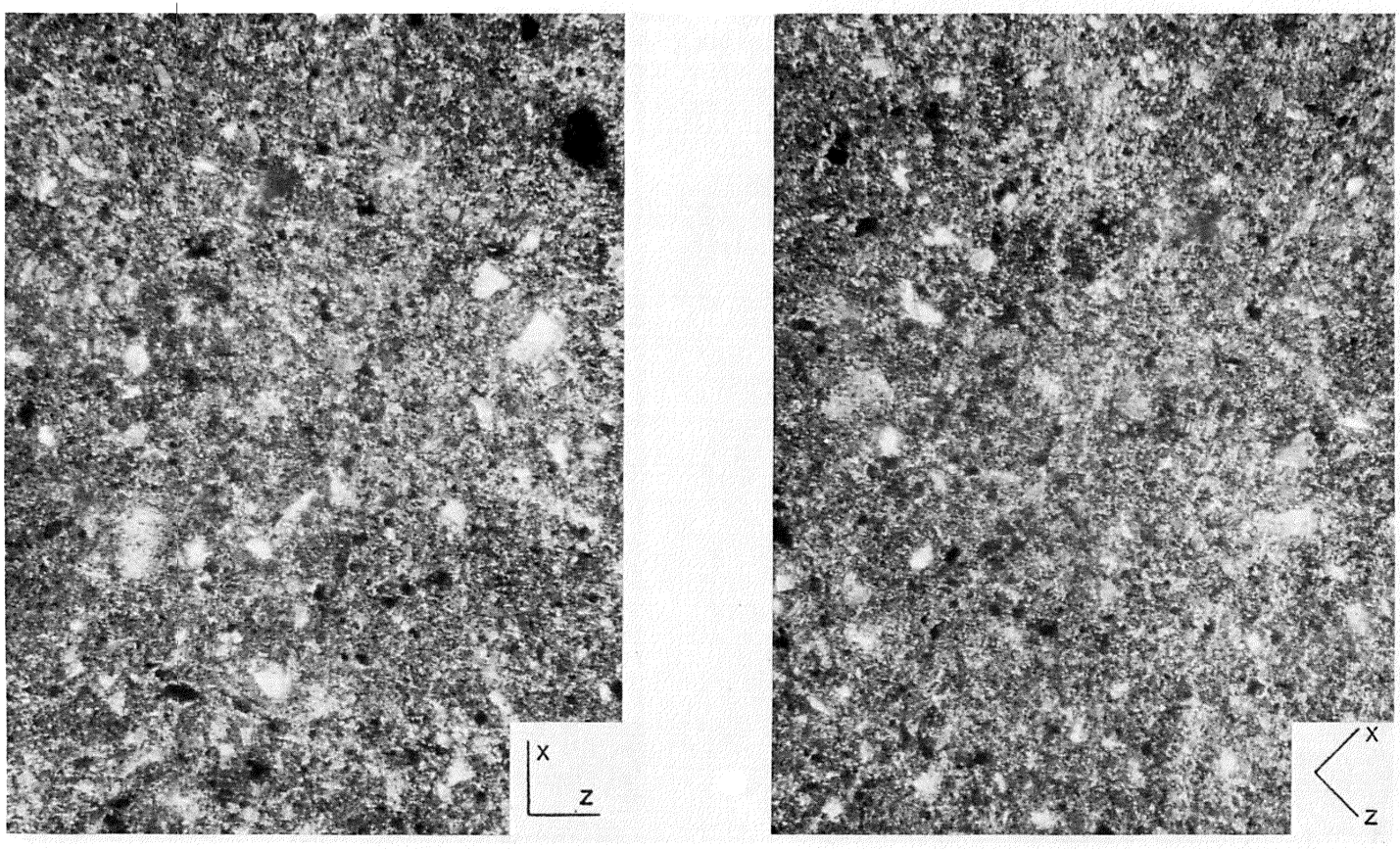

Fig. 25. Photomicrographs of specimen SC10C. Face is normal to trajectory and near impact area. Crossed polarizers, ×20

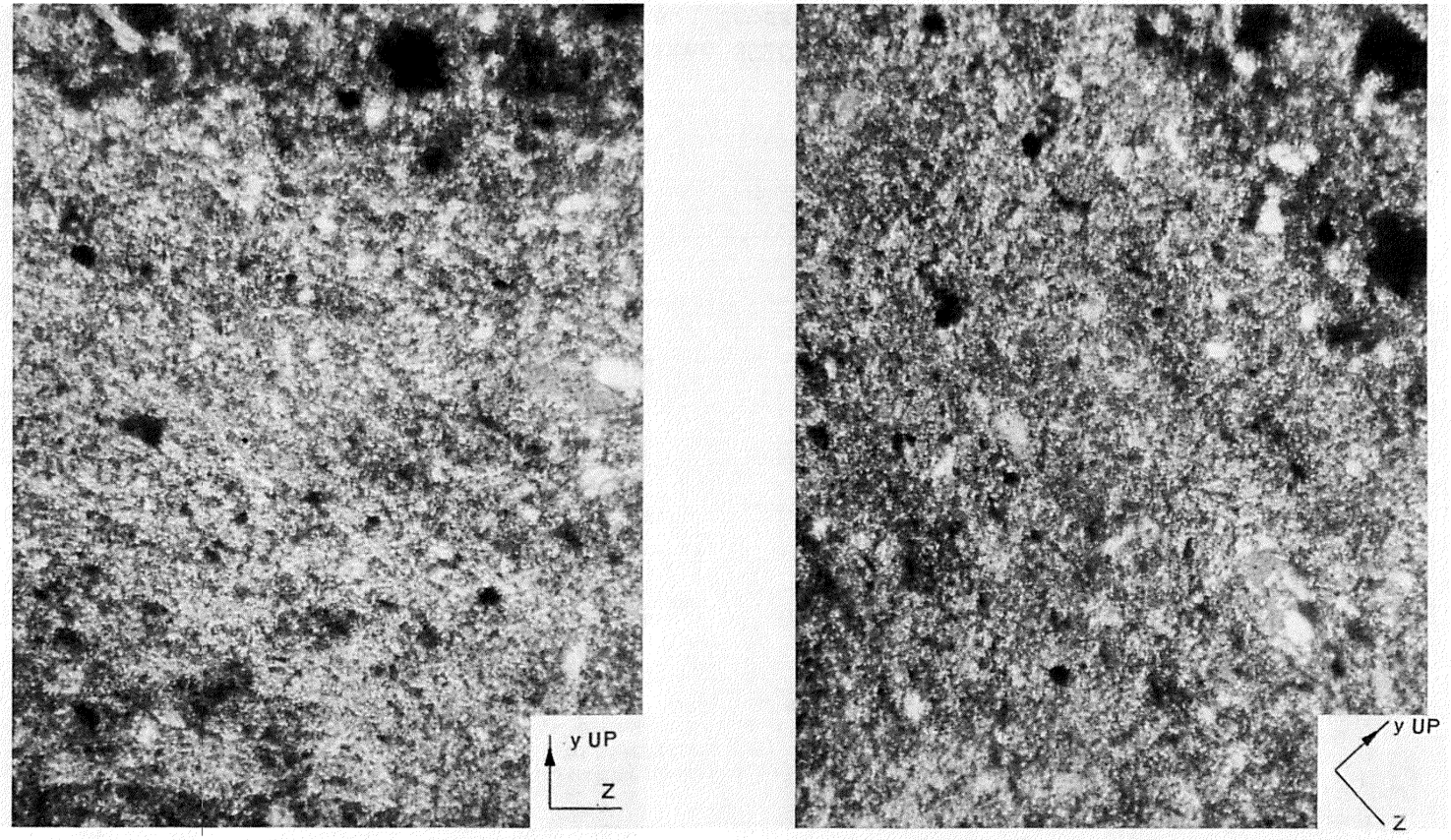

a) UPRIGHT POSITION

b) ROTATED POSITION

Fig. 26. Photomicrographs of specimen SC10C. Face is parallel to trajectory and near impact area. Crossed polarizers, ×20

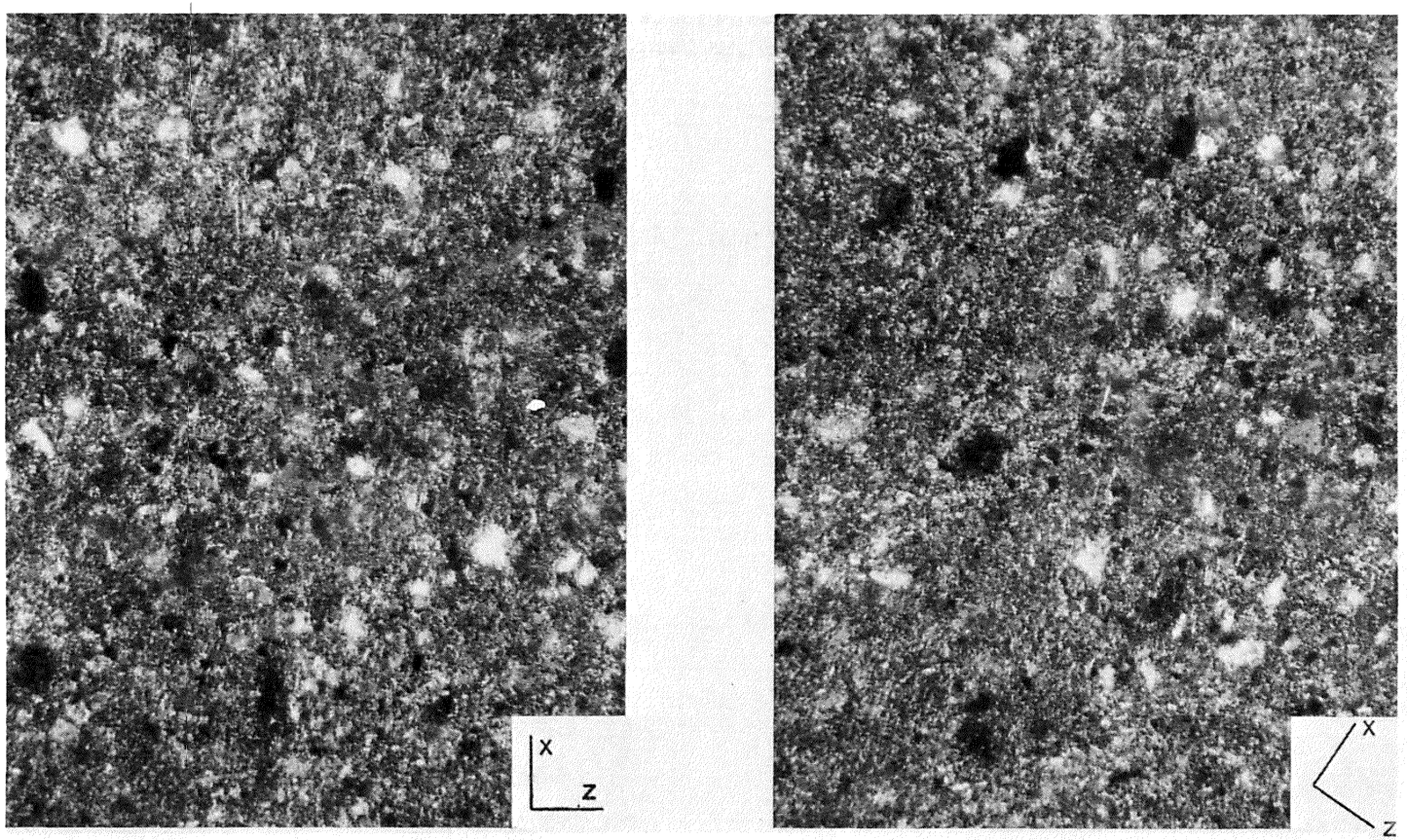

a) x-z PLANE

b) x-z PLANE ROTATED

Fig. 27. Photomicrographs of specimen SC1OX. Face is normal to trajectory and beyond impact area. Crossed polarizers, X20

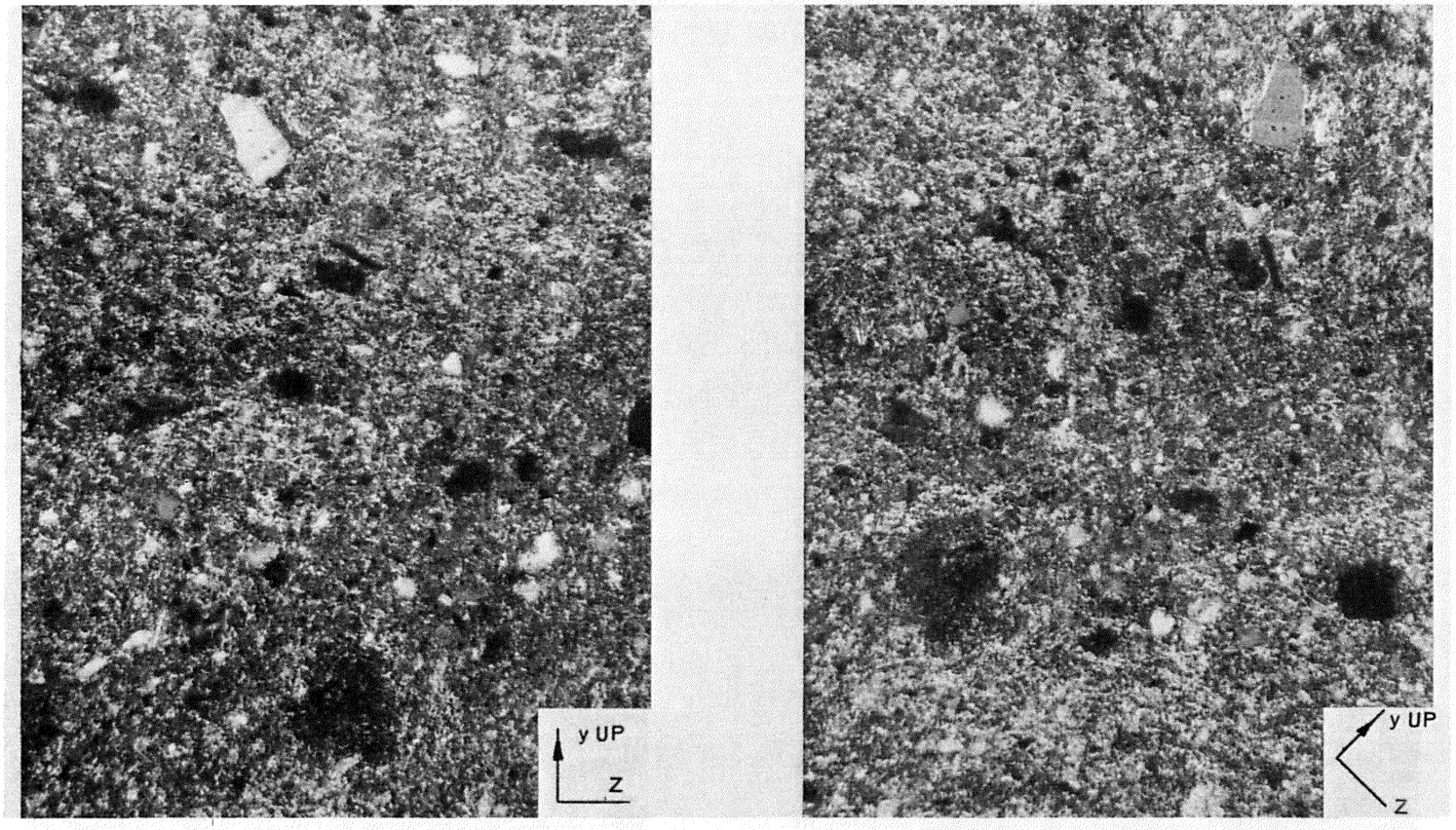

a) UPRIGHT POSITION

b) ROTATED POSITION

Fig. 28. Photomicrographs of specimen SC1OX. Face is parallel to trajectory and beyond impact area. Crossed polarizers, ×20

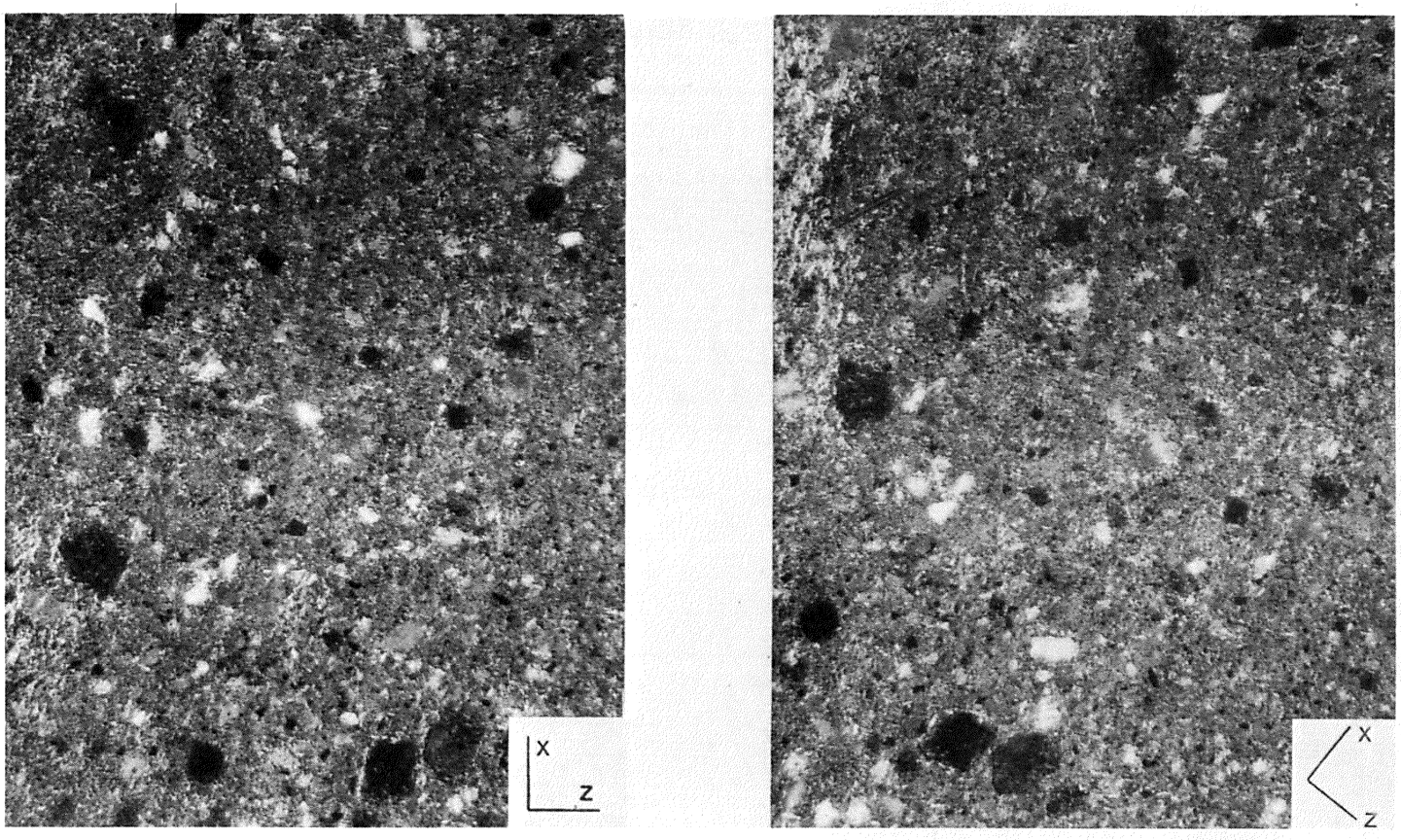

a) x-z PLANE

b) x-z PLANE ROTATED

Fig. 29. Photomicrographs of specimen SC1OX. Face is normal to trajectory and near impact area. Crossed polarizers, ×20

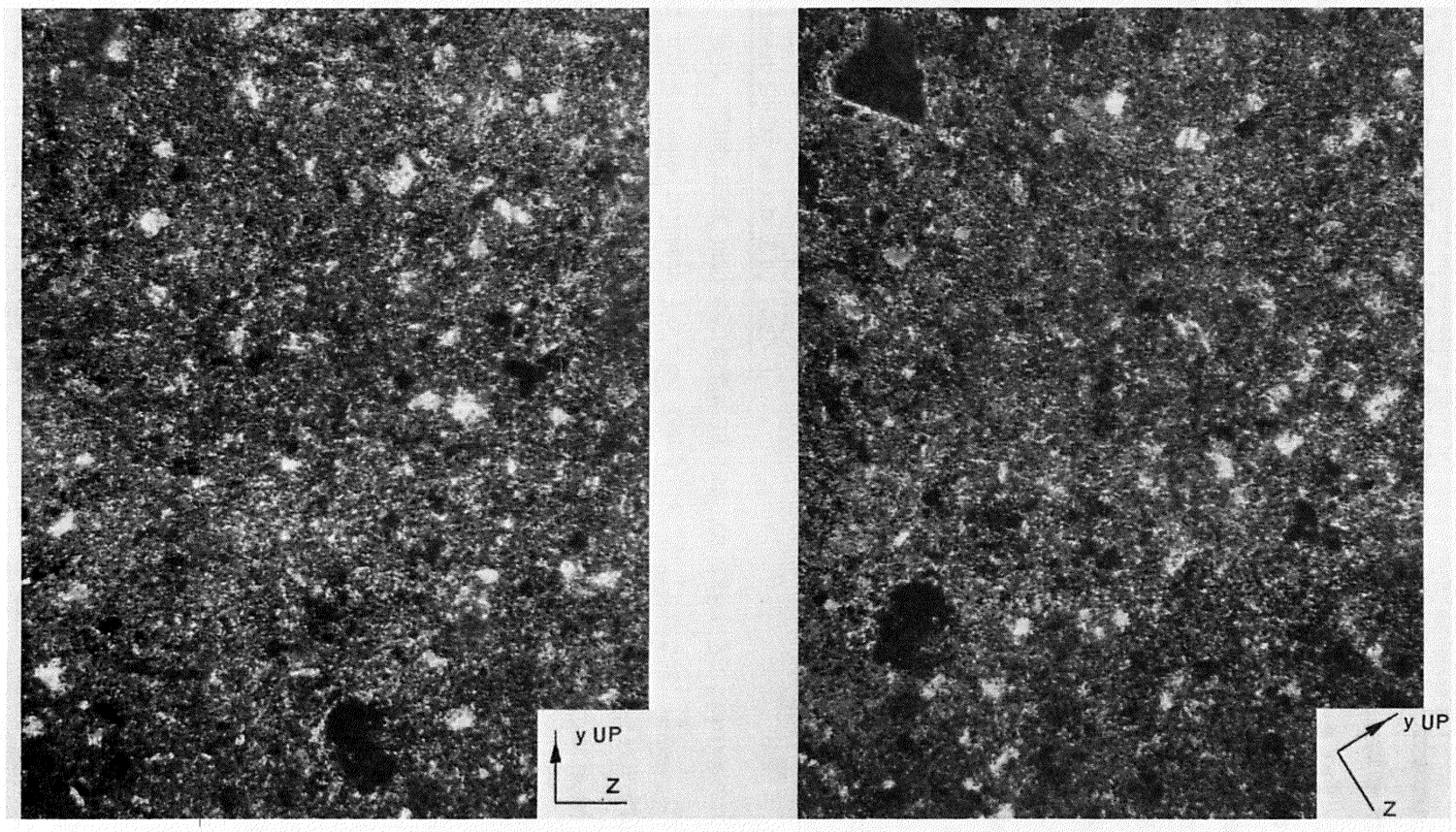

a) UPRIGHT POSITION

b) ROTATED POSITION

Fig. 30. Photomicrographs of specimen SC1OX. Face is parallel to trajectory and near impact area. Crossed polarizers, ×20

Discussion

90. The photomicrographs demonstrate that the clay exhibited a preferred orientation in the region adjacent to as well as beyond the impact crater. The orientation is one of more-or-less face-to-face arrangement with the faces normal to the firing direction and also normal to the direction of compaction. This preferred orientation is believed to be due to compaction. The areas adjacent to the impact crater do not appear to be appreciably different from those beyond. It is concluded that the thin sections do not reveal any significant fabric changes attributable to the ballistic impact.

PART VI: SCANNING ELECTRON MICROSCOPY

91. The examination of clay fabrics by the scanning electron microscope (SEM) has become an increasingly important method of clay analysis. The SEM provides the investigator with a relatively fast and reproducible means of identifying particle arrangement as well as constituent mineralogy. Clay mineral identification is generally based upon shape and size of individual platelets.

Description of SEM Photographs of Specimens 05BC and 011BC

92. Fig. 31 illustrates the locations of SEM samples from specimens 05BC and 011BC. These samples were taken from thin slabs and represent the plane of the trajectory (center) and left and right of the trajectory. The squares on the radiographs indicate the location of the SEM samples and their identification number (SMC-1, -2, etc.)

Specimen 05BC slab B1, SMC-1

93. The SEM photographs shown in fig. 32 represent two magnifications of a face normal to the path of the projectile. The orientation of the clay platelets is nearly parallel to the face. The lighter areas of these and subsequent photographs were caused by nonuniform sample coating. Pore space is well illustrated in fig. 32b.

Specimen 05BC slab D3, SMC-2

94. The face here (fig. 33) is parallel to the trajectory. The lineation indicates a parallel orientation of the platelets, which is roughly normal to this path.

Specimen 05BC slab C2

95. SMC-4 (fig. 34). The face examined is normal to the trajectory. The clay platelets are oriented parallel to the face. The large grain in the upper left of the photograph is most likely feldspar. At X2000 pore structure is evident.

96. SMC-5 (fig. 35). The face here is normal to the trajectory. The clay platelets exhibit well-developed alignment parallel to the sample face. The large grain left of center is probably quartz.

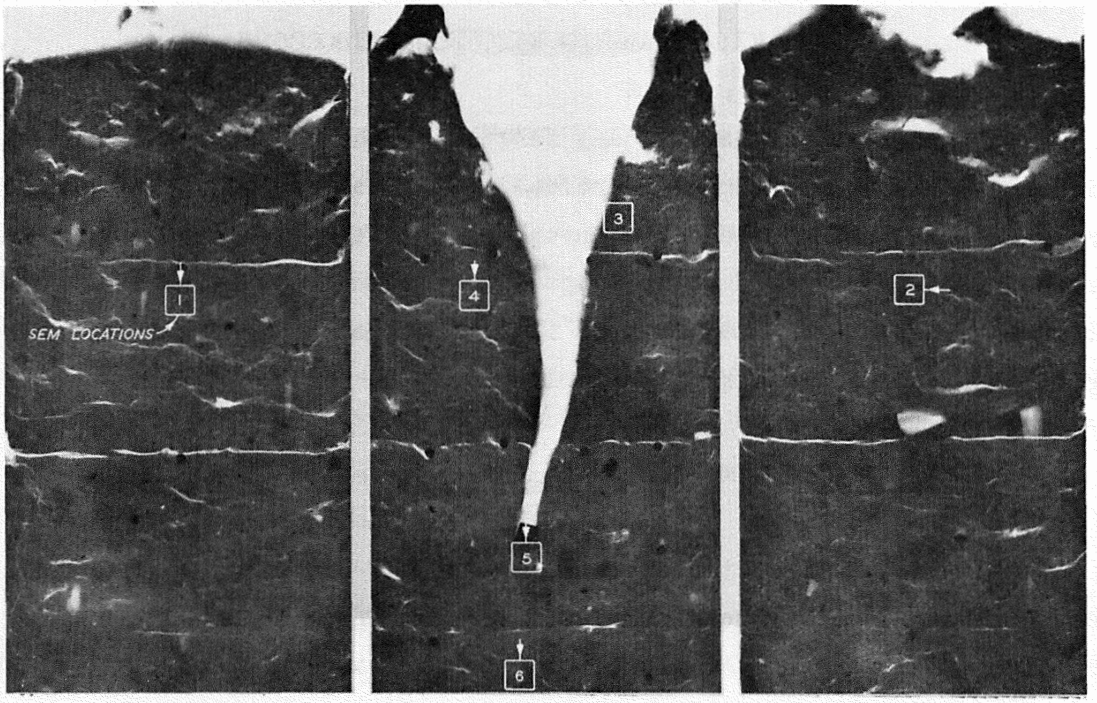

a. SLAB B1 b. SLAB C2 c. SLAB D3

SPECIMEN 05BC

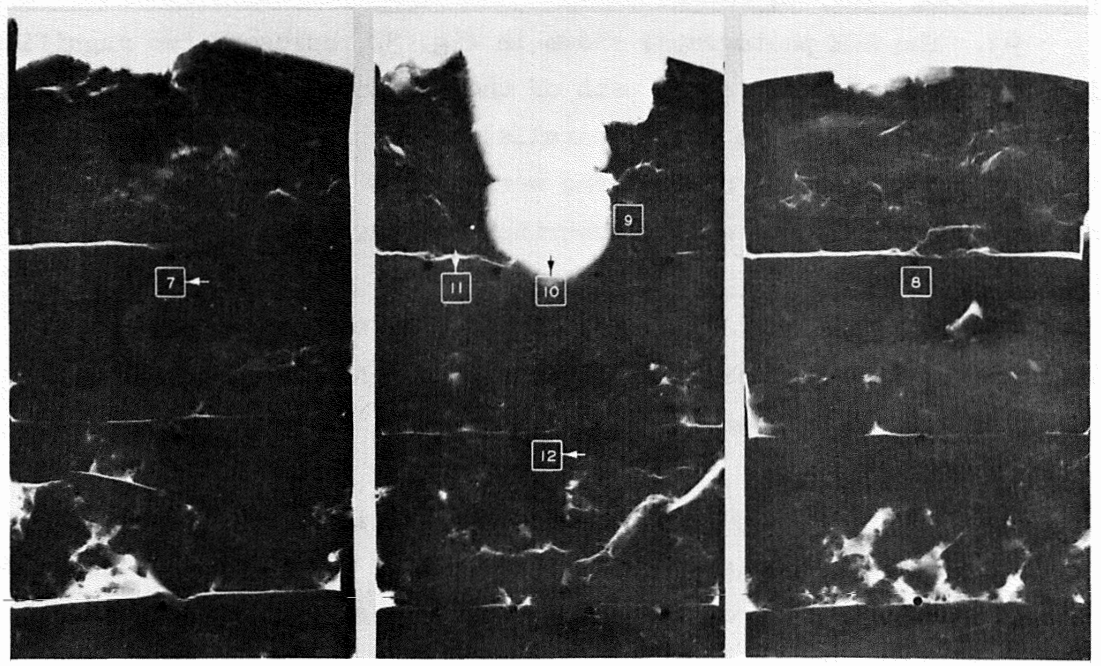

a. SLAB B1 b. SLAB C2 c. SLAB D3

SPECIMEN 011BC

NOTE: NOS. 3,8, AND 9 NOT USED
ARROW POINTING TO SQUARE INDICATES FACE EXAMINED

SCALE IN INCHES

0 2 3

Fig. 31. SEM sample locations, specimens 05BC and 011BC

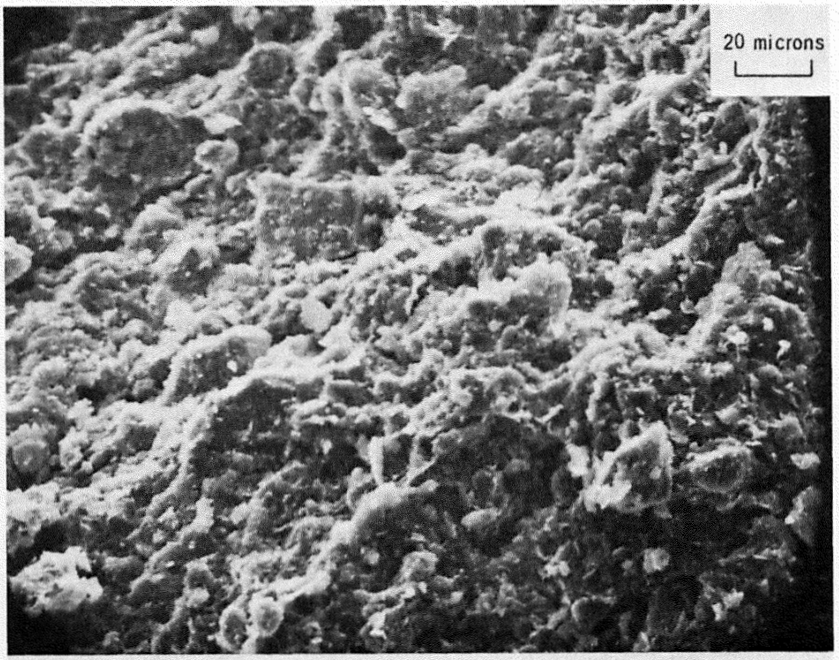

a) X500

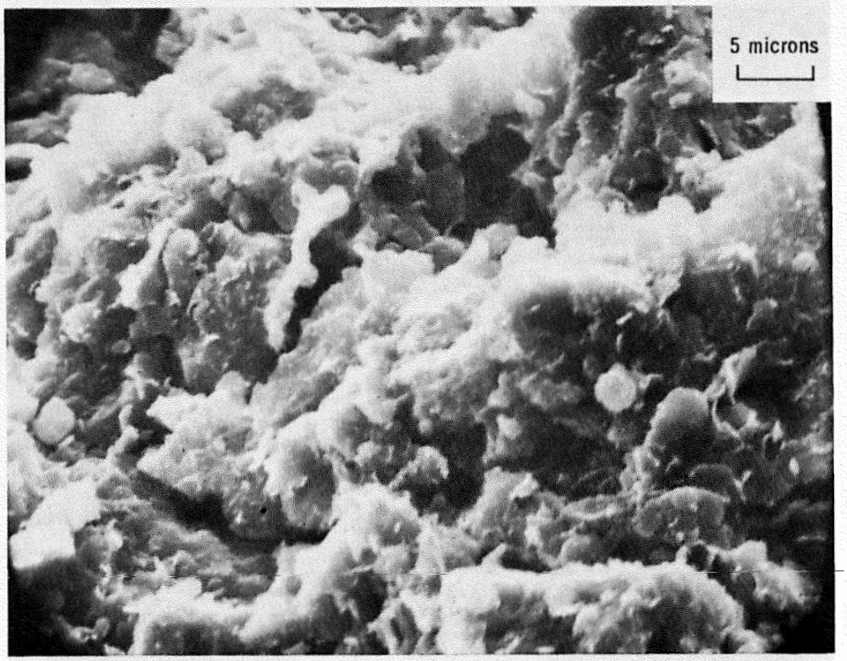

b) X2000

Fig. 32. SEM photographs of specimen 05BC slab B1, SMC-1. Face is normal to trajectory

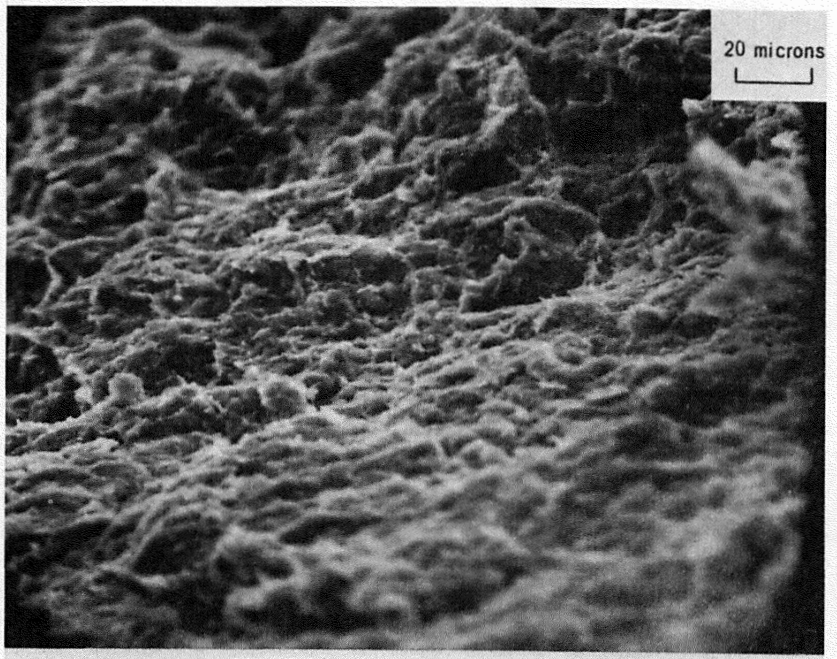

a) X500

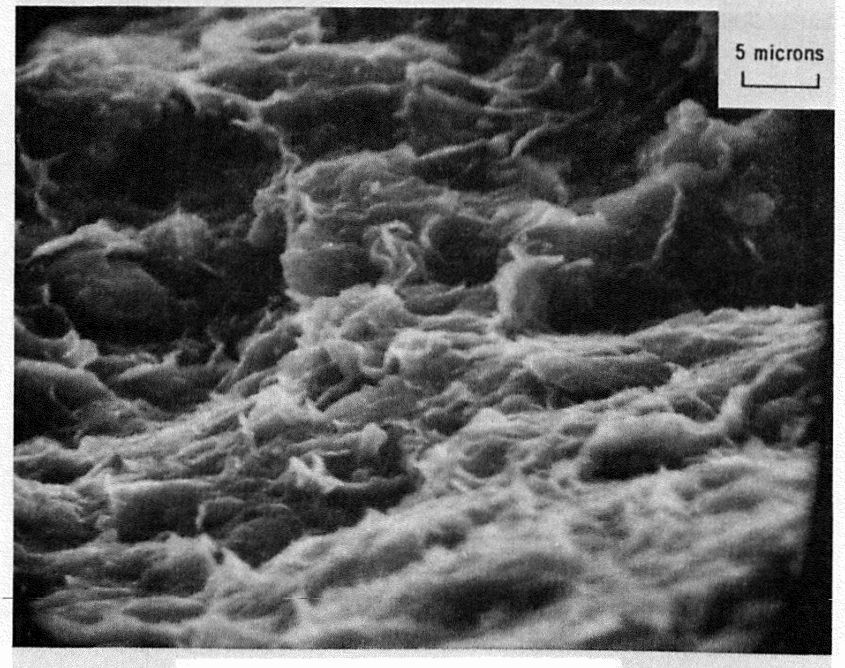

b) X2000

Fig. 33. SEM photographs of specimen O5BC slab D3, SMC-2. Face is parallel to trajectory

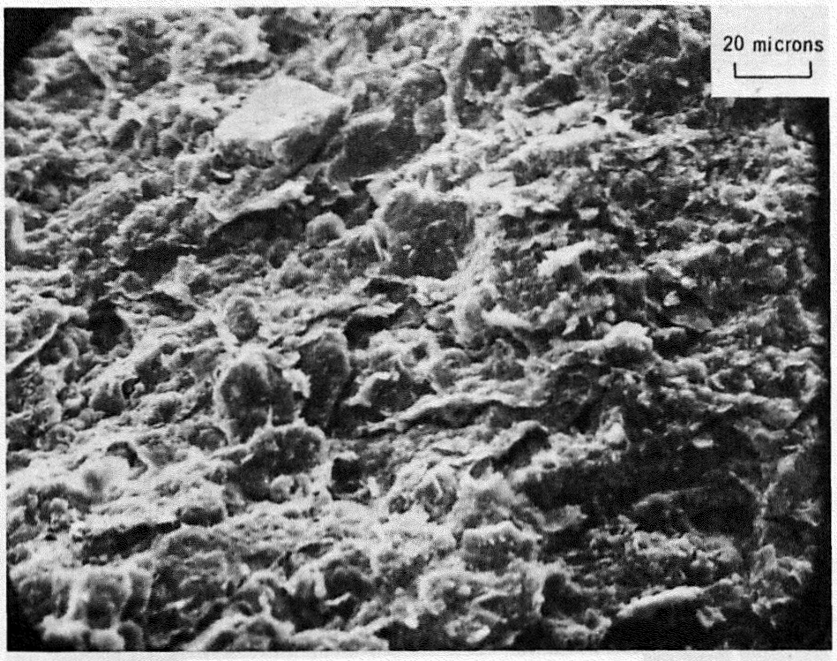

a) X500

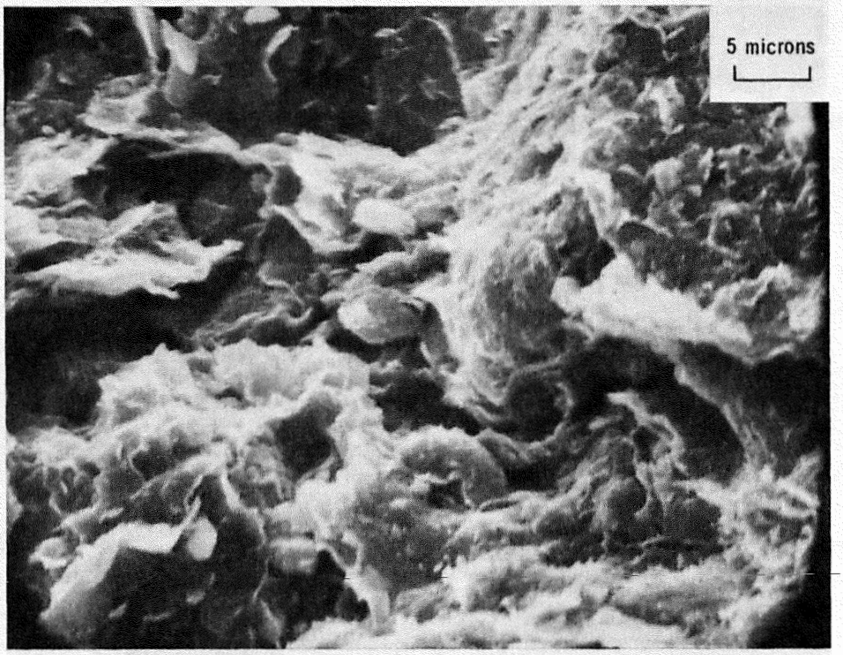

b) X2000

Fig. 34. SEM photographs of specimen 05BC slab C2, SMC-4. Face is normal to trajectory

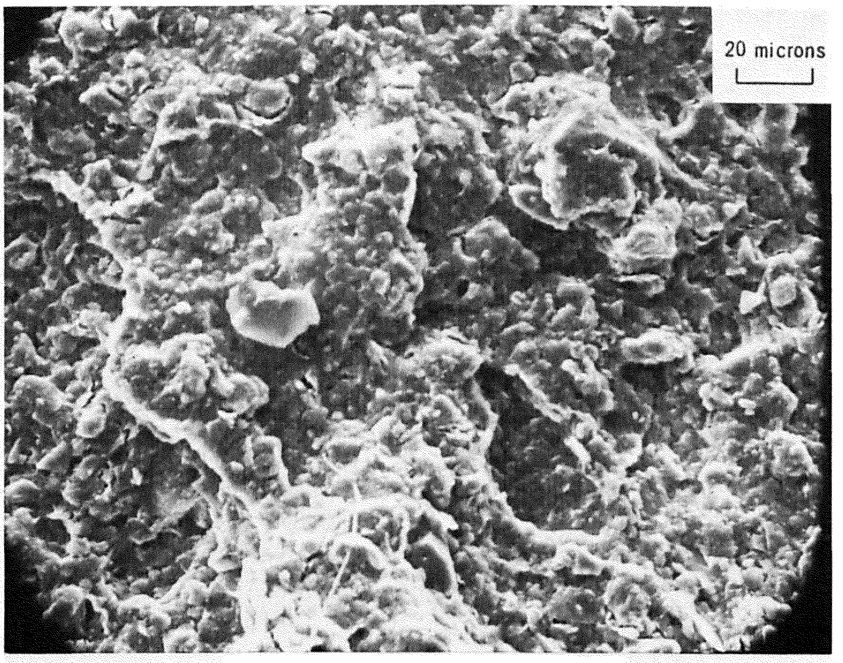

a) X500

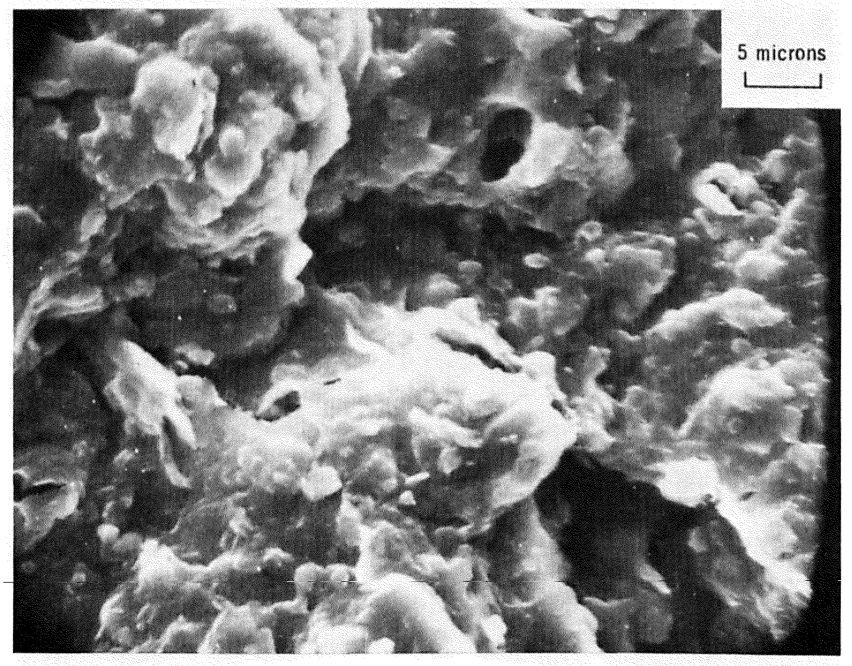

b) X2000

Fig. 35. SEM photographs of specimen 05BC slab C2, SMC-5. Face is normal to trajectory and adjacent to projectile

97. SMC-6 (fig. 36). The face is normal to the trajectory. There appears to be no distinct orientation, and the material seems massive.

Specimen 011BC slab B1, SMC-7

98. The face is parallel to the trajectory (fig. 37). The platelets are parallel and dip to the lower left of the photograph. The higher magnification (fig. 37b) also shows a parallel orientation but parallel to the face. This demonstrates that although the higher magnification can be quite helpful on details, it fails to give an adequate understanding of the general situation. The curling of the small platelets in the X2000 view is characteristic of montmorillonites.

Specimen 011BC slab C2

99. SMC-10 (fig. 38). The face is normal to the projectile path. The clay platelets exhibit a distinct parallel alignment parallel to the face examined.

100. SMC-11 (fig. 39). The face examined is normal to the trajectory. The platelets are roughly parallel to the face, but there is considerable curling which may be due to sample preparation. Note the quartz grain to the left below center.

101. SMC-12 (fig. 40). The face is parallel to the trajectory. Note that here the platelets exhibit a high degree of orientation parallel to the trajectory.

Description of SEM Photographs of Specimens SC10C and SC10X

102. The following descriptions of SEM photographs refer to the two specimens from which thin sections were taken. The areas examined by SEM are adjacent to the areas studied in thin sections.

103. Fig. 22 illustrates the locations of the studied areas within the impacted specimens.

Specimen SC10C beyond impact area

104. SMC-13 (fig. 41). The face is beyond the impact area of SMC-1 and is parallel to the trajectory. A degree of preferred orientation is evident; the platelets appear to be aligned from left to right

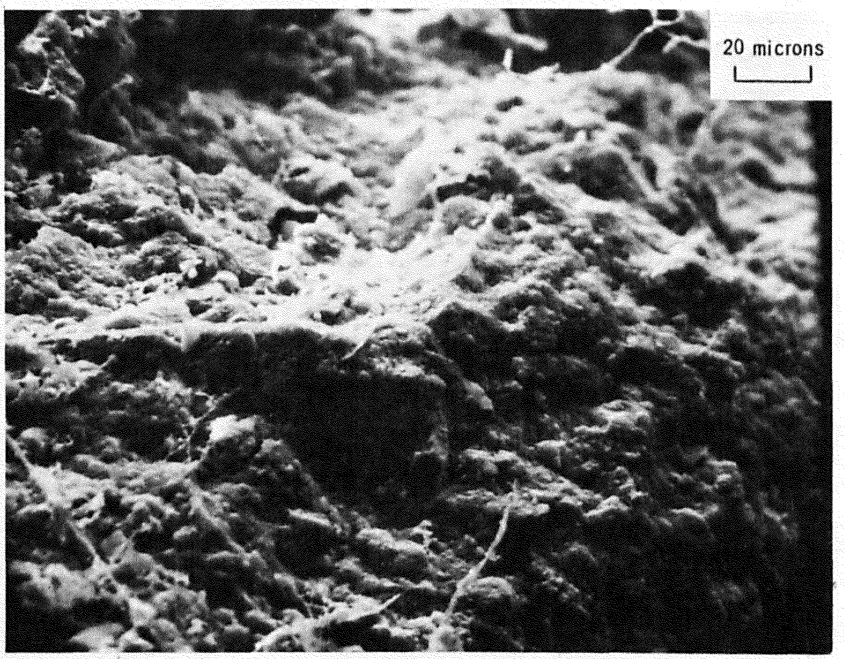

a) X500

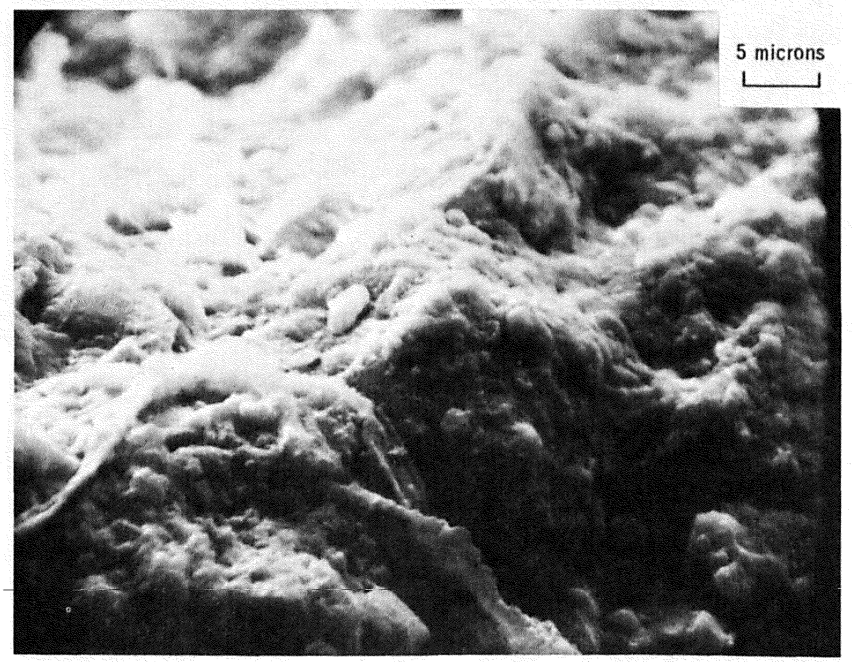

b) X2400

Fig. 36. SEM photographs of specimen 05BC slab C2, SMC-6. Face is normal to trajectory

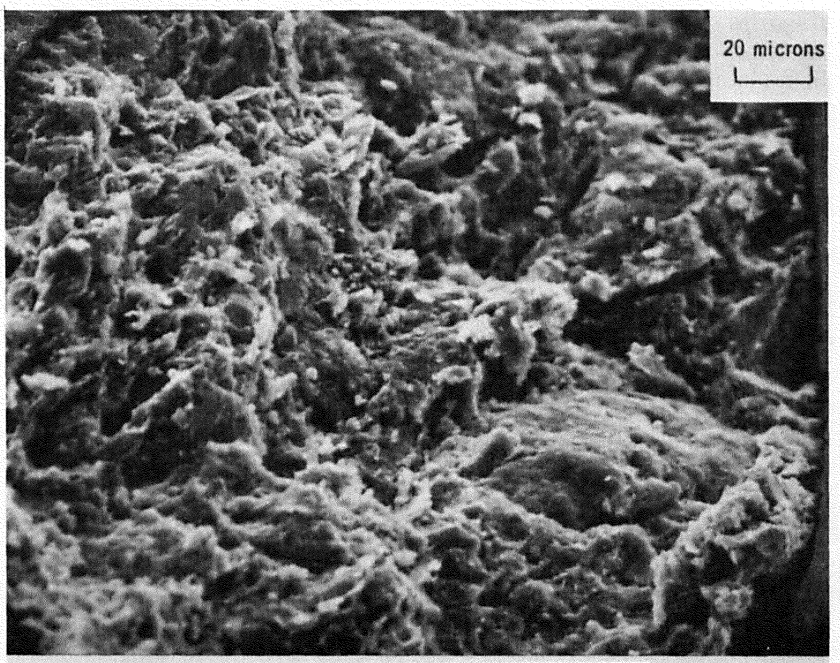

a) X500

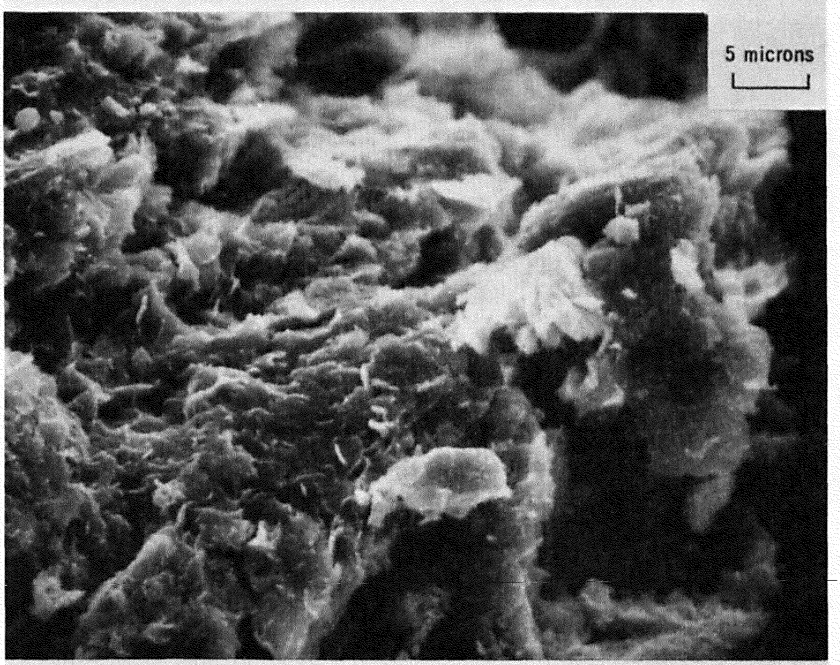

b) X2000

Fig. 37. SEM photographs of specimen O11BC slab B1, SMC-7. Face is parallel to trajectory

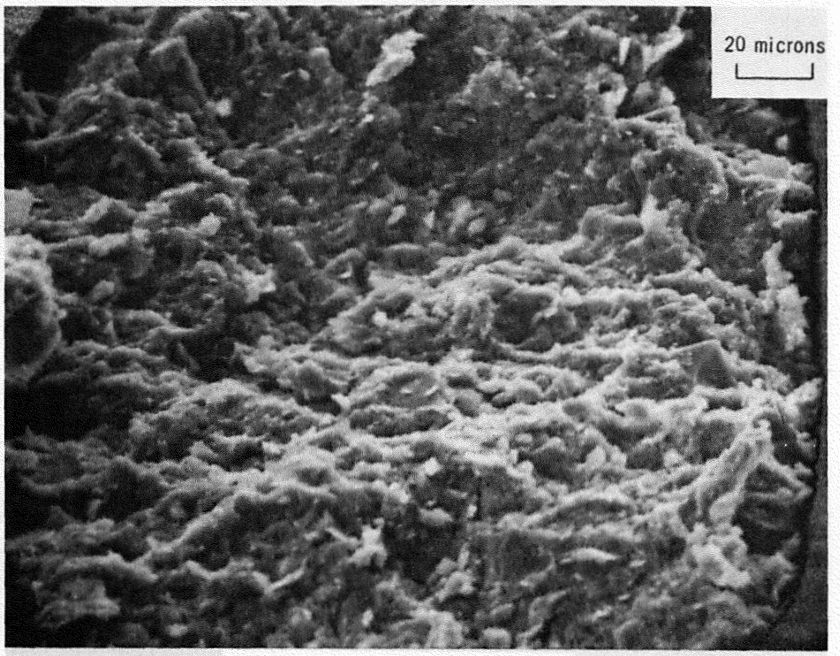

a) X500

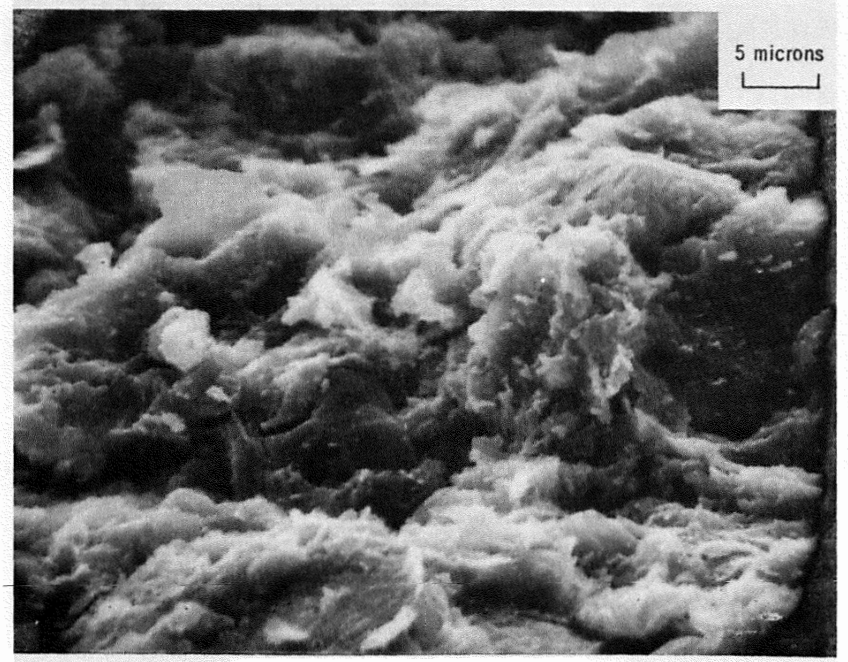

b) X2000

Fig. 38. SEM photographs of specimen O11BC slab C2, SMC-10. Face is normal to trajectory and adjacent to crater

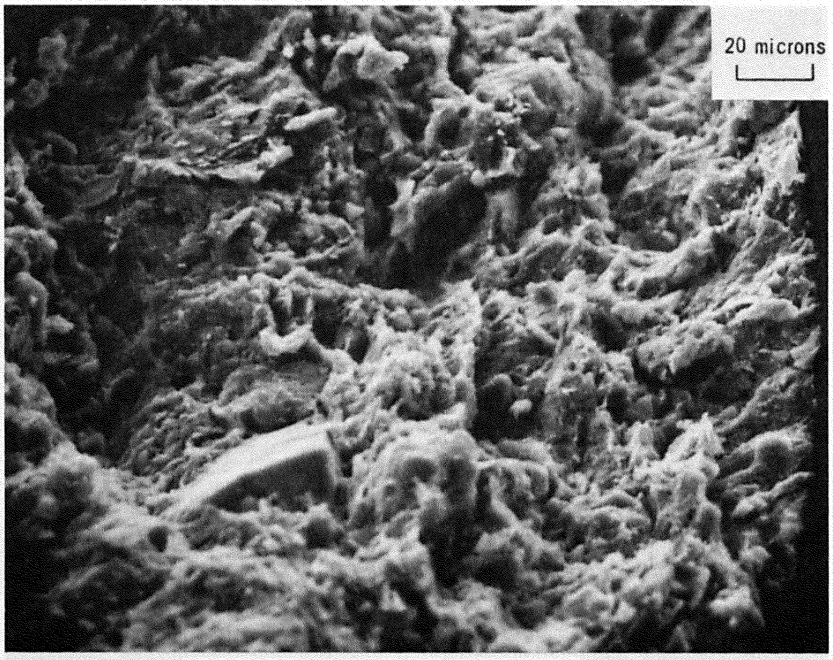

a) X500

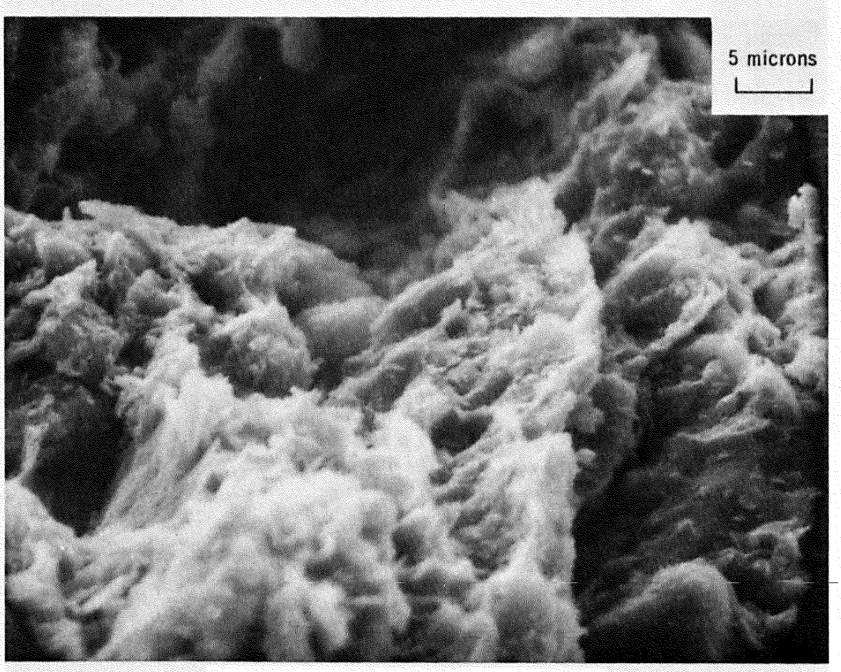

b) X2000

Fig. 39. SEM photographs of specimen O11BC slab C2, SMC-11. Face is normal to trajectory

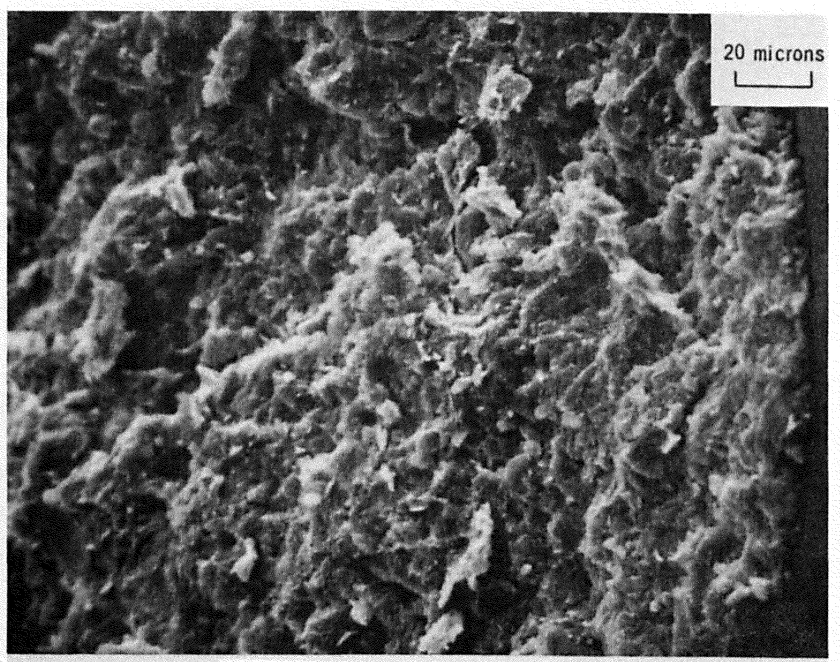

a) X500

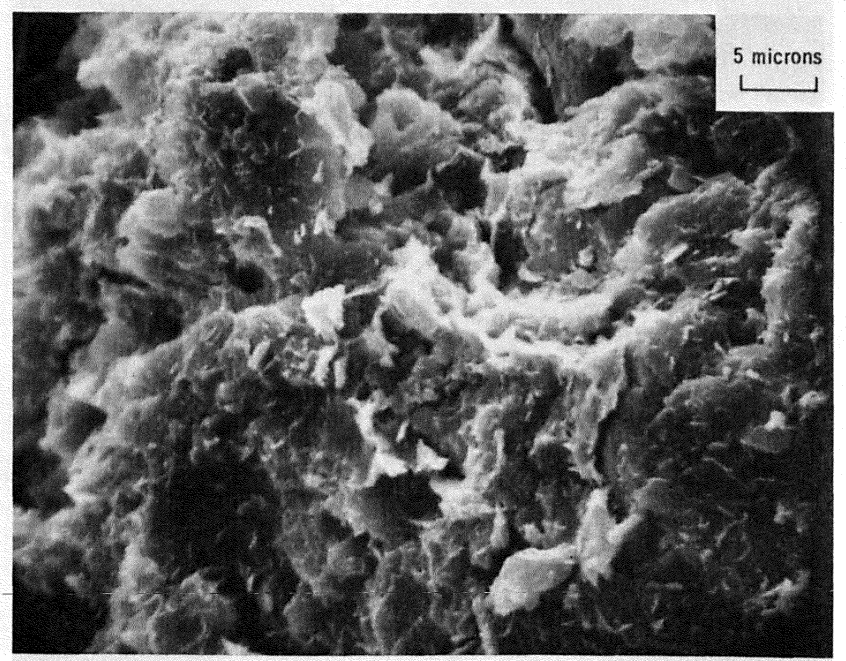

b) X2000

Fig. 40. SEM photographs of specimen O11BC slab C2, SMC-12. Face is parallel to trajectory

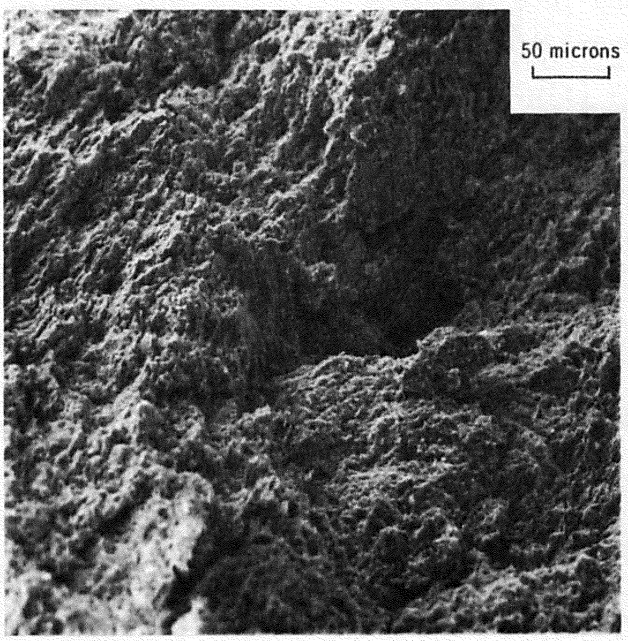

a) X220

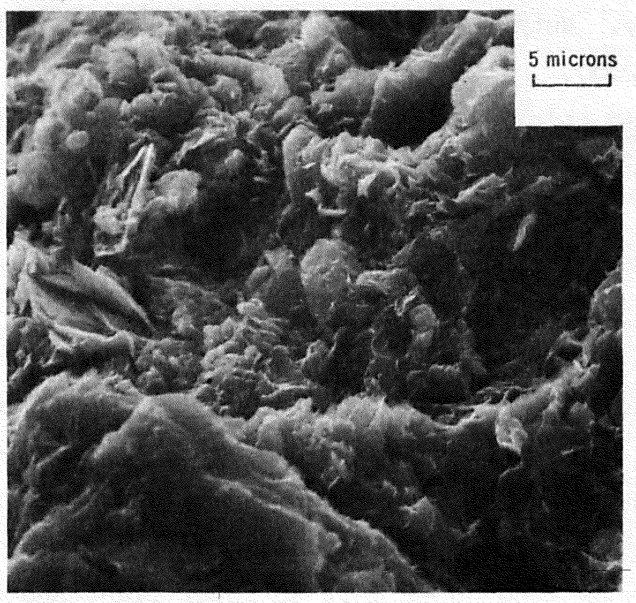

b) X2200

Fig. 41. SEM photographs of specimen SC10C, SMC-13. Face is parallel to trajectory and beyond impact area

and to dip down and into the plane of the photograph (X220). At X2200 magnification the orientation is well expressed.

105. SMC-14 (fig. 42). The face examined is normal to the trajectory. Both magnifications reveal a high degree of preferred orientation which is normal to the trajectory.

Specimen SC10C near impact area

106. SMC-15 (fig. 43). The face examined is normal to the trajectory. Both magnifications reveal a high degree of preferred orientation which is normal to the trajectory.

107. SMC-16 (fig. 44). The face examined is approximately parallel to the trajectory. At X200 magnification there appears to be well-developed platelet alignment roughly parallel to the plane of the photograph. The view at X2000 reveals a parallelism from left to right and a dip to the bottom of the photograph.

Specimen SC10X beyond impact area

108. SMC-17 (fig. 45). The face examined is normal to the trajectory. The platelets exhibit well-developed parallel alignment normal to the trajectory. Note the quartz grain above and to the left of center in the view at X2000.

109. SMC-18 (fig. 46). The face is parallel to the trajectory. Both magnifications reveal well-developed platelet orientation. The alignment trends from left to right and the platelets are dipping toward the bottom of the photographs.

Specimen SC10X near impact area

110. SMC-19 (fig. 47). The face examined is normal to the trajectory. Views at both magnifications reveal well-developed preferred orientation of the platelets. The alignment is normal to the trajectory.

111. SMC-20 (fig. 48). The face examined is subparallel to the trajectory. Both magnifications exhibit moderate preferred orientation. The alignment trends from upper left to lower right and dips to the lower left.

Discussion

112. The SEM photographs demonstrate that, in general, the

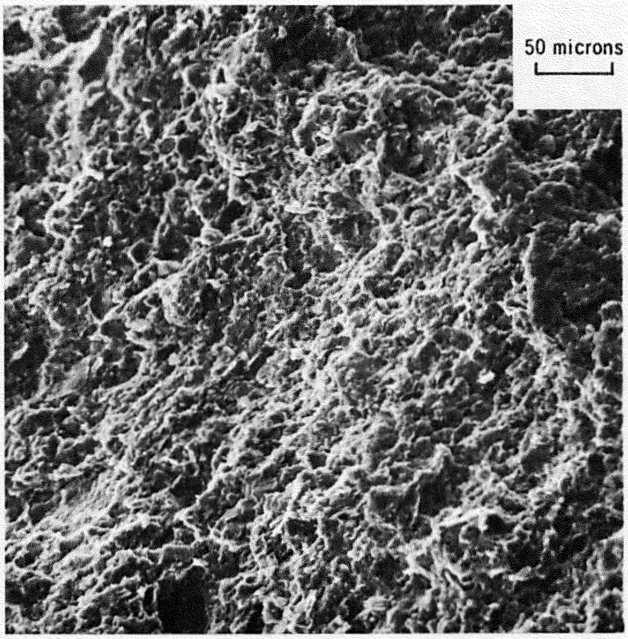

a) X220

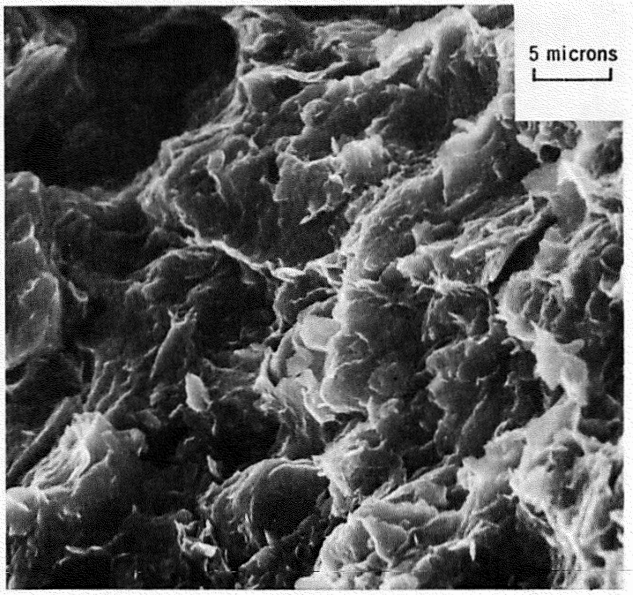

b) X2200

Fig. 42. SEM photographs of specimen SC10C, SMC-14. Face is normal to trajectory and beyond impact area

a) X200

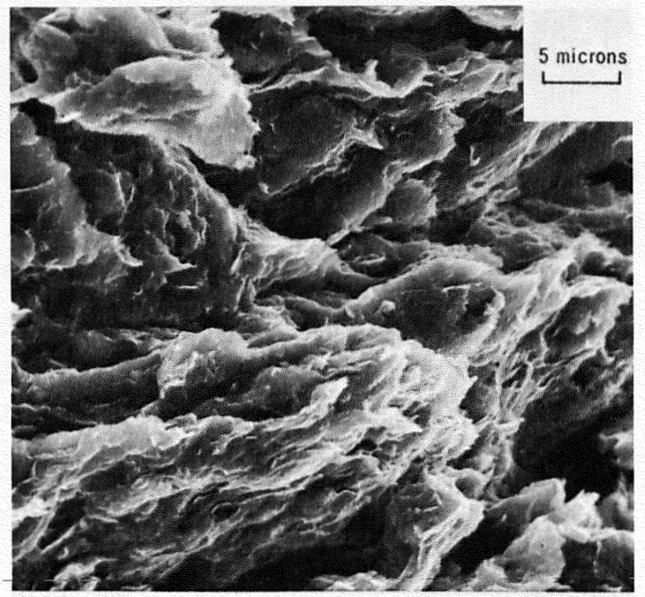

b) X2000

Fig. 43. SEM photographs of specimen SC10C, SMC-15. Face is normal to trajectory and near impact area

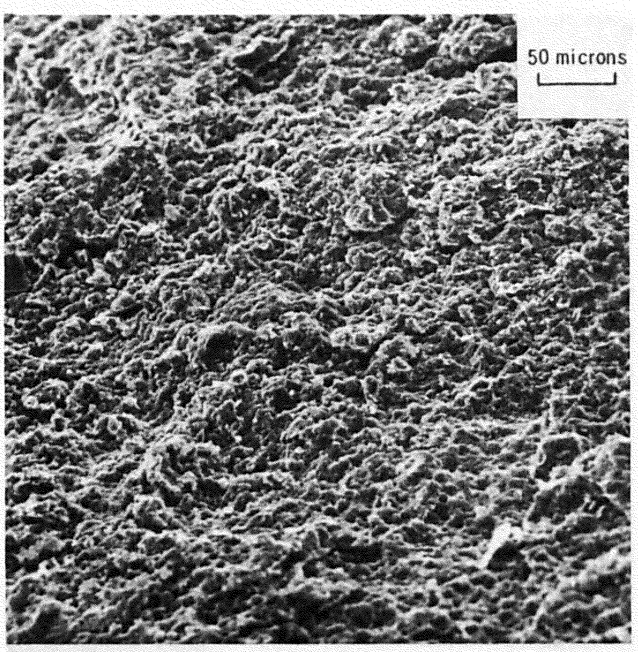

a) X200

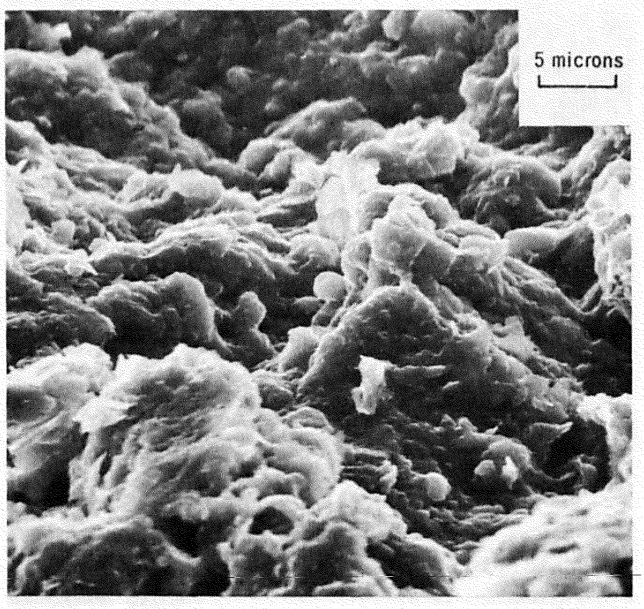

b) X2000

Fig. 44. SEM photographs of specimen SC10C, SMC-16. Face is parallel to trajectory and near impact area

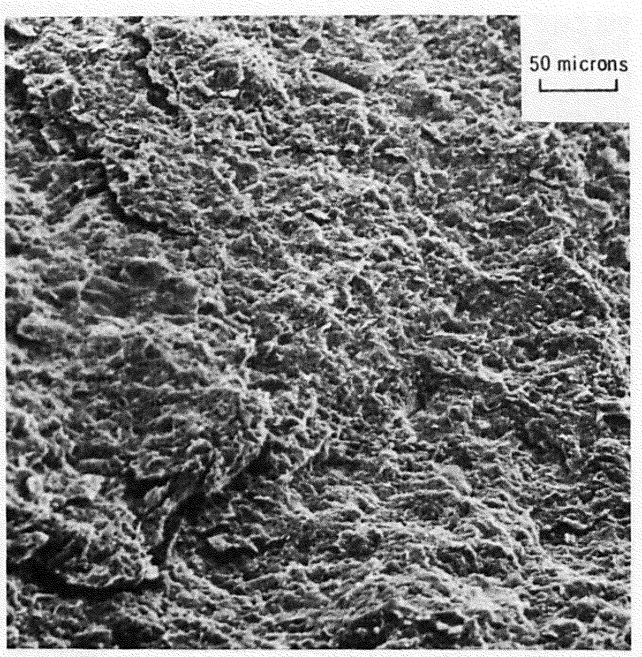

a) X200

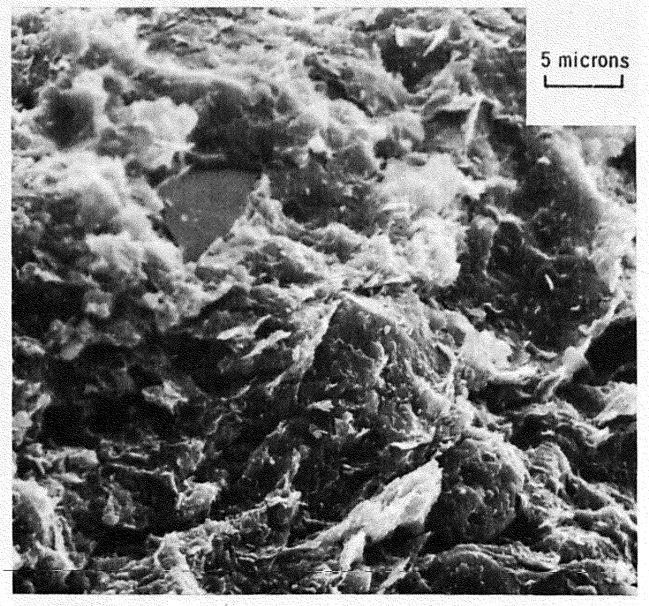

b) X2000

Fig. 45. SEM photographs of specimen SC10X, SMC-17. Face is normal to trajectory and beyond impact area

a) X200

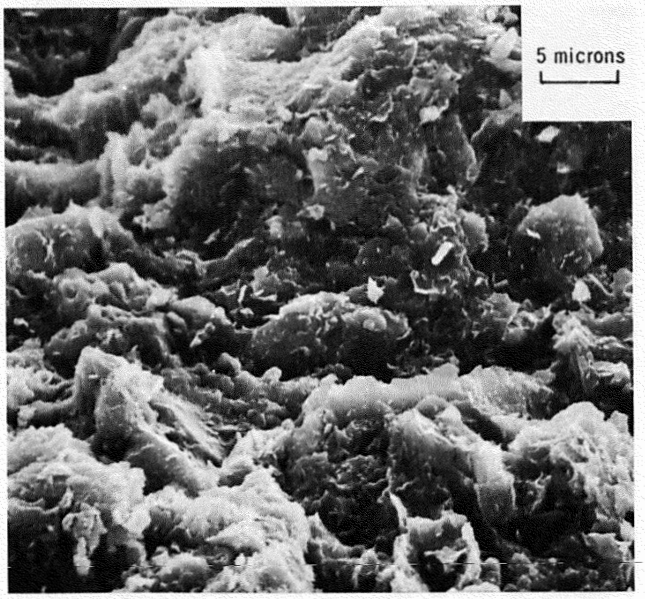

b) X2000

Fig. 46. SEM photographs of specimen SC1OX, SMC-18. Face is parallel to trajectory and beyond impact area

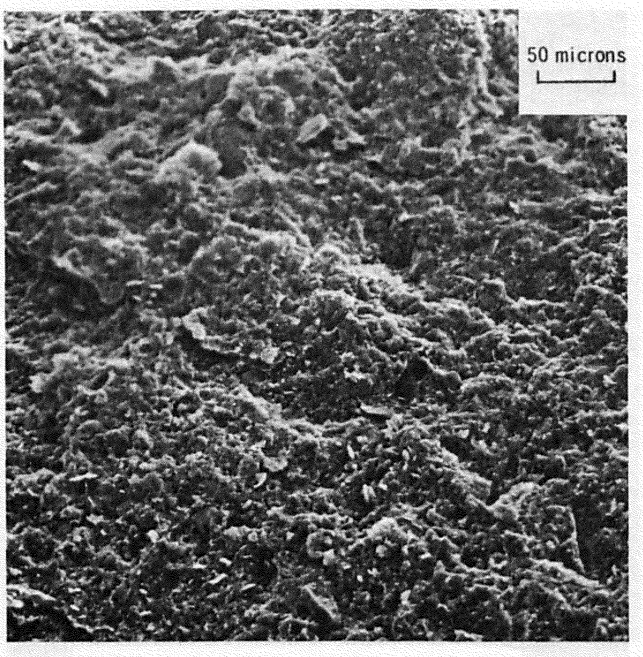

a) X200

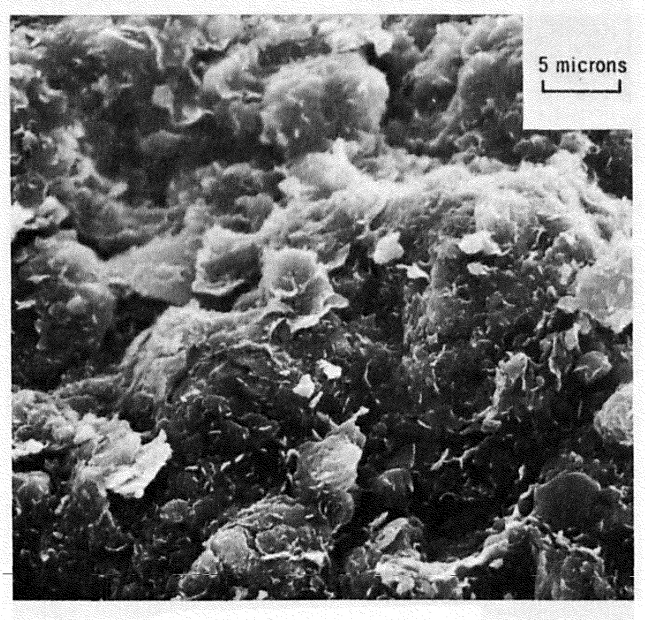

b) X2000

Fig. 47. SEM photographs of specimen SC1OX, SMC-19. Face is normal to trajectory and near impact area

a) X200

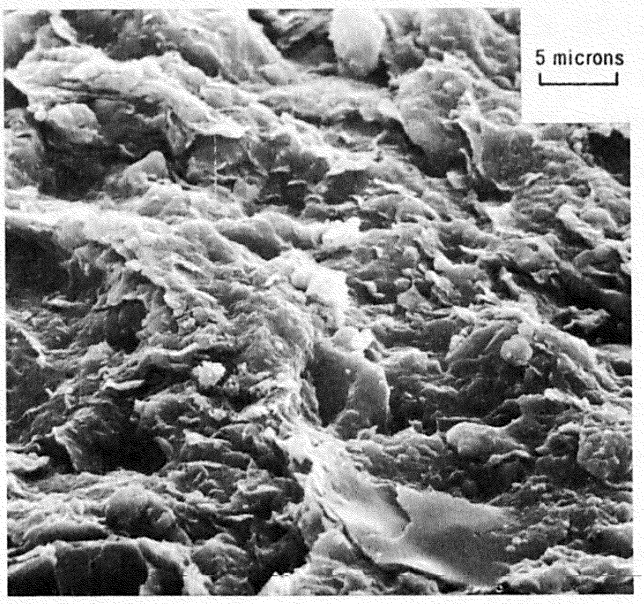

b) X2000

Fig. 48. SEM photographs of specimen SC10X, SMC-20. Face is parallel to trajectory and near impact area

specimens exhibited a rather pronounced preferred orientation of the individual clay platelets. This orientation is approximately parallel to the compacted lifts and normal to the trajectory. There is hardly any difference in degree of orientation between areas near and far from the impact crater. Those samples taken from the walls of the crater did, however, exhibit a smoothing effect due to the passage of the projectile.

113. Selection of the proper magnification is an important aspect of clay-fabric studies. The fabrics encountered in these specimens could be identified with ease at low magnifications (X200 to X500). Generally, higher magnifications did not cover sufficient sample areas and, therefore, did not allow adequate interpretation of the overall fabric.

PART VII: DISCUSSION

114. The use of earth material to protect personnel and equipment from attack by conventional weapons has stimulated interest in the impact resistance of clays and other soils.[6] The depth to which a given projectile will penetrate a particular soil is a function of projectile velocity and the shear strength of the soil. The shear strength is controlled by water content and density. The depth of penetration for a particular soil is an indication of its suitability and the thickness of soil necessary for a protective covering.

115. These practical considerations are directly related to the mechanisms of material deformation.[7] These mechanisms entail an understanding of the changes induced in the material by the penetration of a projectile and include densification and possibly reorientation in clays and densification accompanied by comminution in sands.

116. This investigation intended to demonstrate the applicability of radiography and allied techniques to the detection and evaluation of changes produced by ballistic loading. The vehicle of this study was the loading of laboratory specimens prepared at various densities and water contents and subsequently impacted at both high and low velocities. The use of laboratory specimens plus the need for duplication of specimens required that some form of quality control be provided. The pretest radiographs demonstrated the quality of specimen preparation and permitted the comparison of duplicate specimens. It was evident from the radiographs that, in most cases, sample preparation and duplication were satisfactory. The application of radiography alone for the detection of changes induced by the impact shows greatest promise for the visualization of large-scale effects, e.g., crater geometry, projectile location and trajectory, and other large-scale disruptions produced in the specimen. The comparison of posttest and pretest radiographs did not indicate any disturbance in the region beyond the crater. There was some evidence of density changes in the area beneath and to the sides of the projectile as seen from the radiographs and isodensitometer analyses.

117. The ability to detect and subsequently evaluate small-scale

changes produced by impact is based upon three assumptions as follows:

a. The specimens are more-or-less uniform throughout.

b. Preparation techniques do not appreciably modify the material.

c. There exists a recognizable structural arrangement in the material which can form the basis for detecting changes produced by impact.

If these assumptions are satisfied, isodensitometer analyses and petrographic and SEM techniques may be applied.

118. Examination and comparison of pretest and posttest radiographs will indicate the extent to which the first assumption is satisfied. Experience, on the other hand, has shown that the sample preparation techniques described in this report satisfy the second assumption. The examination of SEM photographs and thin sections revealed that a recognizable fabric or structural arrangement did exist and that it consisted of a more-or-less face-to-face orientation of the clay platelets. The faces of the platelets were normal to the trajectory.

119. The development of the face-to-face orientation is believed to be due to the compaction effort used in preparing the sample. It did not appear that there was any enhancement of this operation directly beneath the projectile. Although it does not seem unreasonable to consider that the penetration of the projectile would, in densifying the clay, produce some enhancement of this orientation, the extent of enhancement may be a function of the degree of original orientation. The nature of this original orientation is probably dependent upon the preparation of the sample.

120. Progressive densification, reorientation, and comminution resulting from the ballistic loading of soils can be more adequately investigated by flash radiography. This procedure would permit the observation of the material at microsecond or nanosecond intervals during the penetration of the projectile. The resulting radiographs and their isodensitometer analyses would provide a visual history of the reactions in the soil including crater development and also allow the computation of soil densities at various stages of impact.

121. Flash radiography would be significantly useful for depicting

the progressive development of the crater system. It is not known to what extent the sabot influences crater geometry and, therefore, some means of visual examination at progressive intervals would be quite useful.

122. Since the penetration of the projectile ejects a portion of the specimen, there is no means of studying the changes induced in the ejected material by posttest radiographs. Isodensitometer analyses of flash radiographs, however, would permit density computations during various intervals of impact.

123. The procedures recommended for studying material properties resulting from ballistic loading are summarized in fig. 49. This flow

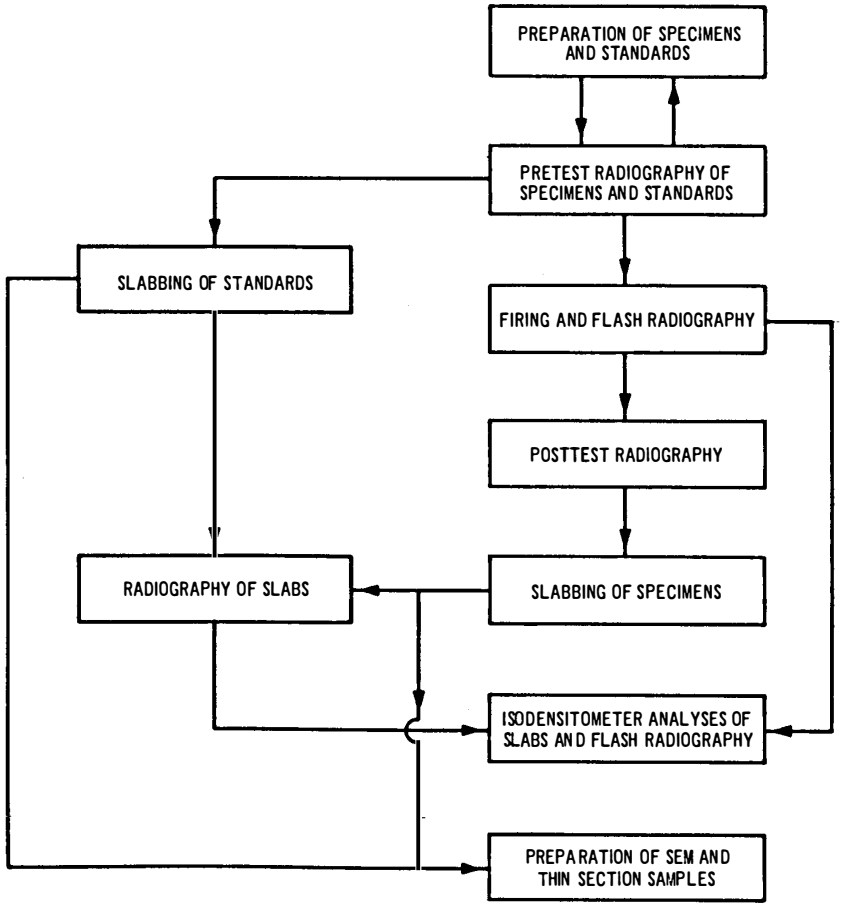

Fig. 49. Flow diagrams illustrating recommended steps and procedures for studying changes in materials induced by ballistic loading

diagram incorporates both flash radiography and the techniques presented in this report.

124. Although the applicability of radiography and allied techniques has been demonstrated for the ballistic loading of clays, the procedures are quite applicable to other soils and, in principal, to all other materials. Cohesionless materials, such as sand, would require some modification of procedures such as impregnation prior to slabbing and subsequent examination by isodensitometer; however, these materials also would be responsive to these methods of investigation.

125. Furthermore, it is concluded that the techniques presented here would also be applicable to other types of dynamic and static loading.

126. The analysis of clay fabrics by petrographic techniques permits the identification of preferred orientation within test specimens. The petrographic procedures utilized in the study were qualitative and required visual inspection and comparison of thin sections. The use of a photoelectric cell to measure the birefringence exhibited by the thin sections at various orientations and to thus quantify the extent of preferred orientation has been shown to provide a rapid and effective means of comparing and evaluating clay fabrics.[5]

127. Another technique that exhibits promise for the quantification of clay-fabric analyses involves X-ray diffraction procedures.[8] In this method the area of interest is X-rayed, and the peak heights or counts per second are determined for selected d-spacings. The degree of preferred orientation exhibited by the clay is proportional to the peak height or count ratio of the basal (001) to nonbasal (0k0) d-spacing.

PART VIII: CONCLUSIONS

128. The radiographic examination of ballistically loaded clay provides useful information regarding the nature of projectile penetration, and the effects of such penetration on the structure and density of the clay.

129. High-velocity impact generally results in deepest penetration, deformation of projectile, and the development of a more complex crater system. For specimens of low density, however, a complex crater system and deeper penetration occur under low-velocity impact.

130. Radiographs of thin slabs provide more detailed information on small-scale changes in the clay and are more useful in this regard than radiographs of bulk specimens.

131. The examination of thin-slab radiographs did not reveal any major fabric alteration beyond the crater.

132. Isodensity tracings made from thin-slab radiographs provided useful data on density variations within the clay and suggest that some densification does occur in the clay directly under the projectile.

133. SEM and petrographic techniques demonstrate that the clay is preferentially oriented with the c-axis more-or-less parallel to the direction of compaction. This orientation is believed to be due to the compaction effort used in preparing the specimens. Also, these techniques do not indicate that there has been any fabric alteration in areas beyond the crater.

134. Flash radiography would provide useful information on material changes that occur during the impact.

LITERATURE CITED

1. Krinitzsky, E. L., "X-Ray Measurement of Soil Densities in Models," Miscellaneous Paper S-72-1, Jan 1972, U. S. Army Engineer Waterways Experiment Station, CE, Vicksburg, Miss.

2. _____, Radiography in the Earth Sciences and Soil Mechanics, Plenum Press, New York, 1970.

3. McMaster, R. C., ed., Nondestructive Testing Handbook, Vol I, Ronald Press, New York, 1959, Section A, p 30.

4. Van Olphen, H., An Introduction to Clay Colloid Chemistry, for Clay Technologists, Geologists, and Soil Scientists, Interscience Publishers, New York, 1963, pp 93-94.

5. Morgenstern, N. R. and Tchalenko, J. S., "The Optical Determination of Preferred Orientation in Clays and Its Application to the Study of Microstructures in Consolidated Kaolin, 1," Proceedings, Royal Society of London, Series A, Vol 300, 1967, pp 218-234.

6. Reeves, G. N. and Rohani, B., "Fragment and Projectile Penetration Resistance of Soils; Literature Review and Preliminary Theoretical Study of Soils as Fortification Material," Miscellaneous Paper S-71-12, Report 1, Jul 1971, U. S. Army Engineer Waterways Experiment Station, CE, Vicksburg, Miss.

7. Rohani, B., "High-Velocity Fragment Penetration of Soil Targets," Proceedings, Conference on Rapid Penetration of Terrestrial Materials, Texas A&M University, 1972, pp 251-280.

8. Diamond, S., "Microstructure and Pore Structure of Impact-Compacted Clays," Clays and Clay Minerals, Vol 19, No. 4, 1971, pp 239-249.

Table 1

Summary of Test Parameters

Sample Parameter	02BC	03BC	Control No. 1	04BC	05BC	Control No. 2	Control No. 4	09BC	010BC	Control No. 5	011BC	012BC	SC10C*	SC10X*
Length, in.	12.90	12.20	11.62	12.42	12.33	12.33	12.60	12.60	12.60	11.76	11.50	11.83	12.00	12.00
Width, in.	4.13	4.13	4.13	4.13	4.13	4.13	4.13	4.13	4.13	4.13	4.13	4.13	12.00	12.00
Height, in.	4.61	4.61	4.61	4.61	4.61	4.61	4.61	4.61	4.61	4.61	4.61	4.61	12.00	12.00
Bulk density wet, pcf	120.00	126.90	128.40	118.40	119.30	119.20	106.70	106.70	106.60	128.00	128.00	128.00	86.30	90.60
Water content, %	35.90	31.30	31.30	42.00	42.00	42.00	67.00	67.00	67.00	28.00	26.00	26.00	28.60	27.00
No. of lifts per specimen	5.00	5.00	5.00	5.00	5.00	5.00	N/A	N/A	N/A	5.00	5.00	5.00	N/A	N/A
No. of blows per lift	25.00	25.00	25.00	25.00	25.00	25.00	N/A	N/A	N/A	50.00	50.00	50.00	N/A	N/A
Projectile velocity, fps	3226	1795	--	3327	1660	--	--	3212	1656	--	3286	1650	1439	3463
Projectile weight, grains	45.00	45.00	--	45.00	45.00	--	--	45.00	45.00	--	45.00	45.00	41.00	41.00
Depth of penetration, in.	7.64	5.39	--	7.68	6.49	--	--	9.76	10.48	--	5.16	4.53	6.30	6.14

Note: N/A designates hand-emplaced.
* Special samples acquired for SEM and petrographic examination.

Table 2

Comparisons of Actual and Computed Bulk Densities

Sample No.	Bulk Density		Difference	
	Actual pcf	Computed pcf	Net, pcf	%*
02BC	120.0	127.5	+7.5	+6.4
04BC	118.8	118.0	-0.8	-0.7
05BC	119.3	122.3	+3.0	+2.5
09BC	106.7	106.5	-0.2	-0.2
010BC	106.6	108.3	+1.7	+1.6
011BC	128.0	132.5	+4.5	+3.5
012BC	128.0	132.0	+4.0	+3.1
Control 1	128.4	127.3	-1.1	-0.9
Control 2	119.2	120.6	+1.4	+1.2
Control 4	106.7	102.7	-4.0	-3.7
Control 5	128.0	130.4	+2.4	+1.9

* Average percent difference is 2.4.

Unclassified

Security Classification

DOCUMENT CONTROL DATA - R & D

(Security classification of title, body of abstract and indexing annotation must be entered when the overall report is classified)

1. ORIGINATING ACTIVITY *(Corporate author)*

U. S. Army Engineer Waterways Experiment Station
Vicksburg, Mississippi

2a. REPORT SECURITY CLASSIFICATION

Unclassified

2b. GROUP

3. REPORT TITLE

RADIOGRAPHIC, PETROGRAPHIC, AND SEM EVALUATION OF BALLISTICALLY LOADED CLAY

4. DESCRIPTIVE NOTES *(Type of report and inclusive dates)*

Final report

5. AUTHOR(S) *(First name, middle initial, last name)*

David M. Patrick

6. REPORT DATE	7a. TOTAL NO. OF PAGES	7b. NO. OF REFS
June 1973	87	8

8a. CONTRACT OR GRANT NO.	9a. ORIGINATOR'S REPORT NUMBER(S)
b. PROJECT NO. 61102A4A061102B52E	Miscellaneous Paper S-73-57
c.	9b. OTHER REPORT NO(S) *(Any other numbers that may be assigned this report)*
d.	

10. DISTRIBUTION STATEMENT

Approved for public release; distribution unlimited.

11. SUPPLEMENTARY NOTES	12. SPONSORING MILITARY ACTIVITY
	Directorate of Military Engineering and Topography Washington, D. C.

13. ABSTRACT

Specimens of highly plastic clay were prepared at densities and water contents ranging from 106 to 128 pcf and 26 to 67 percent, respectively. These specimens were ballistically loaded by impact of a projectile traveling at both low (1660 fps) and high (3327 fps) velocities. Radiographic examination of the specimens revealed the extent and nature of disturbance including crater size and shape, depth of projectile penetration, and projectile deformation. Radiography of thin slabs and isodensitometer studies provided the basis for density measurements. The radiography was supplemented by clay-fabric studies utilizing petrography and scanning electron microscopy (SEM). These techniques indicated that the impact produced negligible fabric disturbance and that some densification had occurred beneath the projectile. Techniques, procedures, and recommendations are given for studying ballistic loading of materials.

DD FORM 1 NOV 68 1473 REPLACES DD FORM 1473, 1 JAN 64, WHICH IS OBSOLETE FOR ARMY USE.

Unclassified

Security Classification

14 KEY WORDS	LINK A		LINK B		LINK C	
	ROLE	WT	ROLE	WT	ROLE	WT
Clays						
Impact loads						
Petrography						
Projectiles						
Radiography						
Scanning electron microscopy						
Soil penetration						
Soil test specimens						